GRV 10-16-06

ANL/EXT-06-45

Argonne NATIONAL LABORATORY

Preliminary Materials Selection Issues for the Next Generation Nuclear Plant Reactor Pressure Vessel

K. Natesan, S. Majumdar, P. S. Shankar, and V. N. Shah

September 2006

ANL/EXT-06-45

Preliminary Materials Selection Issues for the Next Generation Nuclear Plant Reactor Pressure Vessel

K. Natesan, S. Majumdar, P. S. Shankar, and V. N. Shah

September 2006

Argonne National Laboratory
Argonne, IL 60439

Prepared for the
U.S. Department of Energy
Office of Nuclear Energy, Science, and Technology

Argonne is operated by The University of Chicago
under DOE Contract W-31-109-Eng-38.

Executive Summary

The NGNP, which is an advanced HTGR concept with emphasis on both electricity and hydrogen production, involves helium as the coolant and a closed-cycle gas turbine for power generation with a core outlet/gas turbine inlet temperature of 900-1000*C. In the indirect cycle system, an intermediate heat exchanger is used to transfer the heat from primary helium from the core to the secondary fluid, which can be helium, nitrogen/helium mixture, or a molten salt. The system concept for the VHTR can be a reactor based on the prismatic block of the GT-MHR developed by a consortium led by General Atomics in the U.S. or based on the PBMR design developed by ESKOM of South Africa and British Nuclear Fuels of U.K.

This report has reviewed the available information on candidate materials for the construction of RPV and has made a preliminary assessment of several relevant factors to make a judicious selection of the material for the RPV. Some of the factors addressed in this report are availability of commercial alloys for RPV application, their status in ASME Codes for nuclear service, ASME code compliance during steady state and depressurized conduction cooling conditions, baseline mechanical properties, effects of thermal aging on mechanical properties and code compliance over long term, fabrication and welding issues, global assessment of availability/capability of vendors for RPV procurement, and technology gaps in our knowledge base to address some of the technical issues. The assessment included three primary candidate alloys namely, low alloy steel SA508 (UNS K12042), Fe-2.25Cr-1Mo-0.25V steel (UNS K31835), and modified 9Cr-1Mo steel (UNS K90901) for the RPV.

Several conclusions were drawn from this assessment:

Baseline Mechanical Properties: There is sufficient database available for the mechanical properties of SA-508 steel. There is limited data available on the thermal aging effects on the mechanical properties and additional information needs development on the long-term aging effects. The steel is approved for use up to 371°C (700°F) under the ASME Code. At present no data is available on the effects of impure helium on the long-term corrosion and mechanical properties of the material.

There is adequate tensile data on the Fe-2.25Cr-1Mo-0.25V in the temperature range of interest in NGNP RPV. There is only limited creep data available for the steel and additional data are needed, especially at elevated temperatures that encompass depressurized conduction cooldown conditions. However, substantial data on the creep fatigue properties, thermal aging affects on the mechanical properties, performance characteristics in impure helium, and properties of thick section material are needed prior to its selection for NGNP RPV. Furthermore, the steel is approved under ASME Code Section VIII (for non nuclear applications) and is not approved under Section III for use in nuclear systems.

Substantial database on the baseline mechanical properties is currently available for the Modified 9Cr-1Mo steel. Sufficient data are also available on the long-term thermal aging effects on the mechanical properties for this steel. One of the strong points for the selection of this steel is that it is approved in Section III of the ASME Code for nuclear applications. However, the creep-fatigue limits for the steel in the Code is highly conservative and it may preclude its selection for the NGNP RPV application. Furthermore, additional data are needed for the steel in the areas of compatibility in impure helium and mechanical properties of thick sections.

Welding Issues: Pressure vessels of Low alloy steels have been fabricated and used in U.S. light-water reactors and there is substantial experience in welding of both plates rings to form the vessels. Vessels with wall thicknesses varying between 203 to 254 mm (8 to 10 in.) and diameter-to-thickness ratios of ≈20 have been fabricated for the PWRs. In contrast, BWR vessels with much larger diameter and a wall thickness of 152-mm (6-in.) have been fabricated. Pressure vessel materials have performed well in service, and no fatigue-driven cracks have been found in any PWR vessels. The only materials-related variable that appears to affect fatigue is the sulfur content (and distribution as sulfides) in the steel. Low alloy steels with average to high sulfur levels generally exhibit higher crack growth rates in the laboratory than low sulfur steels (<0.010 wt.%).

Vanadium-modified 2.25Cr-1Mo steels are developed for the petrochemical refinery industry service at high temperatures and high hydrogen pressures. These steels were developed so that components having wall thickness in excess of 10 in., and diameters and lengths on the order of up to 20 and 200 ft, respectively, can be fabricated. These steels offer the fabricability and toughness of bainitic microstructures without the difficulties of welding and heat treatment of high chromium martensitic materials such as P91. Stress rupture tests on weldments to 16000 h established that the expected performance of the filler metal, base metal, and HAZ were comparable in strength and within ASME's base metal scatter band. However, for design temperatures in excess of 468°C (875°F), ASME required performance testing of weldments, and additional long-term test data are needed to qualify the welded components for application in NGNP RPV. Temper embrittlement, caused by reduction of bond strength of grain boundaries relative to the grain due to segregation of impurities (P and Sb) at grain boundaries, is of concern. If the grains are insufficiently tempered, the effect is the greatest. Test results for base metal, HAZ, and weld metal exposed for 20000 h at 482°C (900°F) have shown that acceptable toughness is retained for the materials, provided impurity levels were maintained within specific limits.

Modified 9Cr-1Mo steel is a leading candidate for NGNP RPV and it is being evaluated in several programs conducted worldwide. The superior mechanical properties of the 9Cr-1Mo weldment strongly depend on creation of a precise microstructure and maintaining it throughout the service life of the welded component. Welding procedure and post-weld heat treatment play critical roles in creating the microstructure. The most significant problem with welding of 9Cr-1Mo steel is its propensity to Type IV cracking in the heat affected zone. Boron addition seems to reduce cracking susceptibility but additional data are needed to quantify the effect over the long term. Creep-fatigue interaction could be more severe in 9Cr-1Mo weldment compared to weldment of 2.25Cr-1Mo steel. The creep-fatigue data show that the number of cycles to failure decreases with increase in tension hold time for the weldment. Significant additional data are needed to quantify this effect and establish, if any, the maximum reduction in life.

Procurement Issues: The current schedule for the NGNP plant requires that the conceptual and preliminary designs and the application for the construction permit from NRC be completed by the middle of calendar year 2010. The selection of material for the NGNP RPV is one of the critical items to meet the schedule. The NGNP RPV will have dimensions of 8-9 m in diameter and probably 200-300 mm in thickness. Such a vessel is much larger than the current LWR vessels and requires field welding of either ring forgings or plates of the selected material. In the selection of the candidate material for the RPV, the key technical/design issues are the reactor outlet temperature, active vs. passive cooling of the vessel, ASME code compliance under normal and transient conditions, high temperature design methodology currently available, welding and post-weld heat treatment in the field, fabrication expertise to achieve

uniform through-thickness properties in thick sections, and vendor experience and availability in fabrication with different candidate materials.

At present, there exists a substantial experience in fabrication of RPV from SA-508 with several vendors around the world and procurement of a vessel of this material may depend primarily on the availability of a vendor to meet the schedule and not on the technical issues with the material.

Fe-2.25Cr-1Mo-V steel is extensively used in the fossil industries and hydrogenation reactor pressure vessels. There is no available information on existing pressure vessels having dimensions similar to that required in the NGNP RPV. Because of the large scale use of this material in fossil, petrochemical industries, etc. it can be concluded that there is some experience in forging/rolling thick-sections of this material. However, application of this material for NGNP RPV requires substantial additional data on the long term (>10000 h) mechanical properties and ASME Code approval for nuclear service.

Modified 9Cr-1Mo steel has overall superior mechanical properties among the three candidate materials that makes it a primary candidate for use in the NGNP RPV. However, information is lacking on thick-section properties/fabrication experience of this material. An assessment of the potential vendors from all over the world showed that capability and experience to fabricate a modified 9Cr-1Mo vessel of the size required for NGNP are severely lacking. None of the vendors have the capability, at present, to forge thick-section large diameter rings of modified 9Cr-1Mo steel. It was clear that none of the vendors was willing to upgrade their existing facility to facilitate forging of this steel unless an incentive is offered to them (in terms of assured market/customers to order RPV of the modified steel, or in some other form). As ring forging of RPV using modified 9Cr-1Mo steel does not appear to be a feasible option at present, axial welding of plates/ring segments is the alternate choice. However, none of the vendors has experience in manufacturing thick-section plates. Based on our assessment, the selection of this material for RPV may not meet the NGNP schedule because of the procurement limitation.

ASME Code Compliance of RPV: The NGNP RPV needs to be designed using the ASME Section III Code rules. If the RPV wall temperature can be maintained at a sufficiently low temperature, Subsection NB of the Code can be used. Otherwise, Subsection NH has to be followed.

SA508/SA533 steels are ASME Code approved for Class 1 nuclear components and Subsection NB rules are applicable up to 371°C for normal operation. Limited high temperature excursions under off-normal and conduction cooldown conditions are permitted under Code Case N 499. SA-508 forging can be a potential candidate for the pebble bed RPV design since the peak temperature as calculated by RELAP5 is ≤371°C. However, temperatures ≥371°C was calculated when a pebble-bed-specific code was used, which necessitates active cooling of the RPV made of this steel to comply with the ASME Code for transient operation. SA-508 steel is unacceptable for the prismatic core RPV design because the calculated temperatures during normal operation exceed 371°C and active cooling is mandatory, if this steel is selected for the prismatic RPV design.

At present, Fe-2.25Cr-1Mo-V steel is not approved under ASME Code Section III for nuclear service and therefore, no calculation was performed to assess its suitability for both designs of NGNP RPV.

Calculations performed for the modified 9Cr-1Mo steel showed that the peak membrane stress for the pebble bed design RPV is within the ASME Code Subsection NB allowable for the steel. The peak membrane stress for the prismatic design RPV is within the ASME Code Subsection NH allowable (300000 h) for the steel. Stress analysis of the depressurized conduction cooldown condition for both pebble bed and prismatic designs showed the peak temperatures to be in the creep range for the steel, but the stresses are too low to cause any significant creep deformation ($<10^{-6}$).

Contents

Acronyms

BWR	Boiling Water Reactor
CE	Combustion Engineering, Inc.
CGHAZ	Coarse-Grained Heat-Affected Zone
BHN	Brinnel Hardness Number
DBTT	Ductile-Brittle transition Temperature
DOE	Department of Energy
EPERC	European Pressure Equipment Research Council
FATT	Fracture Appearance Transition Temperature
FCAW	Flux Core Arc Welding
FGHAZ	Fine-Grained HAZ
GTAW	Gas Tungsten Arc Welding
GT-MHR	Gas Turbine - Modular Helium Reactor
HAZ	Heat Affected Zone
HIDA	High Temperature Defect Assessment
HRSG	Heat-Recovery Steam Generator
HTGR	High Temperature Gas Reactor
ID	Inside Diameter
IHX	Intermediate Heat Exchanger
KAERI	Korean Atomic Energy Research Institute
LWR	Light Water Reactor
MBN	Magnetic Barkhausen Noise
MHI	Mitsubishi Heavy Industries
MMA	Manual Metal Arc
MT	Magnetic-Particle Testing
NGNP	Next Generation Nuclear Plant
OD	Outside Diameter
PBMR	Pebble Bed Modular Reactor
PCU	Power Conversion Unit
PISC	Program for the Inspection of Steel Components
PWHT	Post-weld Heat Treatment
PT	Penetrant Testing
PWR	Pressurized Water Reactor
PTS	Pressurized Thermal Shock

RPV	Reactor Pressure Vessel
RT_{NDT}	Reference Nil-Ductility-Transition Temperature
SAW	Submerged Arc Welding
SCC	Stress Corrosion Cracking
SMAW	Shielded Metal Arc Welding
UDRPS	Ultrasonic Data Recording and Processing System
USC	Ultra Super Critical
USE	Upper Shelf Energy
UTS	Ultimate Tensile Strength
VHTR	Very High Temperature Reactor System
YS	Yield Strength

Figures

Tables

Preliminary Materials Selection Issues for the Next Generation Nuclear Plant Reactor Pressure Vessel

1. Introduction

In the coming decades, the United States and the entire world will need energy supplies to meet the growing demands due to population increase and increase in consumption due to global industrialization. One of the reactor system concepts, the Very High Temperature Reactor (VHTR), with helium as the coolant, has been identified as uniquely suited for producing hydrogen without consumption of fossil fuels or the emission of greenhouse gases [Generation IV 2002]. The U.S. Department of Energy (DOE) has selected this system for the Next Generation Nuclear Plant (NGNP) Project, to demonstrate emissions-free nuclear-assisted electricity and hydrogen production within the next 15 years.

The NGNP reference concepts are helium-cooled, graphite-moderated, thermal neutron spectrum reactors with a design goal outlet helium temperature of ≈1000°C [MacDonald et al. 2004]. The reactor core could be either a prismatic graphite block type core or a pebble bed core. The use of molten salt coolant, especially for the transfer of heat to hydrogen production, is also being considered. The NGNP is expected to produce both electricity and hydrogen. The process heat for hydrogen production will be transferred to the hydrogen plant through an intermediate heat exchanger (IHX).

The basic technology for the NGNP has been established in the former high temperature gas reactor (HTGR) and demonstration plants (DRAGON, Peach Bottom, AVR, Fort St. Vrain, and THTR). In addition, the technologies for the NGNP are being advanced in the Gas Turbine-Modular Helium Reactor (GT-MHR) project, and the South African state utility ESKOM-sponsored project to develop the Pebble Bed Modular Reactor (PBMR). Furthermore, the Japanese HTTR and Chinese HTR-10 test reactors are demonstrating the feasibility of some of the planned components and materials.

The proposed high operating temperatures in the VHTR place significant constraints on the choice of material selected for the reactor pressure vessel for both the PBMR and prismatic design. The main focus of this report is the RPV for both design concepts with emphasis on material selection.

2. Reactor Pressure Vessel Requirements

The reactor system that is envisioned for both prismatic block and pebble bed designs for NGNP is similar and will consist of a large reactor pressure vessel (RPV) containing the core and internals and a second large vessel for power conversion unit (PCU) containing either the turbine generator or the intermediate heat exchanger and a primary coolant circulator, and a pressure-containing cross vessel connecting the RPV and the PCU.

The reactor design determines the maximum operating temperature of the reactor vessel. The maximum operating temperature then determines the vessel materials that will comply with the design codes and also allow an acceptable lifetime. Some designs, such as the South African Pebble Bed Modular Reactor (PBMR), consider using SA-508 steel for the reactor vessel. SA-508 has been used for reactor vessels in light water reactors and requires a relatively low operating temperature. The PBMR in South Africa calculate a normal operating

temperature of 280°C for the reactor vessel. This low temperature is achieved with a pressure vessel conditioning system that uses an independent coolant stream to keep the reactor pressure vessel at an acceptable temperature. This is not designed as a safety system and thus is assumed to fail during a depressurized conduction cooldown. Other proposed design such as GT-MHR operating at a higher vessel temperature of 495°C requires use of SA-336 (9Cr-1Mo-V) steel.

Gougar and Davis [2006] analyzed both PBMR and prismatic block design concepts to determine maximum temperatures in the reactor pressure vessel during normal operation and during a depressurized conduction cooldown accident. The prismatic design was based on the 600-MW (thermal) GT-MHR. The pebble-bed design was based on the 400-MW PBMR, but the power was increased to 600 MW, the desired power level of the VHTR. Calculations were performed at vessel outlet fluid temperatures of 900 and 950°C. Results from these calculations along with the material properties were used to assess the choice of materials for the RPV and their compliance to ASME Codes during normal and depressurized conduction cooldown conditions.

Some of the factors addressed in this report are availability of commercial alloys for RPV application, their status in ASME Codes for nuclear service, ASME code compliance during steady state and depressurized conduction cooling conditions, baseline mechanical properties, effects of thermal aging on mechanical properties and code compliance over long term, fabrication and welding issues, global assessment of availability/capability of vendors for RPV procurement, and technology gaps in our knowledge base to address some of the technical issues.

3. Materials of Construction

The average reactor pressure vessel wall temperature could vary between 260 and 500°C depending on the RPV design and material selected. This range is based on existing prismatic and pebble bed designs (from Generation IV partners) all over the world. On the lower end, the PBMR design in South Africa has a nominal operating temperature of 260-300°C whereas on the higher side, the prismatic GT-MHR design of General Atomics Corporation has a nominal operating temperature of 495°C [Hayner et al. 2005]. Table 3.1 gives the existing RPV designs, the nominal operating temperatures, and the proposed RPV material in various VHTRs. The temperatures, pressures, etc are valid as of this report and could vary with the evolution of design.

For the construction of the NGNP RPV, potential candidate materials are UNS K12042 (SA-508), UNS K31835 (2.25Cr-1Mo-0.25V steel), and UNS K90901 (modified 9Cr-1Mo steel). The elemental composition of these alloys is given in Table 3.2 [ASME 2004].

Table 3.1: Reactor pressure vessel design parameters of different VHTR concepts [Hayner et al. 2005]

Design Details	Prismatic						Pebble Bed
	GT-MHR (General Atomics)	AREVA (France)	HTTR (Japan)	CEA(France) and EU Prog	Korean RPV	HTR10 (China)	PBMR (S. Africa)
Cycle	Indirect	Indirect					Direct
Reactor Power, MWt	600	600	30				400-500
Height (m) x Diameter (m)	23.7 x 8.2	23.7 x 8.2					28 x 6.2
Wall Thickness, mm (in.)	Not Established	100-200 mm (4-8)					180 (~ 7)
System Pressure, MPa (ksi)	7 (1.01)	5	4 - 4.8				9 - 9.7 (1.3-1.4)
Stress Experienced, MPa (ksi)	137 (20.5) for 200 mm thick	102 (14.8)					171 (24.8)
Nominal Temp. °C (°F)	495 (923)	Cold: < 350 (662) Hot : < 450 (842)	400-440 (752-824)	<370	< 500		260-300 (500-572)
Worst Case Temp., °C (°F)	565 (1049)				< 650		400-500 (752-932) (Short Term Abnormal Condition)
Proposed Material	Possibly Modified 9Cr-1Mo steel	Cold: SA-508 Hot : SA-336 (Modified 9Cr-1Mo)	2.25Cr-1Mo	Modified 9Cr-1Mo steel	SA 508 SA 533 Mod.9Cr-1Mo	SA516 Gr.70	SA-508 Gr. 3 Cl. 1 SA-533 Type B Cl.1

Table 3.2. Composition (wt.%) of candidate RPV forging materials [ASME 2004]

Material	UNS K12042		UNS K31835		UNS K90901	
	ASME#	Grade	ASME#	Grade	ASME#	Grade
Element	SA-508	3, Class 1 & 2[1]	SA-182 & SA-336 SA-541	F22V[2] 22V	SA-182 & SA-336	F91[2]
C	0.25 max		0.11 - 0.15		0.08 – 0.12	
Ni	0.4-1.0		0.25		0.4 max	
Cr	0.25 max		2.0 - 2.5		8.0 – 9.5	
Mn	1.2-1.5		0.3 - 0.6		0.3 – 0.6	
Mo	0.45-0.6		0.9 – 1.1		0.85 – 1.05	
V	0.05 max		0.25 – 0.35		0.18 – 0.25	
P	0.025 max		0.015		0.020 max	
S	0.025 max		0.01 max		0.01 max	
Si	0.15-0.4		0.1 max		0.2 – 0.5	
Nb	-		0.07 max		0.06 – 0.1	
Others	-		B: 0.002 max; Ca:0.015 max; Cu: 0.20 max; Ti:0.030 max; Rare Earth metals: 0.02 max		Al: 0.04 max; N: 0.030-0.070	
Heat treatment	Quench; temper at 621-635°C (min)		Normalize at 899°C (min.); temper at 677°C		Normalize at 1038-1149°C, air cool; temper at 732°C (min.)	

[1]Until 2003, Class 1 and 2 were designated as 3 and 3A respectively.
[2]F indicates forgings

3.1 Baseline Mechanical Properties of NGNP RPV Candidate Materials

The mechanical properties, especially creep, creep-fatigue, and thermal aging behavior, of candidate RPV materials are summarized in this section. The mechanical properties of welds and heat-affected zones are addressed in the Section on welding.

3.1.1 Alloy Steel (UNS K12042)

UNS K12042 steel, having a nominal composition Fe-0.75Ni-0.5Mo-Cr-V, is represented as SA-508 Grade 3 Class 1 and 2 in the ASME Boiler and Pressure Vessel code [ASME 2004]. Both Class 1 and Class 2 components made of this steel have the same elemental composition range, which is listed in Table 3.2. SA-508 steel forgings are currently used for applications in light-water reactors where the operating temperature is ≈300°C. The steel is typically used in the quenched and tempered (tempering at 621-635°C/1150-1175°F) condition. For evaluation of weld quality and weld metal and heat affected zone properties, the alloy can be subjected to simulated post-weld heat treatment. As SA-508 steel is approved under Section III of the ASME Boiler & Pressure Vessel (B&PV) code for use in nuclear components, it is a prime candidate for VHTR reactor pressure vessels operating at temperatures below the creep regime. As per the Code, there is no time limit for the operation of components made of SA-508 as long as the operating temperatures are maintained <371°C, the temperature below which creep deformation is negligible [ASME 2004].

3.1.1.1 Mechanical Properties

There is an extensive database on the mechanical properties of SA508 steel up to about 300°C. For consideration of this material for the NGNP reactor pressure vessel, where the wall temperature could exceed 371°C depending on RPV design, creep and creep-fatigue response and thermal stability become important factors, in addition to elevated temperature tensile properties. Even where the nominal operating temperature is <300°C [as in the case of PBMR design (Table 3.1)], the material could experience higher temperatures during depressurized conduction cooling conditions that may result in creep deformation.

A compilation of elevated temperature tensile properties of SA-508 steel can be obtained from reports published by Reddy and Ayres [1982] and Harris et al. [1986]. Tensile data up to 727°C are available from these reports. From room temperature up to 593°C, SA-508 was observed to be highly strain-rate sensitive [Ellis and Byrnum 1990].

Short-term (up to 48 hrs) creep data on SA-508 was obtained in the temperature range of 398-649°C [Reddy and Ayres 1982] while creep rupture data was generated in the range of 627-752°C by Harris et al. [1986]. Ellis and Byrnum [1990] evaluated the creep rupture behavior of SA-508 in the range of 371-593°C and their results are plotted in Figure 3.1a. Fig. 3.1b shows the corresponding creep rate vs. rupture life curve. It should be noted that creep as well as tensile data were obtained on quenched and tempered specimens (with a ferrite+bainite microstructure) subjected to a simulated post-weld heat treatment for 40 h at 607°C. There was no observable change in either microstructure or hardness after creep testing at 371 and 427°C. However, at 482°C, a slight spheroidization was observed while creep testing at 593 had a significant spheroidized microstructure accompanied by a decrease in hardness. The R_B hardness of specimen tested at 482°C was 92 and it decreased to 81 at 593°C. A decrease in creep strength at higher temperatures could occur in quenched and tempered steels compared to normalized and tempered steels.

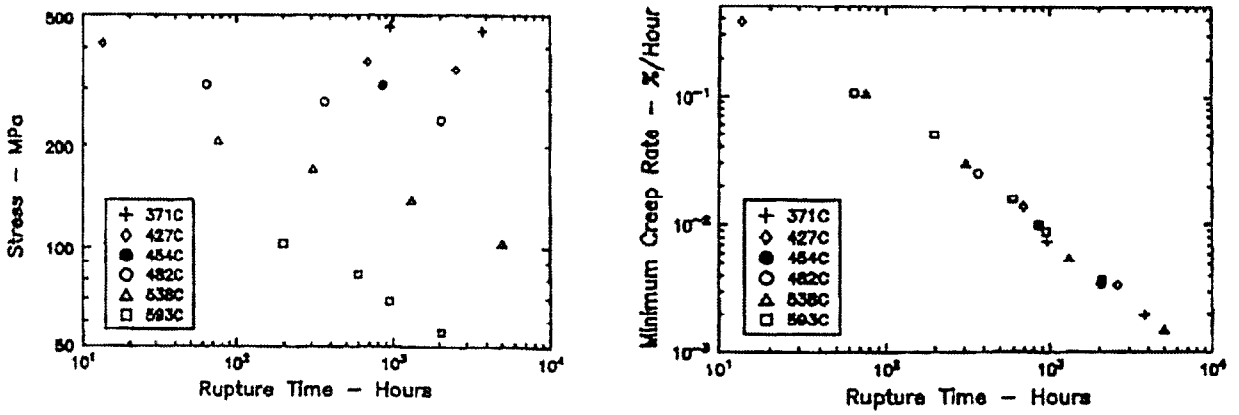

Figure 3.1. Creep response of SA-508 in the range 371-593°C (a) Applied Stress Vs. Rupture Life (b) Creep rate Vs. Rupture Life, [Harris et al. 1986].

Recently, Wu et al [2005] has evaluated the uniaxial creep and creep crack growth behavior of SA-508 Class 2 as-received (ferrite+pearlite microstructure) and simulated coarse-grained heat-affected zone (CGHAZ) having tempered martensite microstructure. They reported that both uniaxial creep and creep crack growth life reduced significantly at higher temperatures, e.g., the creep crack growth life of a CGHAZ was reduced by a factor of five as

the temperature increased from 320 to 340°C at a given stress. Also, creep crack growth life for CGHAZ was less than that for the as-received material, especially at lower stresses. Also, they observed intergranular fracture during creep crack growth tests in CGHAZ whereas the uniaxial creep tests resulted in transgranular fracture.

Long-time stress relief treatments on quenched and tempered SA-508 steel were found to either increase or decrease the fracture toughness compared to those without such treatments [Longsdon 1982]. Stress relieving at 538°C increased the toughness while treatment at 607°C decreased the fracture toughness. A similar trend in the Charpy impact properties was also observed. Nevertheless, the fracture toughness of the steel in the quenched and tempered condition and in all the stress relieved conditions were above the ASME specified reference K_{IR} curve [Longsdon 1982]. In another study [Kwon et al. 2004], thermal aging of a SA-508 welded to a CF-8M did not result in any change in microstructure and Charpy impact properties of the SA-508.

Several studies have evaluated the effects of long-term thermal aging on mechanical properties of SA-508 steel [Fukakura et al. 1993, Devan et al. 1993 & 1996, Gunawardane et al. 2006]. Devan et al. [1993 and 1996] characterized the Chapry impact, tensile, and J-fracture toughness of SA-508 class 2 material after thermal exposure at 282°C up to 103000 h while Gunawardene et al. [2006] evaluated the thermal aging effect of the same material at longer aging times, up to 209000 h. The material had been removed from Oconee Unit 3 reactor vessel head. Table 3.3-3.5 shows the tensile, impact, and fracture toughness properties, respectively after aging at different times.

Table 3.3 clearly indicates that there is no significant change in the tensile properties even after 209000 h of thermal aging. Very minimal hardening may have occurred as seen by the decrease in the reduction of area and the increase in total elongation. Charpy impact testing was performed as per ASTM E 185-82 to clearly identify the transition temperature at absorbed energy of 41 J (30-ft-lb). As can be seen in Table 3.4, there is a small increase in the transition temperature after aging at 209000 h but this increase was within 95% confidence bounds for typical Chapry data. Table 3.5 shows that there is not much variation in the toughness value of the unaged and the 103,000 h (≈12 years) aged condition at both test temperatures. However, the 209,000 h (≈ 24 years) aged condition clearly indicates a substantial increase in fracture toughness but the difference in toughness value of the two 209,000 h specimens (tested at 121°C and 288°C) is quite large. More tests are necessary to verify the effect of aging, if any, on fracture toughness.

Table 3.3 Tensile test results of SA-508 Class 2 forging after 209,000 h thermal aging [Gunawardene et al. 2006]

Test temperature (°C)	0.2% Yield Strength (MPa)	Ultimate Tensile Strength (MPa)	Total Elongation (%)	Reduction in Area (%)
21	405	581	24	70
121	388	551	23	69
304	379	582	27	67

Table 3.4. Chapry V-notch impact test results of SA-508 forged material as a function of thermal aging time [Gunawardene et al. 2006, De Van et al. 1993]

Material Condition	41J Transition Temperature, °C
Unaged	-37
Aged 103,000 h	-32
Aged 209,000 h	-23

Table 3.5 Fracture toughness response of SA-508 steel after thermal aging [Gunawardene et al. 2006, De Van et al 1996]

Test Temperature (°C)	Material Condition	J_{IC} or J_Q, (kJ/m^2)
121	Unaged	132
	Unaged	159
	Aged 103,000 h	221
	Aged 103,000 h	224
	Aged 209,000 h	482
288	Unaged	191
	Unaged	231
	Aged 103,000 h	221
	Aged 103,000 h	182
	Aged 209,000 h	296

Fukukara et al. [1993] observed that thermal aging at 450°C for up to 10000 hrs did not affect the tensile properties of SA-508 Class 1 base metal in the quenched and tempered condition. The ductile-brittle transition temperature (evaluated by Charpy impact testing) of thermally aged base metal at 350 and 400°C did not change significantly. In the case of 450°C thermally aged material, the ductile brittle transition temperature increased by a maximum of 20°C after 10000 hrs aging. Fracture toughness, J_{IC} was measured at room temperature on unaged and aged (400 and 450°C) base metal. The fracture toughness decreased by about 30% in the 10000 hr 450°C aged condition compared to the unaged condition. The toughness decreased from ≈200 kN/m in the unaged condition to ≈135 kN/m in the 450°C, 10000 hr aged condition. The decrease in fracture toughness after 400°C was lower than the decrease observed after 450°C aging.

3.1.1.2 ASME Code Allowables

The minimum property requirements for yield strength (YS), ultimate tensile strength (UTS), and elongation and the various stress allowables (St, Smt, etc.) for SA-508 steel are given in the ASME B&PV Code Section II, Part D [ASME 2004]. Figure 3.2(a-b) shows the code allowables for YS and UTS along with tensile property results from Harris et al. [1986]. It can be seen that the YS data of Harris et al. [1986] meet the minimum requirement while the UTS seems to tend toward the lower side. The Code allows for unlimited operation of the alloy

component when the temperature is <371°C. During accident conditions, if the temperature exceeds 371°C, ASME Code Case 499-2 [ASME 2001] gives the requirements to operate under such elevated temperatures. Essentially, Class 1 nuclear components made of SA-508 class 3 forgings and their weldments maybe used in the temperature range of 371-427°C, for a cumulative time of 3000 h, and in the range 427-538°C, for a maximum time of 1000 h. The number of anticipated events should not exceed 3, when the metal temperature exceeds 427°C. Figures 3.3 and 3.4 show the minimum requirements for creep and creep-fatigue that are specified in the code case. Additional design rules for operating at temperatures in the creep regime can be obtained from the code case.

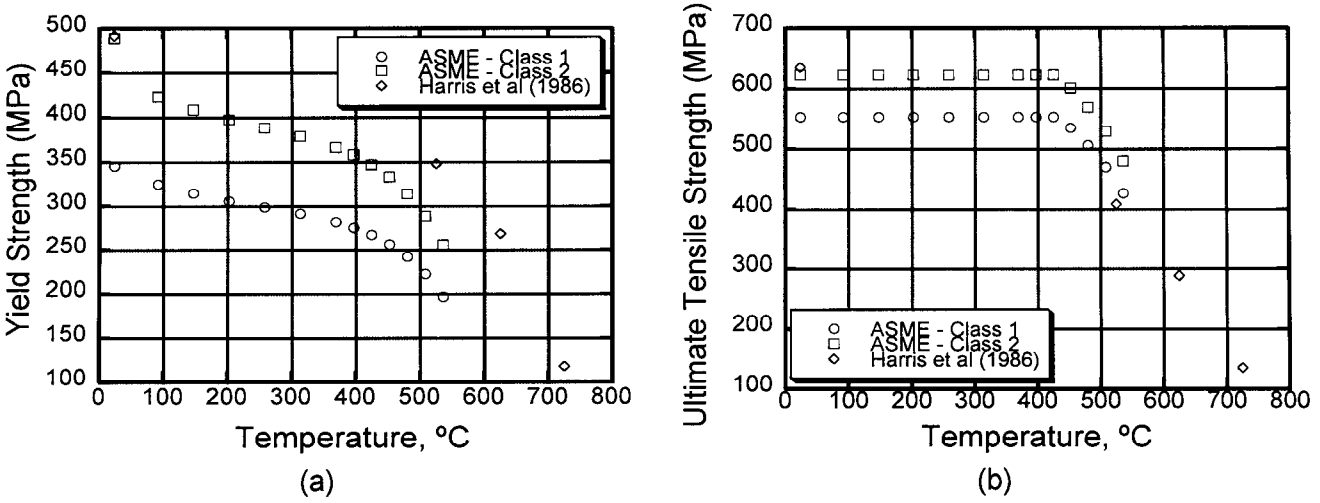

Figure 3.2. Comparison of ASME minimum tensile property requirements with literature values (a) YS and (b) UTS.

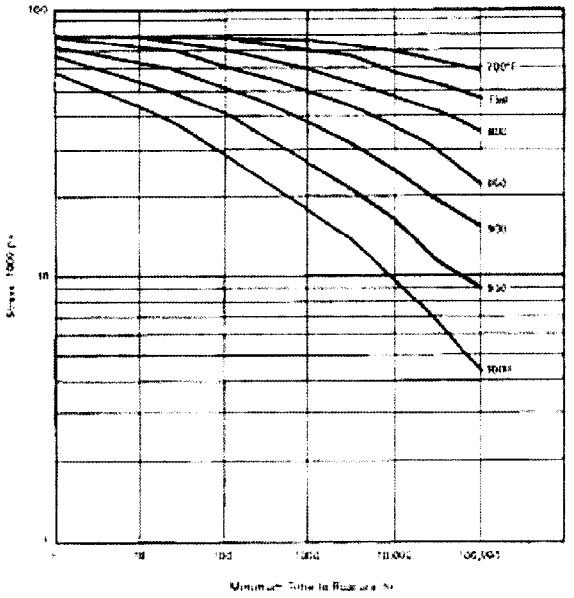

Figure 3.3. Minimum creep rupture requirements for SA-508 from ASME Code Case N-499-2 [ASME 2001].

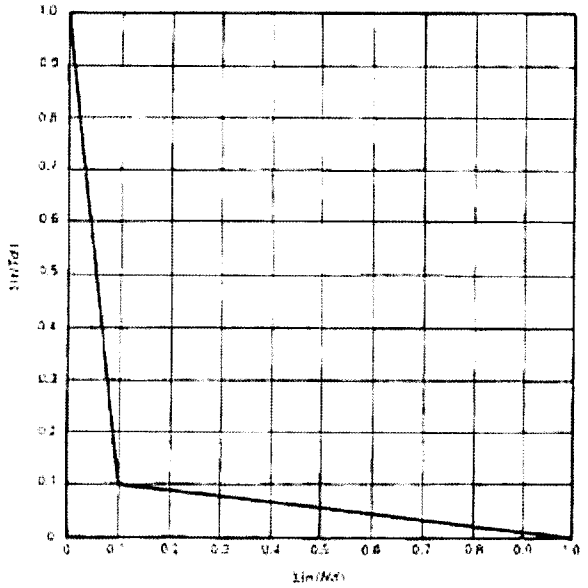

Figure 3.4. Creep-fatigue damage envelope for SA-508 from ASME Code Case N-499-2 [ASME 2001].

3.1.2 Fe- 2.25Cr-1Mo-0.25V Steel (UNS K31835)

UNS K31835 steel, having a nominal composition of Fe-2.25Cr-1Mo-0.25V, is permitted for structural use under ASME specification SA-336 (Grade F22V), SA-182 (Grade F22V), and SA-541 (Grade 22V) in the ASME B&PV Code [ASME 2004]. SA-336 forging is the standard for construction of large pressure vessels. The composition of UNS K31835, listed in Table 3.2, is identical for all three ASME specifications. UNS K31835 steel is a vanadium-modified 2.25Cr-1Mo steel and is extensively used in the fossil and petroleum industries. In addition to vanadium, the alloy also contains small amount of other elements such as boron, titanium, etc. as indicated in Table 3.2. Conventional 2.25Cr-1Mo steel (without vanadium addition) is the primary reactor pressure vessel candidate for the Japanese HTTR reactor, which operates at nominal temperature range of 400-440°C [Tachibana 2005].

Addition of vanadium offers increased tensile and creep rupture strengths, and increases hardenability when compared to conventional 2.25Cr-1Mo steel [ASM 1990]. In addition, vanadium also improves resistance to hydrogen attack, which is an important attribute for hydrogen reactors/petrochemical industries. The microstructure of 2.25Cr-1Mo-0.25V steel is typically bainitic, which offers better short-term creep resistance compared to ferrite-pearlite microstructures [ASM 1990]. For long life service, creep strength is offered by the presence of various fine carbides of chromium, vanadium, molybdenum, etc. The stability of carbides increases in the following order of alloying elements: Cr, Mo, V, and Nb. The hardening (implies secondary hardening) produced by these carbides increases with an increase in tempering temperature. Furthermore, low-chromium-vanadium modified steels such as 2.25Cr-1Mo-0.25V offer the fabricability and toughness of bainitic microstructures without special precautions that are needed for welding and heat treating high-chromium martensitic materials (e.g. 9cr or 12Cr steels [Imgram et al. 1990]. During heat treatment of thick sections (>300 mm), the objective is to avoid the formation of proeutectoid ferrite, which affects hardenability. Achievement of fully bainitic microstructures through the thickness is facilitated by the addition of small amounts of boron [Ishiguro et al. 1982, Klueh and Swindeman 1986]. As per the ASME code [ASME 2004], all three grades of 2.25Cr-1Mo-0.25V steels are to be used in the normalized (at a minimum temperature of 899°C) and tempered (at a minimum temperature of 677°C) condition.

3.1.2.1 Mechanical Properties

Several studies [Ishiguro et al. 1982, Klueh and Swindeman 1986, Imgram et al. 1990, Prager 1998, Hucinska 2003, Tsuchida et al. 2004] have been performed on evaluating the mechanical properties and thermal stability of 2.25Cr-1Mo-0.25V steels. The study of Imgram et al [1990] contains an exhaustive database on tensile and creep results on several heats obtained from different forging manufacturers. The vanadium content in different heats was in a range of 0.25-0.35 wt.%. The different heats of the alloy were in the form of 50.8-mm-thick plates, which were austenitized, air cooled, and tempered. The specimens for tensile testing were slowly cooled after tempering to simulate post-weld heat treatment of heavy wall vessel construction. Using ASME procedures, ratio trend curves for yield and tensile properties were established and are shown in Figure 3.5. The yield or tensile ratio is the ratio of yield or tensile strength at a given temperature to those at room temperature.

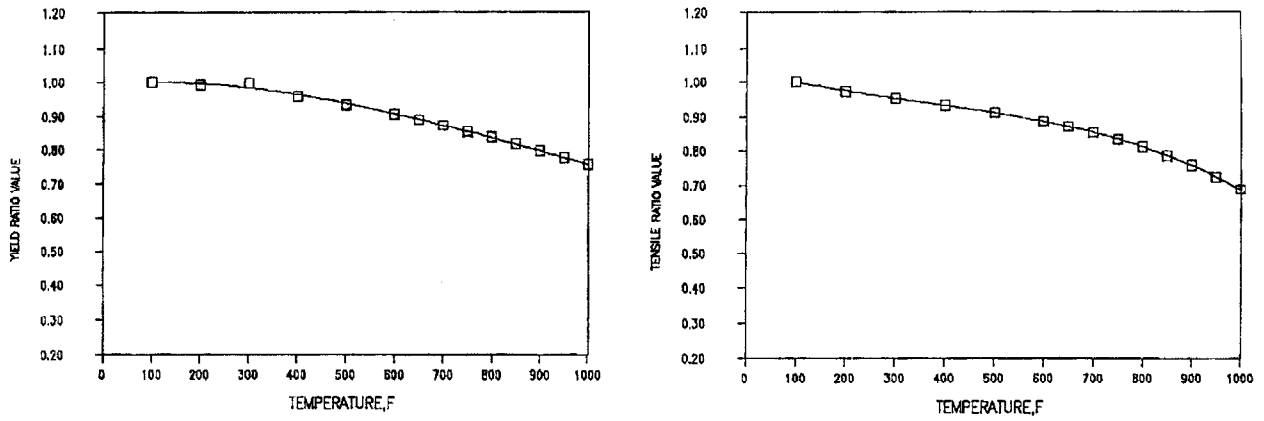

(a) (b)

Figure 3.5. Ratio trend curves of YS and UTS ratio as a function of temperature (a) YS and (b) UTS [Imgram et al. 1990].

Ishiguro et al. [1982] evaluated the mechanical properties of several 2.25Cr-1Mo steels with varying amounts of V, B, and Ti. Table 3.6 summarizes the results of room temperature tensile and Charpy impact toughness properties of VB6 heat of 2.25Cr-1Mo-V steel at different simulated plate thicknesses that is obtained by a programmed cooling after austenitization. The chemical composition of the VB6 heat is 2.3Cr-0.97Mo-0.21V-0.0022B-0.022Ti with minor alloying additions of Si, Mn, Ni, Al, P, S, N and trace elements As, Sb, and Sn. It can be seen that the tensile properties remain the same for all the thicknesses while the fracture appearance transition temperature (FATT) slightly increased over the range of plate thickness. Table 3.7 shows the effect of austenitizing temperature on the tensile and impact properties for a simulated 200-mm thick plate. As evident from the table, a higher austenitizing temperature results in higher yield and tensile strengths and higher impact transition temperature. At higher austenitizing temperature, a larger amount of vanadium in solution available for subsequent precipitation results in higher strength. Figure 3.6a shows a comparison of elevated temperature tensile properties of VB6 steel with those for the conventional 2.25Cr-1Mo steel. As evident in the figure, the VB6 steel has significantly higher yield and tensile strengths compared to the conventional 2.25Cr-1Mo steel from room temperature to 650°C. The VB6 heat, in this case, was a 50 mm thick plate austenitized at 950°C for 5 h followed by programmed cooling to simulate the quarter thickness location of a 200-mm thick water quenched plates, and subsequently tempered at 690°C for 2 h. The conventional 2.25Cr-1Mo

steel received the same heat treatment to that of VB6. In contrast to the above result, Klueh and Swindeman [1986] observed that a V-Ti-B modified 2.25Cr-1Mo steel had lower tensile strength than a conventional 2.25Cr-1Mo steel as illustrated in Fig. 3.6b. The difference in the tensile behavior of the conventional 2.25Cr-1Mo steel in these two studies [Ishiguro et al. 1982, Klueh and Swindeman 1986] is attributed to differences in microstructures, bainite+polygonal ferrite in Ishiguro et al. study and fully bainitic in the work of Klueh and Swindeman. Even in the fully bainitic microstructure, there was some evidence of lath structure with precipitates present on lath boundaries.

Table 3.6. Summary of tensile and impact test results for Heat VB6 simulating 100- to 400-mm thick, water quenched and tempered plates [Ishiguro et al. 1982].

Thickness (mm)	0.2% Proof stress (MPa)	Ultimate tensile strength (MPa)	Elongation (%)	Reduction of area (%)	FATT (°C)
100	529	625	26.5	80.4	-31
200	524	616	26.1	80.0	-17
300	535	622	25.4	80.2	-14
400	520	617	26.5	82.3	-7

Table 3.7. Effect of austenitizing temperature on tensile and impact properties for VB6 heat simulating 200-mm thick water quenched and tempered plates [Ishiguro et al. 1982].

Austenizing temperature (°C)	0.2% Proof stress (MPa)	Ultimate tensile strength (MPa)	Elongation (%)	Reduction of area (%)	FATT (°C)
920	490	589	25.8	80.1	-20
950	524	616	26.1	80.0	-17
980	557	637	24.7	78.3	-6

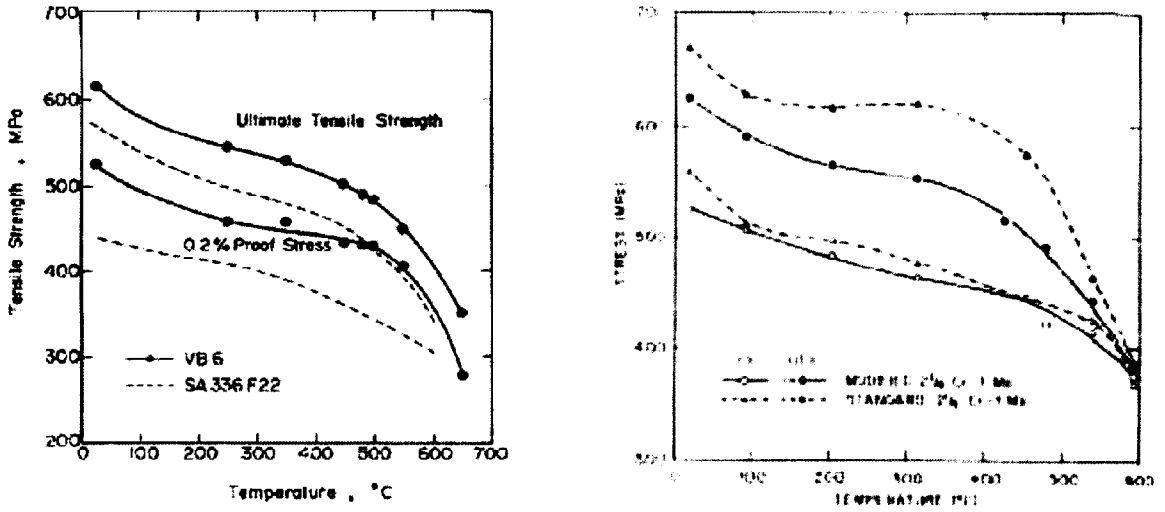

(a) (b)

Figure 3.6. Comparison of tensile properties of vanadium-modified 2.25Cr-1Mo (VB6) steel with conventional 2.25Cr-1Mo steel (SA336-Grade F22). [Ishiguro et al. 1982, Klueh and Swindeman 1986]].

The creep behavior of conventional 2.25Cr-1Mo steel was lower than the bainitic vanadium modified 2.25Cr-1Mo steel in studies by both Ishiguro et al [1982] and Klueh and Swindeman [1986]. Figure 3.7(a-b) shows the respective stress vs. life curves. Figure 3.7b indicates that except at high stress low life region, creep resistance of the modified steel is better than the conventional steel in the temperature range 482-538°C. Figure 3.8 shows the scatter band in creep data of conventional steel vs. modified steels plotted as rupture strength vs. Larson Miller Parameter, clearly indicating the superior creep properties of the modified steel. The superior creep strength was attributed to the higher room temperature strength and precipitation of fine carbides of vanadium and titanium [Ishiguro et al. 1982]. Higher creep strength in the modified steel due to precipitation of fine carbides (of vanadium and titanium) with a high dislocation density was also confirmed by Klueh and Swindeman [1986] using TEM observations.

The creep rupture behavior of 2.25Cr-1Mo-0.25V steel from different heats produced by various forging manufacturers is shown in Figure 3.9 [Imgram et al. 1990]. All five heats were furnished as 50.8 mm thick plate, austenitized by the manufacturers, air cooled and tempered. The final microstructure was bainitic in all heats. As evident in the figure and understandably so, the creep strength is higher at lower temperatures. The Larson-Miller Parameter curve for the steel is shown in Figure 3.10 [Prager 1998]. Figure 3.11 shows a comparison of the creep strength of vanadium modified 2.25Cr-1Mo steel with a high chromium modified 9Cr-1Mo steel [Tsuchida et al. 2004]. The heat treatment of the vanadium modified 2.25Cr-1Mo steel consisted of austenitization at 980°C, tempering at 730°C for 5h, which was followed by a simulated post-weld heat treatment at 705°C for either 6 or 30 h. The microstructure was tempered bainite with V, Mo and Cr precipitates in the matrix and some evidence of lath structure having globular M_7C_3 precipitates along grain and lath boundaries. As evident in the figure, the creep strength of this steel is comparable to modified 9Cr-1Mo up to ≈500 h in the temperature range of 450-600°C, but decreases at longer rupture life.

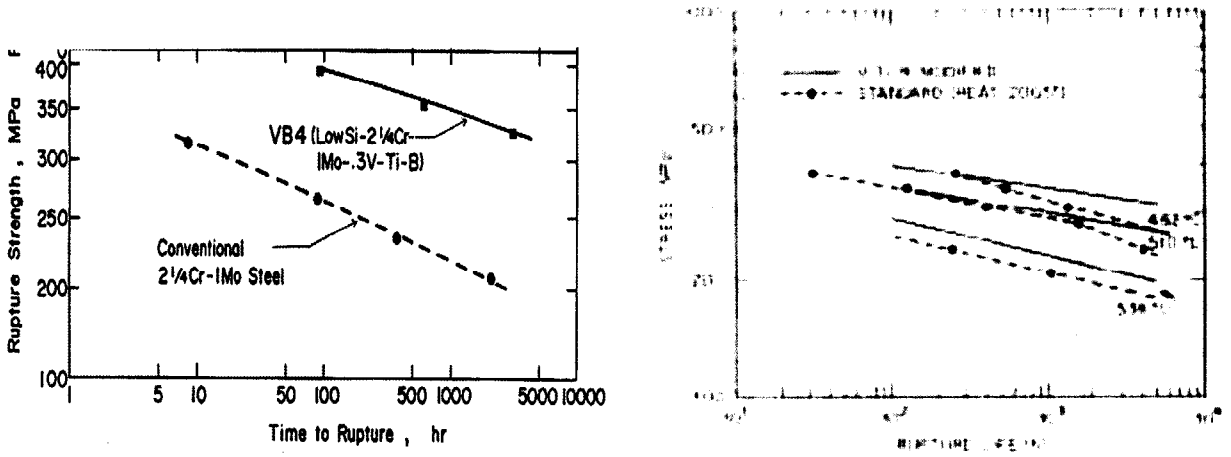

(a) (b)

Figure 3.7. Comparison of creep rupture behavior of conventional vs. vanadium modified 2.25Cr-1Mo steel from two studies. (a) Ishiguro et al [1982] and (b) Klueh and Swindeman [1986].

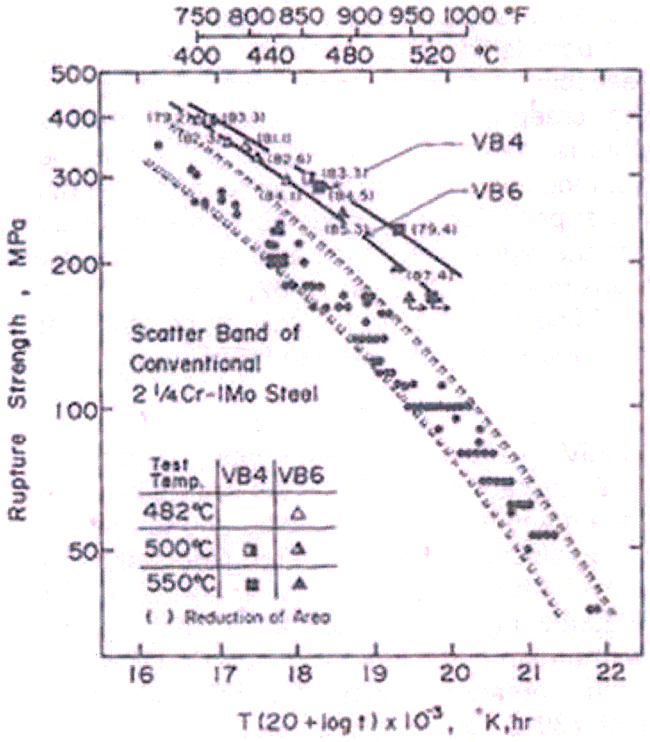

Figure 3.8. Creep rupture response of standard 2.25Cr-1Mo steel and modified 2.25Cr-1Mo-V steel [Ishiguro et al. 1982].

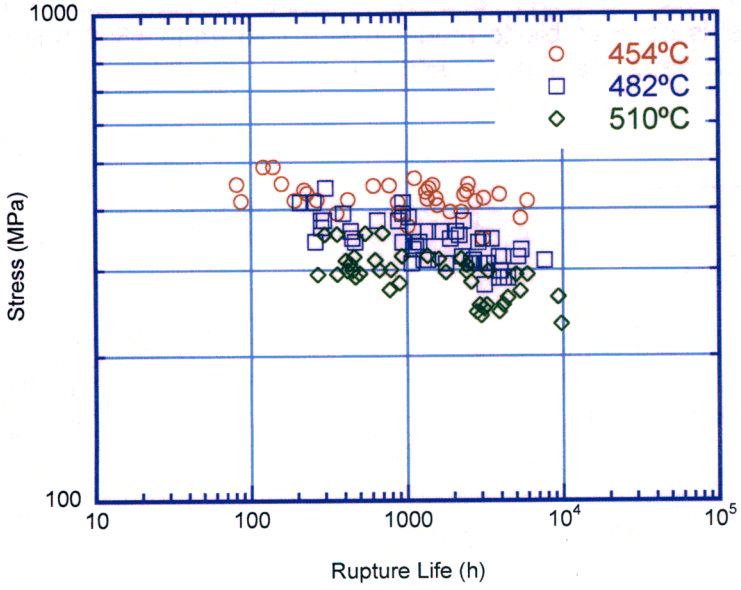

Figure 3.9. Creep rupture behavior of 2.25Cr-1Mo-0.25V steel at different temperatures. [Imgram et al. 1990].

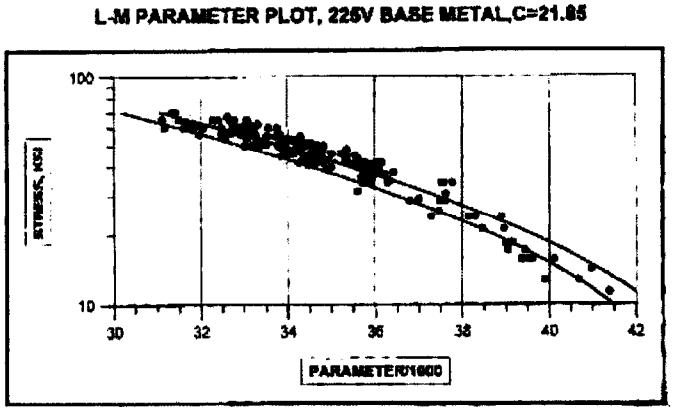

Figure 3.10. Larson-Miller Parameter plot for alloy 22V [Prager 1998]

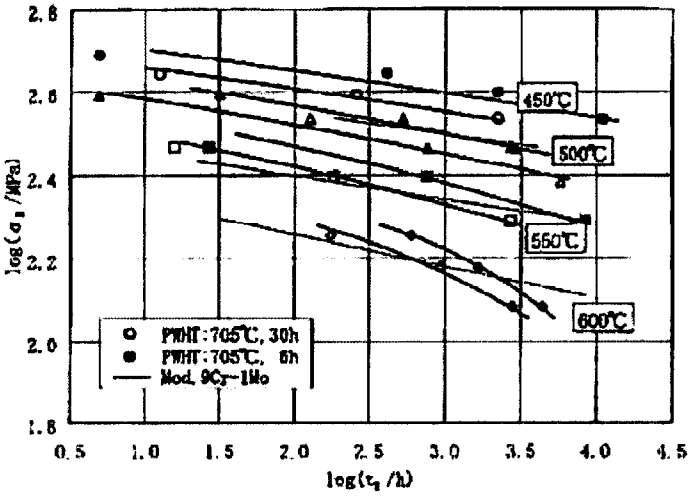

Figure 3.11. Comparison of creep data of 2.2.5Cr-1Mo-V steel with modified 9Cr-1Mo steel. [Tsuchida et al. 2004].

3.1.2.2 Thermal Aging Effects on Mechanical Properties

Long term operation of reactor structural components like pressure vessels could cause a significant change in the material microstructure and may alter the mechanical performance due to thermal aging of the component. Temper embrittlement or temper aging embrittlement is a time and temperature dependent process that could occur due to thermal aging, thereby affecting component performance. The thermal stability of 2.25Cr-1Mo-0.25V steels has been evaluated by an isothermal exposure and by a step cooling method [Ishiguro et al 1982, Prager 1998]. The step cooling method is an accelerated aging technique to characterize thermal aging response and should be cautiously used in design.

Table 3.8 shows the transition temperature and its shift at an absorbed energy of 40 ft-lb for different heats (BM1, BM2 and BM4) of 2.25Cr-1Mo-0.25V and for a conventional 2.25Cr-1Mo steel (BM3). BM2 had a high phosphorus content (0.018 wt.%) and also contained small amounts of Sb, Sn and As. BM1 and BM4 had lower phosphorus contents and did not contain Sb, Sn or As. It is clear from the table that the modified steel with higher purity has lower impact properties before exposure and shows good toughness retention after thermal aging. BM2 has poor impact properties probably due to the presence of high concentration of phosphorus and other impurities. The results of the accelerated aging study by Ishiguro et al [1982] are shown in

Table 3.9. All three heats VB6, VB7 and VB8 had impurities P, Sn, Sb, and As, with the highest levels in VB8 and the lowest in VB6. As seen in Table 3.8, all three heats showed very little change in transition temperature after the step cooling. This is in contrast to the results in Table 3.8 [Prager 1998], which indicated poor impact properties for the steel with higher impurities. Ishiguro et al [1982] attributed the low susceptibility to temper embrittlement, partly to the low Si content and partly to the presence of Ti and B. Although B and Ti were present in all the heats evaluated by Prager [1998], the Si contents were higher (0.07-0.11%) compared to a Si content of 0.02% in all the heats studied by Ishiguro et al [1982]. Furthermore, Prager [1998] studied the thermal aging behavior by a step cooling method and indicated that it was not a good method for such characterization. Clearly, more studies are needed to establish the effect of Si, Ti, B, V, and other impurities on thermal aging and resulting temper embrittlement of 2.25Cr-1Mo-0.25V steels.

Table 3.8. Charpy impact 40 ft-lb temperature after isothermal exposure at 482°C [Prager 1998]

Steel	Chemical composition	Isothermal exposure time at 482°C (900°F)								
		5000 h			10000 h			30000 h		
		Tr_{40} (°C)	ΔTr_{40} (°C)	Tr_{40} $+2\Delta Tr_{40}$ (°C)	Tr_{40} (°C)	ΔTr_{40} (°C)	Tr_{40} $+2\Delta Tr_{40}$ (°C)	Tr_{40} (°C)	ΔTr_{40} (°C)	Tr_{40} $+2\Delta Tr_{40}$ (°C)
BM1	V mod. -low. P	-60	-5	-70	-57	-2	-61	-55	0	-55
BM2	V mod. -high. P	54	47	148	56	58	181	75	68	211
BM4	V mod. -med. P	-31	-4	-39	-26	1	-24	-24	3	-18
BM3	Conventional	-37	-1	-39	-34	2	-30	-31	5	-21

Table 3.9. Charpy impact transition temperatures before and after step cooling method [Ishiguro et al. 1982]

Sample No.	FATT[a] (°C)		Tr_{40}[b](°C)		Absorbed energy[c] (J)	
	Before	After	Before	After	Before	After
VB6	-17	-23	-30	-36	274	272
VB7	+2	+5	-13	-18	274	272
VB8	+2	+10	-8	-4	269	269

[a]Transition temperature at shear fracture of 50 percent.
[a]Transition temperature at absorbed energy of 40 ft·lb.
[a]Absorbed energy at upper shelf temperature.

Very recently, Kim et al [2006] studied the susceptibility to temper embrittlement of 2.25Cr-1Mo and 2.25Cr-1Mo-0.25V steel (V=0.29wt.%) forgings of size 400 mm thick and 2.3 m inner diameter. In the vanadium modified steel, P= 0.006 wt.% while in the standard steel, P≈0.007 wt. %. Both the steels were subjected to a simulated post-weld heat treatment at 650-700°C. Both the steels had a tempered bainite structure. Charpy V-notch 54 J transition temperature (vTr_{54}) and 50% shear fracture appearance transition temperature ($FATT_{50}$) were measured as a function of aging time up to a maximum of 50000 h. The aging temperatures ranged from 430°C to 515°C. Fig. 3.12 shows the variation of FATT and vTR_{54} with aging time at two different temperatures. It is evident from the figure that at both aging temperatures, the vanadium-modified steel has better resistance to temper embrittlement than the standard

2.25Cr-1Mo steel. This result also reinforces Prager's [1998] result (Table 3.8) that low-P in steel reduces susceptibility to temper embrittlement.

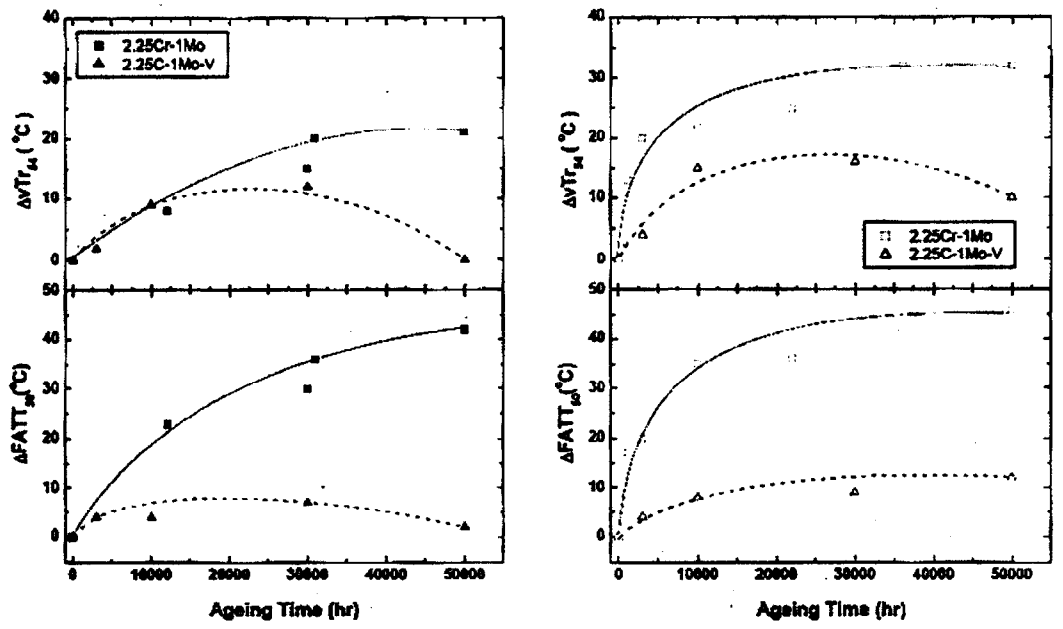

a) 454 °C b) 515 °C

Figure 3.12 Average shift of fracture appearance transition temperature ($FATT_{50}$) and 54J transition temperature (vTr54) by isothermal aging for 50000 h of 2.25Cr-1Mo and 2.25Cr-1Mo-0.25V steels.

3.1.2.3 ASME Code Allowables

Conventional 2.25Cr-1Mo steel (without vanadium addition) is code approved under Section III of the ASME code for use up to 593°C service. On the other hand, 2.25Cr-1Mo-0.25V steel (UNS K31835) is approved only under Section VIII of the ASME Code for temperatures up to 482°C. Additional mechanical property data, especially in the areas of thermal aging, creep-fatigue, helium interactions, including thick-section properties of the 2.25Cr-1Mo-0.25Vsteel are needed for inclusion in Section III of the ASME code.

3.1.3 Fe-9 Cr-1Mo-V Steel (UNS K90901)

UNS K90901 is ferritic steel having a nominal composition of Fe-9Cr-1Mo-V. Forgings of this steel are allowed for use in pressure vessel components under ASME specifications SA-336 (Grade F91) and SA-182 (Grade F91), of which SA-336 is the standard for construction of large pressure vessels. The elemental composition of the UNS K90901 steel is given in Table 3.2 and is identical for both SA-182 and SA-336 specifications. The 9Cr-1Mo-V steel (also called modified 9Cr-1Mo steel) is the primary/potential reactor pressure vessel candidate in several Generation IV high temperature reactor programs, *viz.,* CEA (France) and EU program, Korean RPV concept, and AREVA's hot vessel concept.

The 9Cr-1Mo-V steel is a modified alloy of conventional 9Cr-1Mo ferritic steel developed at Oak Ridge National Laboratory [Sikka et al. 1981]. It shows a remarkable increase in stress rupture strength, achieved by addition of small amounts of vanadium, niobium, and nitrogen.

This alloy is much more resistant to thermal fatigue than austenitic stainless steels because of its lower thermal expansion coefficient (at least 30% lower) and higher thermal conductivity. This alloy provides good mechanical properties at elevated temperature when produced and heat treated to form the proper microstructure. As per the ASME Code [ASME Code 1991], UNS K90901 steel is to be used in the normalized (in the temperature range of 1038-1149°C) and tempered (at a minimum temperature of 732°C) condition. The microstructure is typically 100% tempered martensite but sometimes a small amount of δ-ferrite can be formed depending on the tempering temperature [Orr and Woolard 1997, Klueh 2005]. The dominant precipitate in the microstructure is vanadium-rich $M_{23}C_6$ particles (M indicates metal) along the prior austenite grain boundaries and on lath boundaries. In addition, fine MX precipitates of V and Nb (VN, NbC, etc) of size 100 nm or less are present. The 9Cr-1Mo-V steel derives its strength primarily from solid solution strengthening with the V- and Nb-containing precipitates contributing to both high temperature strength and creep resistance.

3.1.3.1 Mechanical Properties

Heat treatment of the modified 9Cr-1Mo steel is critical to produce the desired microstructure and mechanical properties. For this steel, a normalization treatment (air cooling) is sufficient to produce a fully martensitic structure. However, the normalization temperature can have an effect on the tensile and creep-rupture properties of the steel [Totemeier et al 2006]. Figure 3.13 shows the effect of normalization temperature on the room-temperature strength and hardness of modified 9Cr-1Mo steel. It is evident that a normalization temperature below 925°C has a significant effect on the strength and hardness whereas between 925-1050°C, the properties are relatively constant. The difference in properties is attributed to difference in microstructure after normalization: While the microstructure consisted of low dislocation density polygonized ferrite at normalization temperatures below 900°C, it was entirely martensitic above 900°C. It should however, be noted that the observed tensile and hardness properties at all normalization temperatures were above the minimum requirements specified by ASME for Grade 91 steel.

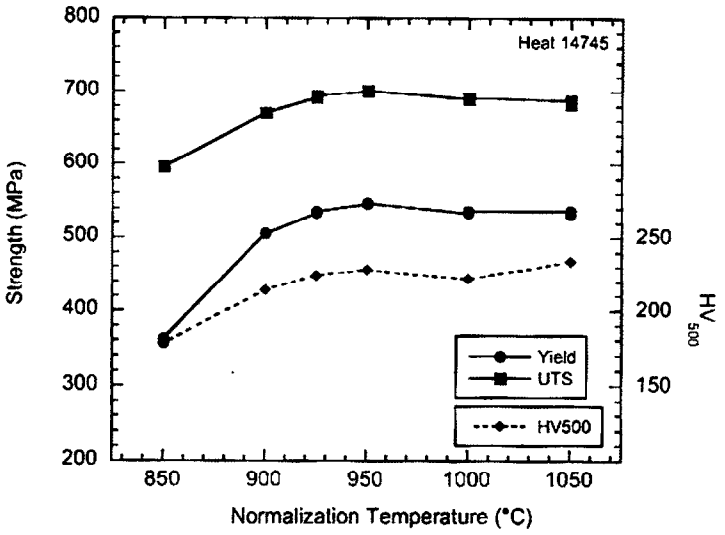

Figure 3.13. Effect of normalization temperature on the room-temperature mechanical properties of modified 9Cr-1Mo steel [Totemeier et al. 2006]

The creep rupture strength was lower at a normalization temperature of 925°C than at 1050°C. This reduction in rupture strength was more pronounced for higher test temperatures and lower stresses as shown in Fig. 3.14a. The corresponding variation of minimum creep rate

with stress is shown in Fig. 3.14b. Furthermore, at a test temperature of 600°C and an applied stress of 145 MPa, the creep-rupture strength continuously decreased with decreasing temperature. The rate of decrease was larger when the normalization temperature was less than 950°C. The reduction in creep strength is attributed to the presence of ferrite at normalization temperatures of 850-900°C, and to subtle changes in MX precipitates resulting from coarsening and incomplete dissolution during normalization between 925-1050°C. The creep rupture lives of specimens normalized at temperatures less than 925°C fell below the ASME minimum curve for Grade 91 steel.

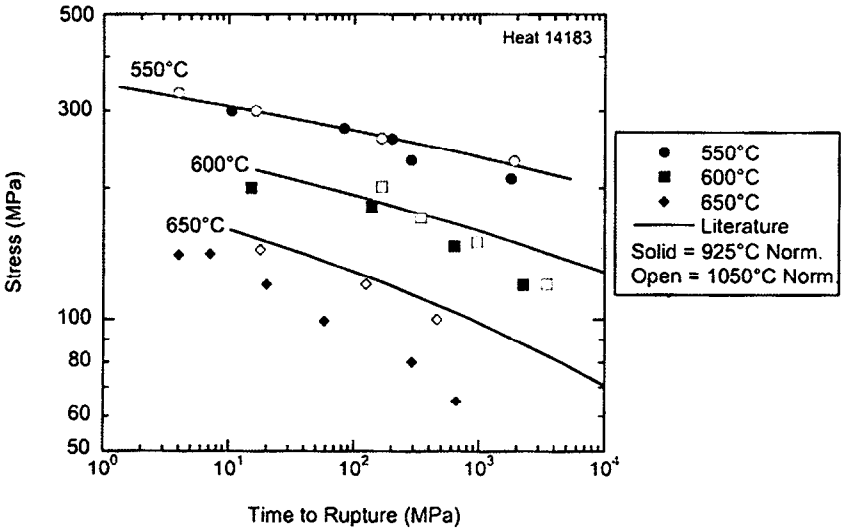

(a)

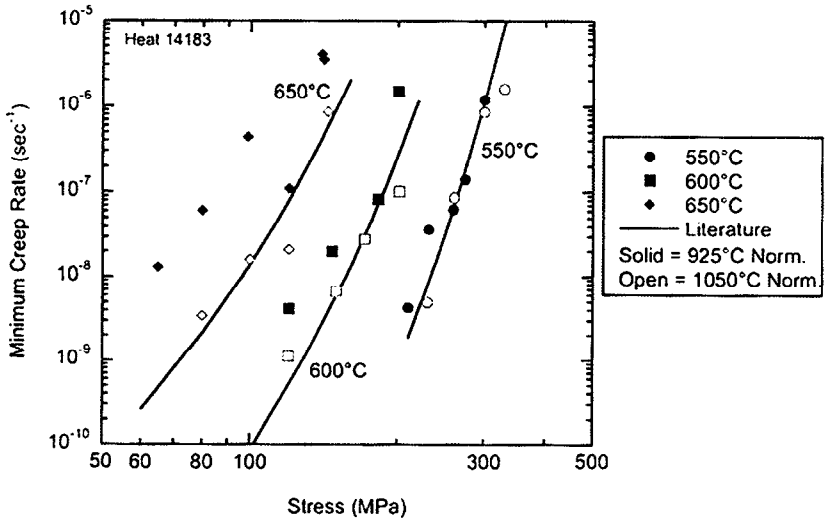

(b)

Fig, 3.14 Creep rupture behavior of modified 9Cr-1Mo steel normalized at 925 and 1050°C. Literature data is from [Sikka et al, 1983] (a) Stress vs. Rupture Life (b) Stress dependence of creep rate

Extensive studies have been conducted on a nominally Fe-9Cr-1Mo class of ferritic steels to evaluate their tensile, creep rupture, and low-cycle fatigue properties [Sikka et al. 1981, Brinkman et al. 1990, Swindeman et al. 1998]. Long-term aging effects on the mechanical properties have been determined for these steels (Swindeman et al. 1998, Swindeman et al.

2000, Klueh and Harris 2001). Fig. 3.15 shows the creep rupture behavior of modified 9Cr-1Mo steel in the range of 550–650°C at 25°C intervals [Sklenicka 1994]. The creep deformation characteristics may be described by the Norton equation with two values of Norton's stress exponent *n* with values around 17 at 550°C and around 10 at 650°C. Figure 3.16 shows the stress dependence of P91 (P indicates piping) steel along with other variants of the 9Cr-1Mo steel at 600 and 650°C [Ennis and Czyrska-Filemonowicz 2002]. In the high stress region, the difference in the secondary creep rates of the three steels is relatively small, whereas the difference between the steels becomes more pronounced in the low stress region. At high stresses, the value of n is around 16 whereas at low stress it is 6. A varying stress dependence of minimum creep rate was also observed in a recent study [Anderson et al. 2003], in which the value of n was 22 at high stresses and ≈4 at low stresses. The change in the value of n indicates a change in the creep characteristics brought about by a change in the operating creep mechanisms. Kloc et al. [1998] conducted creep tests at very low stresses (<10 MPa) in addition to high stress tests. The observed behavior is illustrated in Fig. 3.17, i.e., a value of n = 1 at very low stress and a higher value at higher stresses. Again, the change in n is attributed to different creep mechanisms. A comprehensive review on modified 9Cr-1Mo steel and other advanced ferritic-martensitic steels and their structure-property relationships can be found in the paper by Klueh [2005].

Figure 3.18 shows the creep rupture behavior of modified 9Cr-1Mo steel, tested in the Korean RPV program [Ryu 2005]. Creep rupture strength of 130MPa at 600°C and 100000 hr was observed. In the figure, N00 indicates 0 wt.% N in steel, N10 indicates 0.1 wt.% N, etc [Ryu 2006]. The 100000 hr creep rupture strength of 130MPa at 600°C was observed for a steel having 0.08% N. The creep strength increases with increasing N content up to 0.8 wt.% and then decreases. The optimum creep strength at 0.8%N is attributed to minimum lath width and also the precipitation of fine Cr_2X precipitates [Kim et al. 2004]. At 0.10%N steel, reduction in creep strength was attributed to the coarsening of Cr_2X precipitates.

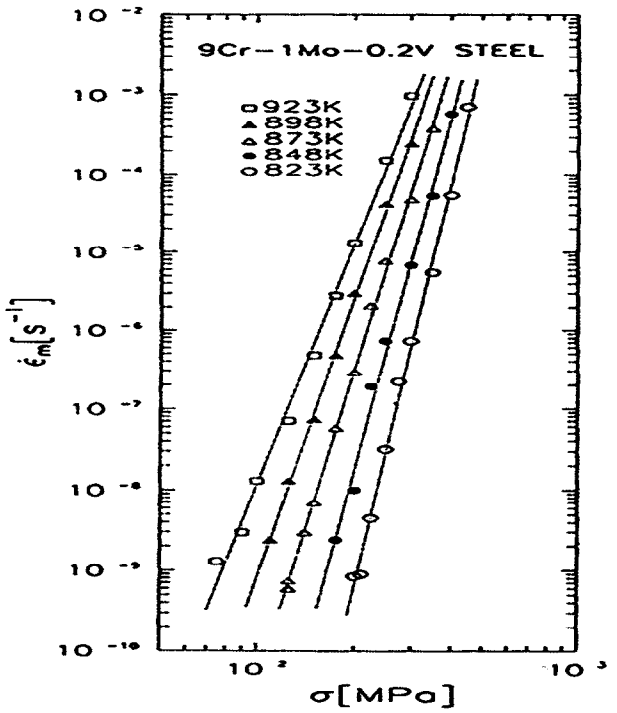

Figure 3.15. Stress dependence of minimum creep rate of modified 9Cr-1Mo steel [Sklenicka, 1994].

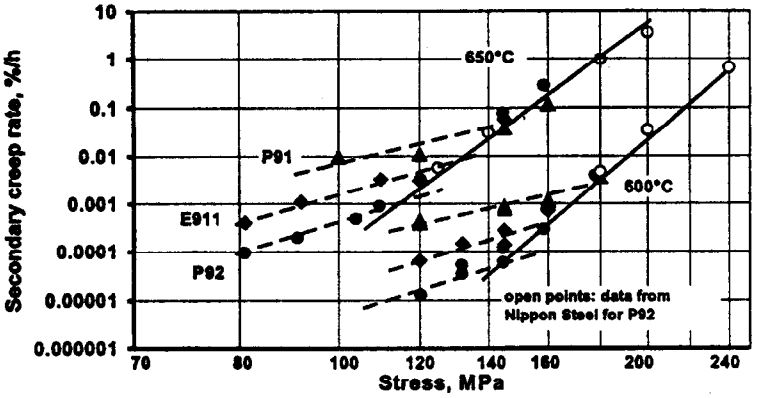

Figure 3.16. Secondary creep rates for P91, P92, and E911 [Ennis and Czyrska-Filemonowicz 2002].

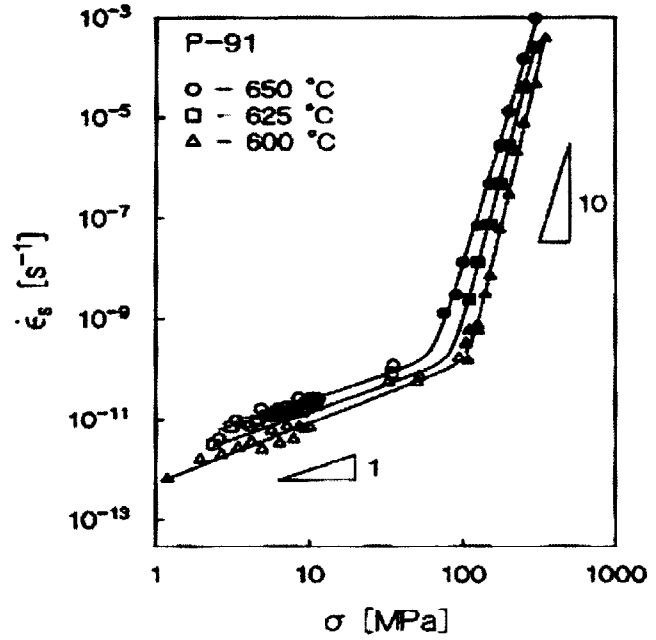

Figure 3.17. Stress dependence of creep rate of P91 steel at very low and higher stresses [Kloc et al. 1998]

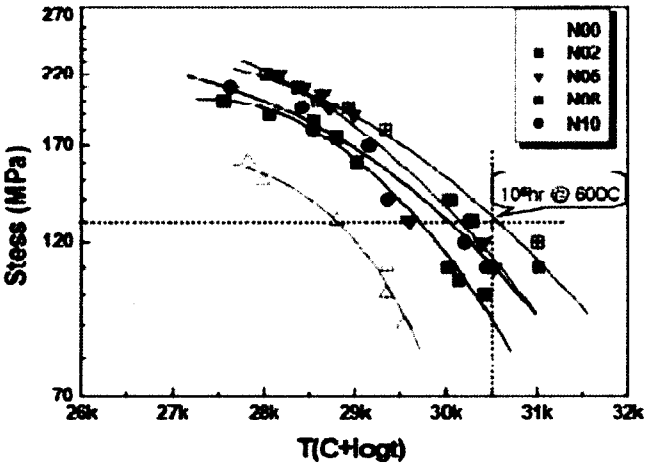

Figure 3.18. Creep response of modified 9Cr-1Mo steel [Ryu 2005].

Low-cycle fatigue and creep-fatigue behavior of modified 9Cr-1Mo steel has been evaluated in several studies [Hoffman 1982, Jones 1983, and Ebi and McEvily 1984, Mannan and Valsan 2004, 2006, Mannan et al. 2005, and Nagesha et al. 2005]. The cyclic stress-strain curves at 50% of the number of cycles to failure are shown in Fig. 3.19 [Ebi and McEvily 1984]. The results indicate a higher cyclic strength for the hot-rolled material compared with that for the hot-forged material. Also included in Fig. 3.19 are correlations that relate cyclic stress and cyclic strain. Ebi and McEvily [1984] also measured fatigue crack propagation rate as a function of crack length by measuring the fatigue striation spacing on the failed test specimens. They concluded that the crack propagation rate was similar for both the hot-rolled and hot-forged materials when tested in air (see Fig. 3.20). But they reported that the crack growth rates were lower in vacuum than in air for the hot-rolled material.

Mannan and Valsan [2004, 2006] and Mannan et al. [2005] evaluated the effect of strain rate, dynamic strain aging, and test temperature on low cycle fatigue, and hold-time effect on creep-fatigue behavior of modified 9Cr-1Mo steel. They performed tests on normalized and tempered 25-mm-gage length, 10 mm gage diameter specimens machined from hot-forged and heat-treated 70 mm diameter rods. The cyclic stress-strain response showed brief hardening for the first few cycles followed by a gradual and a continuous softening regime. Hardening was attributed to dynamic strain aging effects while softening was attributed to coarsening of precipitates. Fig. 3.21 shows the effect of test temperature at a given strain rate on the low-cycle fatigue behavior. As evident in the figure, the effect of temperature was more pronounced at lower strain amplitudes (±0.25%). The decrease in fatigue life with increase in temperature was attributed to the combined effects of oxidation and dynamic strain aging [Mannan and Valsan 2006]. Failure at 600°C was strongly influenced by oxidation, especially at the lower strain amplitudes. Fig. 3.22 shows the variation of fatigue life with strain rate at different temperatures. At strain rates $<3 \times 10^{-3}$/s, fatigue life reduction was attributed to oxidation at 550 and 600°C while at 500°C, it was due to oxidation and dynamic strain aging. Under conditions of low temperatures and high strain rates, oxidation effects were not significant.

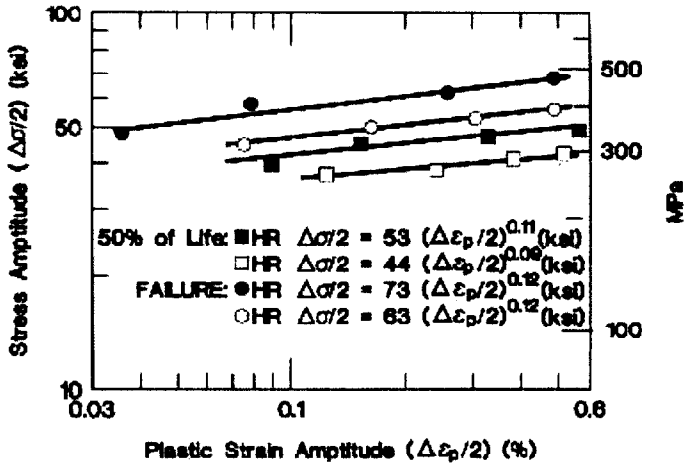

Figure 3.19. Cyclic stress-strain properties of hot-rolled and forged materials of modified 9Cr-1Mo steel [Ebi and McEvily 1984].

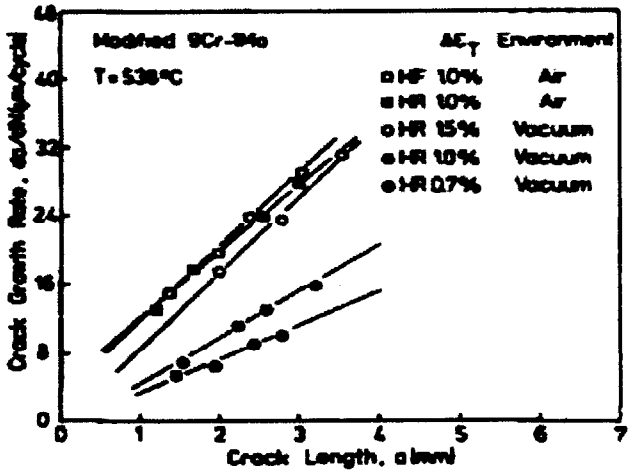

Figure 3.20. Fatigue crack propagation rate as a function of crack length for modified 9Cr-1Mo steel [Ebi and McEvily 1984].

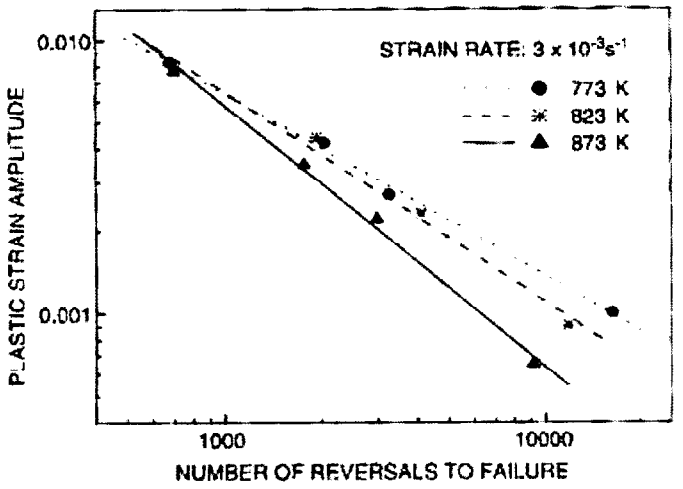

Figure 3.21. Low cycle fatigue life of modified 9Cr-1Mo steel in air at various test temperatures [Mannan et al. 2005]

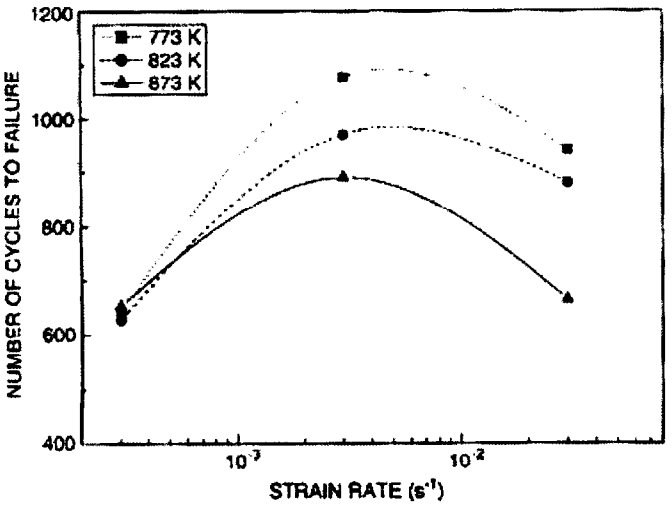

Figure 3.22. Effect of strain rate on the low cycle fatigue behavior of modified 9Cr-1Mo steel in air [Mannan et al. 2005]

Creep-fatigue interaction tests were conducted [Mannan et al 2005, Nagesha et al. 2005] by introducing tensile hold times in the range 1-30 min at test temperatures of 550 and 600°C. Fig. 3.23 shows the effect of hold-time on fatigue life at 600°C. The fatigue life decreases sharply with addition of hold time but appears to saturate after ≈30 minutes hold time. The reduction in fatigue life was attributed to oxidation occurring during fatigue. Furthermore, compression hold was observed to be more detrimental to fatigue life than tensile hold due to the oxide behavior (formation, cracking, spalling etc).

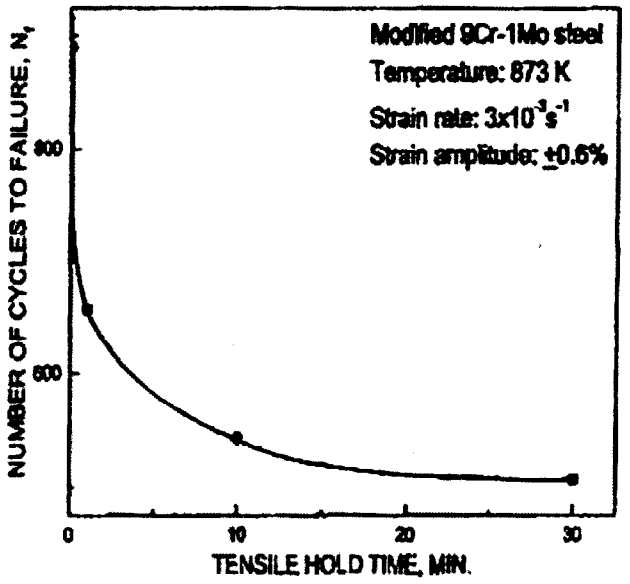

Figure 3.23. Effect of hold time on the fatigue life of modified 9Cr-1Mo steel in air at 600°C. [Mannan et al. 2005]

3.1.3.2 Thermal Aging Effects on Mechanical Properties

Figure 3.24 shows the ultimate tensile strength after long-time aging, which is compared to a trend curve for unexposed material. Plates aged for 75000 h were tested at the aging temperature. For aging at 482°C (900°F), little effect was noticed. If anything, a slight increase in strength was observed. The ultimate strength at 649°C (1200°F) was significantly below the trend curve for typical material.

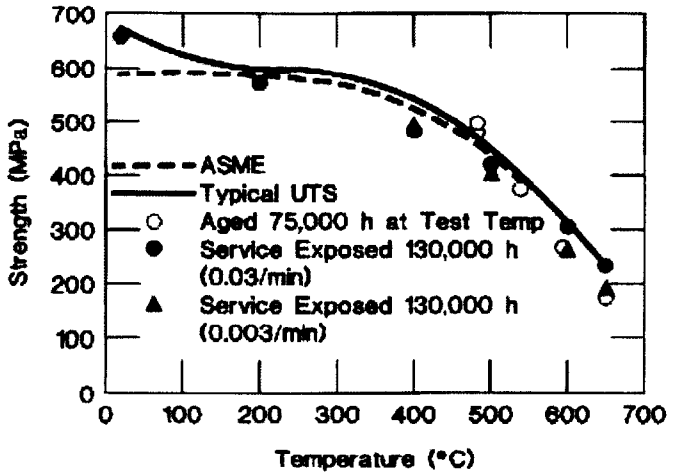

Figure 3.24. Comparison of ultimate tensile strength of unexposed Grade 91 with aged and service-exposed materials [Swindeman et al. 2000].

A more detailed analysis of the influence of aging time and temperature is reported elsewhere [Brinkman et al. 1990, Alexander et al. 1993]. The material exposed to service conditions for 130000 h was tested at several temperatures. It was reported that the strength fell below the trend curve for typical as-tempered material. At a comparable strain rate, the strength of the service-exposed material was similar to the aged material at 593 and 649°C (1100 and 1200°F).

The effect of long-term aging on the impact energy can be seen in Fig. 3.25, which shows that the upper shelf energy (USE) decreases with aging time [Sikka 1985]. Fig. 3.26 shows the effect of aging time and temperature on the ductile-brittle transition temperature (DBTT) and the USE. The figure indicates maximum worsening of impact properties at 500-550°C aging temperature. There is some recovery of impact properties at higher aging temperatures and/or at prolonged aging times as indicated in the figure. The recovery is attributed to local changes in microstructure and composition. Laves phase and other embrittling phases can form during tempering, thermal aging, and/or during creep testing [Klueh and Harris 2001]. Initial composition of the steel can also affect impact properties, e.g., steel with a lower Si content has a lower DBTT compared to higher Si steel. In short, the magnitude of embrittlement produced by thermal aging is dependent on steel composition and initial microstructure, aging temperature and time, and the induced microstructural and local compositional changes. Further details on the effect of thermal aging on the impact properties can be found elsewhere [Klueh and Harris, 2001].

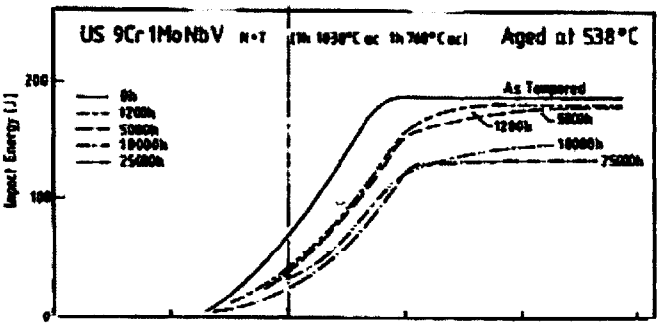

Figure 3.25. Effect of aging time on the impact energy of modified 9Cr-1Mo steel [Sikka, 1985].

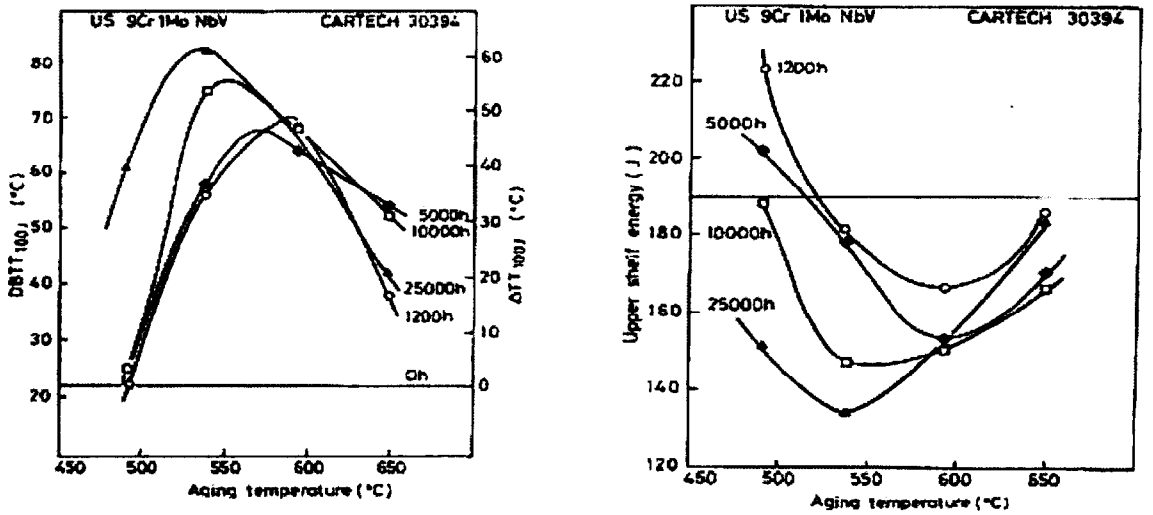

Figure 3.26. Effect of aging temperature and time on Charpy V-notch impact DBTT and USE of modified 9Cr-1Mo-V steel containing 0.4% Si [Sikka 1985, Wall 1987].

Creep curves for service-exposed and unexposed modified 9Cr-1Mo steel are shown in Fig. 3.27 for tests conducted at 600°C (1112°F) and 100 MPa (14.5 ksi). The service-exposed material exhibited a creep rate that was ten times greater than the unexposed steel. The unexposed material remained in the primary creep stage to beyond 15000 h. Creep curves for the service-exposed Grade 91 tested at different temperatures are shown in Fig. 3.28. At 100 MPa, the creep rates at 625 and 600°C (1157 and 1112°F) accelerate around 1% strain, whereas the creep rates at 575 and 550°C (1067 and 1022°F) showed no acceleration around 1% strain after 20000 h. The minimum creep rates at 100 MPa for three aging conditions are compared to the unexposed behavior in Fig. 3.29. These data are plotted against the reciprocal of absolute temperature, and the trend indicates activation energy as well as relative creep strength. The steeper slopes indicate higher activation energy. The lowest value for reciprocal temperature corresponds to the highest temperature of testing (700°C). With decreasing test temperature (increasing reciprocal temperature), data tended to diverge. The service-exposed material exhibited the highest creep rate, and the data for material aged 25000 h at 649°C mingled within the trend. Material aged 10000 h at 649°C exhibited lower creep rates, whereas the unexposed material exhibited the lowest rates.

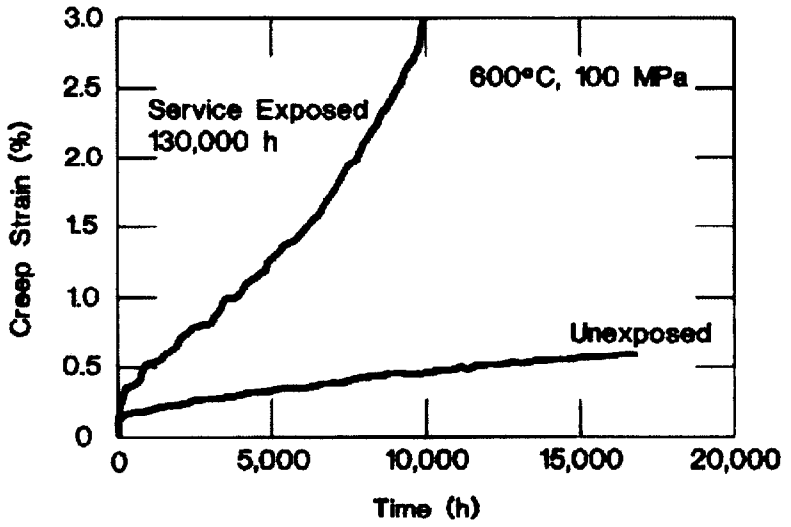

Figure 3.27. Comparison of creep curves for unexposed and service-exposed Grade 91 at 100 MPa [Swindeman et al. 2000].

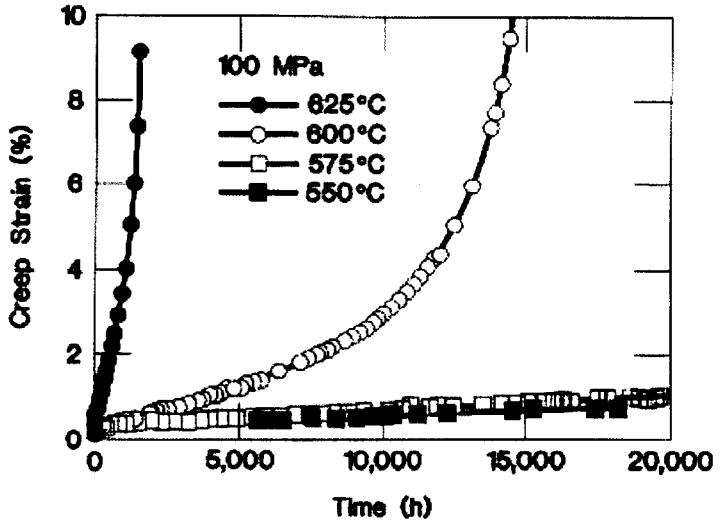

Figure 3.28. Creep curves for service-exposed Grade 91 at 100 MPa and several temperatures [Swindeman et al. 2000].

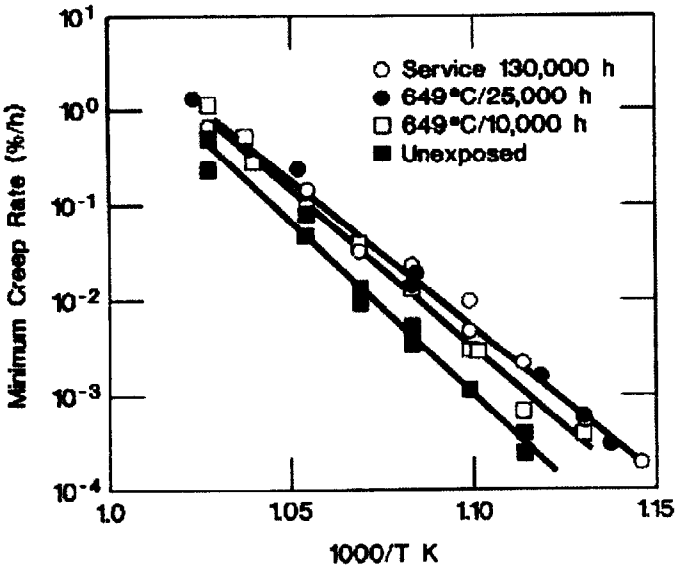

Figure 3.29. Comparison of isostress plots of minimum creep rate of Grade 91 for several material conditions at 100 MPa [Swindeman et al. 2000].

For a given temperature, the creep rates for all conditions varied by less than a factor of ten. The slopes of the lines drawn through the data indicated that the activation energy for creep of the service-exposed material was lower than that for the unexposed material. A plot of rupture life versus the reciprocal temperature for the 100 MPa isostress data is shown in Fig. 3.30. With the exception of one short-time test result on material aged 25000 h at 649°C, the aged and unexposed materials exhibited the same temperature dependence. The unexposed material had the longest life, and material aged 25000 h at 649°C had the shortest. The service-exposed material showed different temperature dependence. The slope of the line drawn through the data indicated lower activation energy for rupture than the unexposed material. The rupture lives for different conditions varied by less than a factor of ten at any temperature examined. The rupture life of the pressurized tube was included in the plot, and the point fell on the trend for the uniaxial tests.

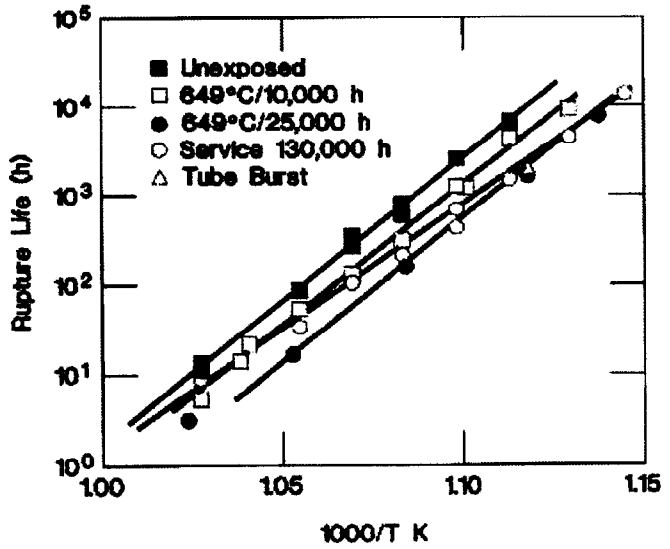

Figure 3.30. Comparison of isostress plots of rupture life for Grade 91 for several material conditions at 100 MPa [Swindeman et al. 2000].

Although the temperature dependence of the rupture life of service exposed material appeared to differ from that for the aged materials, the Monkman-Grant correlation for all conditions was similar. Data for several heats of unexposed material are compared to the aged and service-exposed materials in Fig. 3.31. All data follow the same trend. As is often the case, the trend for the long-time data was not as well defined as shorter time data. Rupture data for more than forty tests on aged and service-exposed materials are plotted in Fig. 3.32 as stress versus the Larson Miller parameter. A parametric constant of 30 was selected for the correlation. Included in the plot are rupture data for a large number of tests on unexposed material. Results clearly show that the rupture lives for the aged and service-exposed materials fell near the lower strength or shorter life side of the scatter band for the unexposed material. At the higher values of the Larson Miller parameter, the strength of the severely aged materials was reduced to about 80% of the average for the unexposed material. Changes in strength were attributed to coarsening of the metallurgical substructure of the tempered martensite in the material [Swindeman et al. 2000].

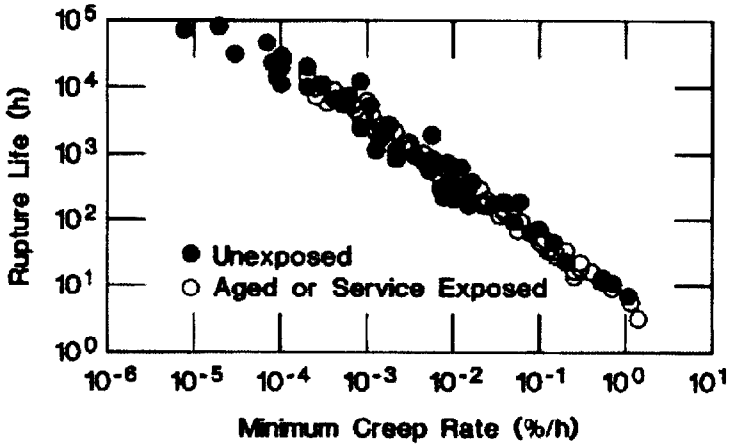

Figure 3.31. Monkman-Grant plot for unexposed, aged, and service-exposed Grade 91 steel [Swindeman et al. 2000].

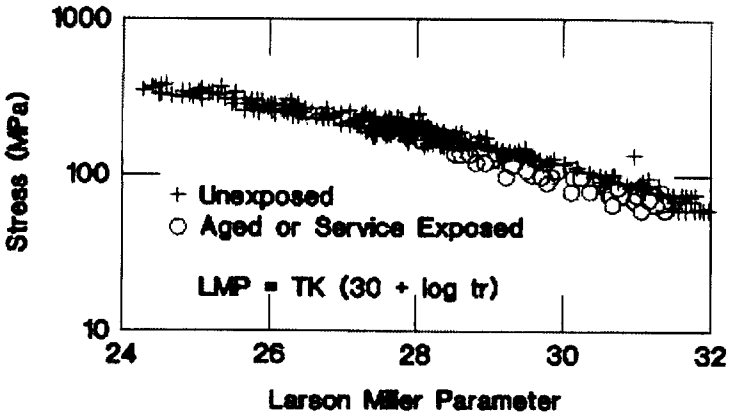

Figure 3.32. Stress versus Larson-Miller parameter for unexposed, aged, and service-exposed Grade 91 steel [Swindeman et al. 2000].

During service exposure for long times, the stress and temperature of a component does not always stay constant. The minimum creep rate is sensitive to changing temperature and stress during service exposure. Thermally induced softening over predicts the rupture life when extrapolating from high to low stress, and under estimates life when extrapolating from low to high stress [Swindeman et al. 2005]. Further details of this on-going study at ORNL to evaluate the behavior of modified 9Cr-1Mo at changing times and temperatures can be found elsewhere [Swindeman et al 2005].

3.1.3.3 Thick Section Properties

Knowledge of thick section properties is critical for the successful design RPV for the NGNP, whose wall thickness is expected to be between 100-300 mm depending on the design and material. Most of the studies of modified 9Cr-1Mo steel have been done on thin sections (thickness <100 mm). It is difficult to achieve uniform through-the-thickness microstructure in forgings of 200 mm or more. Therefore, assuming that a thick section will perform in the same manner as a thin section is non-conservative. Figure 3.28 shows the creep rupture strength versus Manson-Mendelson parameter of standard 9Cr-1Mo steel [Choudhary et al. 1999]. The average and the minimum solid lines in the graph correspond to thin sections while the data points correspond to data developed on 300 mm thick forgings. The curve shows data on both quenched and tempered and simulated post-weld heat treated specimens. It is clear from the figure that the thick section rupture strength is lower than the average creep data for thin sections (solid line). The reason for this is attributed to the coarseness of the subgrain structure. For the modified 9Cr-1Mo steel, a 10% reduction in creep strength was noted for thick sections compared to thin sections [Barlow et al. 1990]. Figure 3.29 shows the creep rupture strength of grade 91 steel on thick (>75mm) and thin (<75mm) plates [Kimura 2005]. As evident in the figure, no significant difference was observed between the thick and thin plates. Actual thickness information was not provided in that study. CEA, France has initiated a program to evaluate the thick section properties of the modified 9Cr-1Mo steel [Seran at al. 2004]. They have reported impact properties on 30mm thick plate and found a good correlation between Charpy impact and toughness (K1c) data. They also observed that if a ferrite phase is present, there is non-negligible embrittlement of the material.

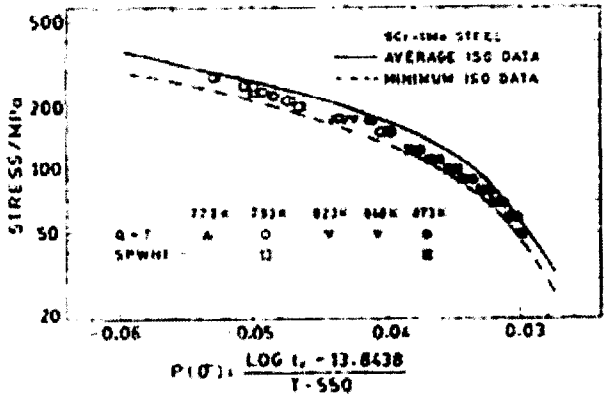

Figure 3.33. Comparison of creep rupture strength of thick and thin sections of 9Cr-1Mo steel [Choudhary et al. 1999].

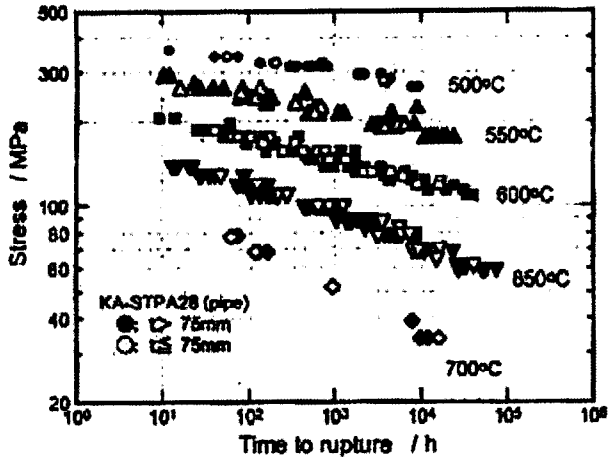

Figure 3.34. Comparison of creep rupture strength between thick and thin plates of modified 9Cr-1Mo steel [Kimura 2005].

Mechanical properties data on modified 9Cr-1Mo-V steel in helium environments, pertinent to service in NGNP reactor, is currently not available. The effect of impurities in helium on the creep, corrosion, and oxidation behavior needs to be established.

The radiation levels expected in the NGNP is expected to be very low (<0.1 dpa). There is no available data for these steels at this low dpa level. Although data at higher dpa levels affect mechanical properties, the effect of radiation on mechanical properties is expected to be negligible to minimal for the RPV in NGNP system. Some experimental tests to evaluate the effect of irradiation on mechanical properties would be desirable.

3.1.3.4 ASME Code Allowables

9Cr-1Mo-V materials in various forms have been adopted in a number of ASTM/ASME standards. Many are listed in the ASME Boiler and Pressure Vessel Code Section II, Part D, allowable stress tables with a maximum temperature rating of 649°C (1200°F) for ASME Code Section I and Section VIII, Division 1, and rating of 371°C (700°F) for Section III, Class 1, 2, and 3. The 9Cr-1Mo-V steel has also been approved for structural use until 649°C in Section III, Subsection NH. For pressure vessel applications, SA-182 is primarily used for flanges, fittings, valves, whereas SA-336 is the standard for construction of large pressure vessels. Gas turbine modular helium reactor (GT-MHR) design at a nominal operating temperature of 495°C is in the creep regime for this steel. Appropriate use of creep data and other design allowables of 9Cr-1Mo-V steel from subsection NH for the design of SA-336 pressure vessel need to be addressed. Relevant knock-down and/or safety factors to account for thick sections, helium environment, etc should be determined by experimentation and modeling before applying subsection NH rules for construction of the SA-336 vessel.

3.1.3.5 Advanced Ferritic-Martensitic Steels

The advantages that higher-chromium steels (e.g., modified 9Cr-1Mo steel) offer compared to low-alloy steels in terms of better elevated temperatures properties and increased oxidation resistance has been a driving force to constantly modify and refine the composition and microstructure to achieve better performance. Several high-chromium steels with W addition and higher chromium (>10wt.% Cr) steels have been found to provide better properties than grade 91 steel.

Table 3.10 presents the chemical composition of three additional grades of 9Cr-1Mo-V steels along with Grade P9 steel. The steel designated P91 (modified 9Cr-1Mo steel) was developed at Oak Ridge National Laboratory (Sikka et al. 1981). It shows a remarkable increase in stress rupture strength, achieved by addition of 0.2wt.% V, 0.06wt.% Nb, and 0.05wt.% N. The steel designated P92 was developed at Nippon Steel, in which a further increase in stress rupture strength was achieved by addition of 1.8wt.% W and reduction of the Mo content from 1 to 0.5wt.%. Similar steel, designated E911, was developed in a European program and it contains 1wt.% Mo and 1wt.% W and offers stress rupture strength similar to P92. This development of 9Cr-1Mo-V steels is illustrated in Figure 3.35, which shows the 100000-h stress rupture strength of Grades P9, P91, P92, and E911 at 600 and 650°C.

Table 3.10. Chemical composition (in wt.%) of several grades of 9Cr-1Mo steels

Element	P9	P91	P92	E911
C	Max. 0.15	0.10	0.124	0.105
Si	0.20-0.65	0.38	0.02	0.20
Mn	0.80-1.30	0.46	0.47	0.35
P	Max. 0.030	0.020	0.011	0.007
S	Max. 0.030	0.002	0.006	0.003
Cr	8.5-10.5	8.10	9.07	9.16
Mo	1.70-2.30	0.92	0.46	1.01
W	-	-	1.78	1.00
V	-	0.18	0.19	0.23
Nb	-	0.073	0.063	0.068
B	-	-	0.003	--
N	-	0.049	0.043	0.072
Ni	-	0.33	0.06	0.07
Al	-	0.034	0.002	--
Heat treatment		1 h at 1050°C + 1 h at 750°C, air cool	2 h at 1070°C + 2 h at 775°C, air cool	1 h at 1050°C + 1 h at 750°C, air cool
100000-h stress rupture strength at 600°C (MPa[a])	35	94	115	110

[a]Values for P91 from Canonico [1994], for P92 from Wachter et al. [1995], and for E911 from Staubli et al. [1998].

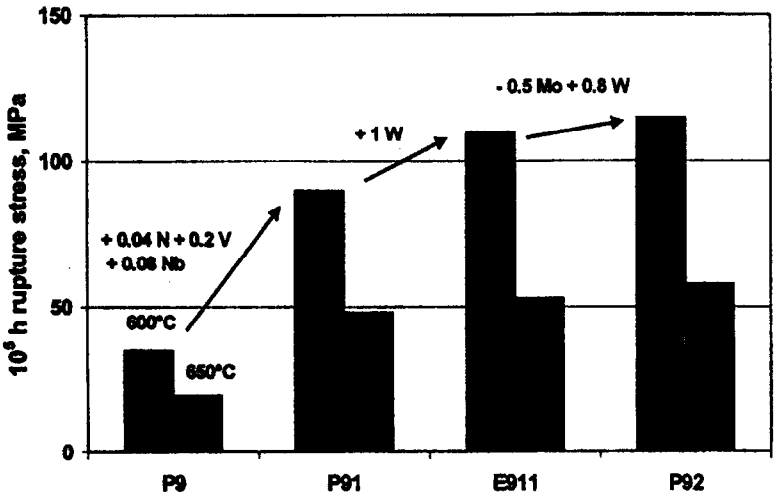

Figure 3.35. Rupture stress in development of 9%Cr steels [Ennis and Czyrska-Filemonowicz 2002].

Lee et al. [2006] in a recent paper evaluated creep rupture properties of P92 steel at 550-650°C up to ≈63000 h. They observed that the stress exponent, n decreases from 17 in short-term high stress short-term creep to 8 in low stress long-term creep. This was in agreement with the results of Ennis and Czyrska-Filemonowicz [2002], who observed such behavior in P91, E911 and P92 steel (Fig. 3.16). Lee et al [2006] did not notice any significant difference in activation energies though. Furthermore, at high stress low life regime, a ductile fracture was observed whereas at low stress long life, a brittle intergranular fracture was observed. The occurrence of intergranular fracture was attributed to the coarsening of Laves phase.

Creep-fatigue data at 700°C of modified 9Cr-1Mo steel is shown in fig. 3.36 along with the data for other ferritic steels. The creep-fatigue life of grade 91 steel is lowest and ductility is

highest compared to ferritic steels with W additions, 12 Cr compositions, and oxide dispersion strengthened steels. In addition, low-chromium steels based on 3Cr-3WV in composition have better properties than modified 2.25Cr-1Mo-0.25V steels discussed in Section 3.2. Although there is insufficient mechanical property database and the absence of ASME code that prevent them from being used for the NGNP, they may be potential candidates for future reactors. The review paper by Klueh [2005] provides the current state-of-knowledge of these advanced steels.

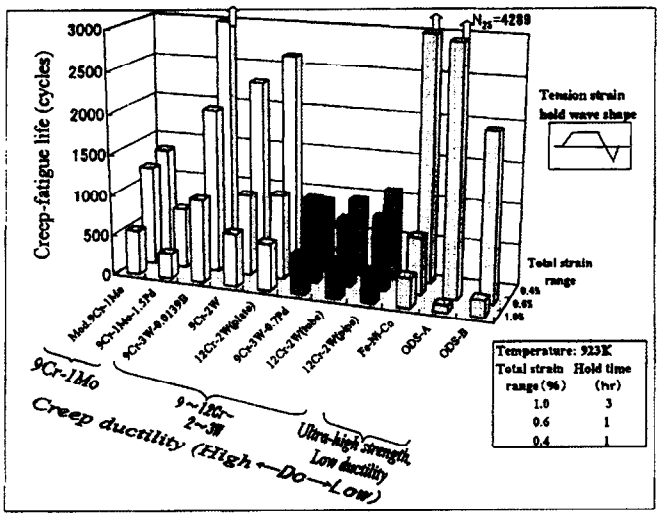

Figure 3.36. Comparison of creep fatigue behavior of modified 9Cr-1Mo steel with other ferritic steels at 700°C [Kimura et al. 2003]

3.2 Welding of Candidate Materials

3.2.1 Fabrication and Welding of Low-Alloy Steel Pressure Vessels

This section summarizes the experience related fabrication and welding of light water reactor (LWR) pressure vessels, which were fabricated with low-alloy pressure vessel steels. The three U.S. PWR NSSS vendors are Babcock & Wilcox Company (B&W), Combustion Engineering, Inc. (CE), and Westinghouse; all three vendors have similar vessel designs with wall thicknesses varying between 203 to 254 mm (8 to 10 in.) and diameter-to-thickness ratios of approximately 20. In contrast, boiling water reactor (BWR) vessels are much larger in diameter, and have a 152-mm (6-in.) wall thickness. Vessels designed by Westinghouse were fabricated by B&W, CE, Chicago Bridge and Iron Company, Societe des Forges et Ateliers du Creusot in France, or Rotterdam Dockyard in the Netherlands. Several Westinghouse vessels were initially fabricated by B&W, but were later finished by Rotterdam Dockyard or CE. All B&W and CE NSSS reactor vessels were fabricated by their in-house shops. Owing to the larger downcomer region and resultant larger water gap between the core and the vessel wall in a B&W-designed and fabricated vessel, the vessel in a B&W plant is exposed to a relatively lower level of radiation.

Fifty-three of the 73 PWR vessels operating in 1994, were fabricated using formed steel plates of either SA302 Grade B (SA302B) steel for earliest vessels or SA533 Grade B Class 1 (SA533B-1) steel for the other vessels. Nickel-modified SA302B (SA302B Mod.) is the early equivalent of SA533B-1. Twenty of the later B&W and foreign-supplied vessels were fabricated using ring forgings of SA508 Class 2 (SA508-2) or SA508 Class 3 (SA508-3) rather than plates. The volume of weld metal is significantly reduced in these vessels because there are no longitudinal weld seams; future nondestructive examinations are thus minimized. Furthermore, fewer weld seams are located in the central core region. The upper shell course of the vessels

contain the nozzles and is typically at least 30% thicker (to account for nozzle penetrations) than the intermediate or lower shell courses. The nozzles are all forgings of SA508-2 or SA508-3.

Table 3.11 lists examples of chemistry and mechanical properties for these various base metals and welds used in fabrication of pressure vessels for eight U.S. PWR plants, which cover the designs by all three U.S. NSSS vendors. The vessels in Table 3.11 were fabricated either by Babcock & Wilcox or Combustion Engineering. Note that in 1973, limits were placed upon the allowable amounts of copper (Cu) and phosphorus (P) for the reactor vessel base metals in the core region to minimize the embrittlement sensitivity of the steels. Copper, in particular, is a tramp element that showed up in many steel products fabricated from recycled automotive scrap that contained some copper wiring and radiators. Note that nickel (Ni) has also been shown to increase radiation embrittlement sensitivity, even though it is an important alloying element for pressure vessel steels.

Table 3.11. Composition and mechanical properties for PWR pressure vessel materials[a]

		Chemical Composition		Mechanical Properties[b]		
Plant	Steel	Cu	Ni	Initial RTndt (°F)	Initial USE (ft-lb)	Initial Yield Stress (ksi)
A	SA 508-3 (forging)	0.3	0.73	-30	152	64
	Weld (Linde 80)	0.3	0.65	40	78	72
B	SA 533B-1 (plate) Weld	0.10	0.46	30	77	67
	(non-Linde 80)	0.20	1.00	-56	94	74
C	SA 508-2 (forging) Weld	0.16	0.80	38	85	70
	(non-Linde 80)	0.09	0.11	19	95	64
D	SA 508-2 (forging) Weld	0.04	0.75	20	133	68
	(Linde 80)	0.35	0.68	-5	70	69.2
E	SA 302B-M (plate) weld	0.19	0.48	0	71.8	64
	(non-Linde 80)	0.18	1.05	-56	118	64
F[x]	SA 533B-1 (plate) Weld	0.04	0.68	-10	136.5[d]	62[d]
	(non-Linde 80)	0.07	0.09	-50	109	63
G	SA 302B-1 (plate) Weld	0.20	0.06	1	91	60
	(Linde 80)	0.25	0.54	-5	70	73
H	SA 533B-1 (plate) Weld	0.06	0.60	30	107	69
	(non-Linde 80)	0.04	0.10	-800	134	72

MPa = 6.894 ksi, °C=5/9 (°F-32).

a. The data for chemical composition, initial RT_{NDT}, and initial upper shelf energy (USE) are from the licensees' responses to Generic Letter 92-01. The data for initial yield stress are from the reactor vessel radiation surveillance programs. All these data are from the same plate, forging, or weld at a given plant.

b. Upper shelf energy and yield stress data for all base metals (plate or forging) are from the longitudinal direction (see Figure 6 in Section 1-3), unless otherwise noted.

c. All data for this plant are from the reactor vessel radiation surveillance program.

d. Data are from the transverse direction.

Pressure vessel materials have performed very well in service, and no fatigue-driven cracks have been found in any PWR vessels. The only materials-related variable that appears to affect fatigue is the sulfur content (and distribution as sulfides) in the steel. Low alloy steels with average to high sulfur levels generally exhibit higher crack growth rates in the laboratory than low sulfur steels (<0.010 wt%). As shown in Table 3.9, only the SA508-3 forging material has low sulfur, and the levels in other steels are typical of most U.S. vessels (including the weld metal) [Stahkopf et al. 1987].

Automatic submerged arc welding (SAW) was usually employed except for complicated geometries and repairs; manual shielded metal arc welding (SMAW) was used in these special cases. Narrow gap SAW was used in some vessel girth welds to help reduce the amount of weld volume [Stahlkopf et al. 1987]. The B&W-fabricated vessels were made mostly using SAW and Linde 80 flux, which introduces micro inclusions and results in low initial upper shelf toughness properties. Other SAW flux types (for example, Linde 0091, 1092, and 124) used by the other manufacturers produce welds with similar mechanical properties, but with upper shelf energy and upper shelf toughness levels significantly higher than those for the Linde 80 flux welds. For example, in Table 3.11 the initial upper shelf energy for Linde 80 flux welds is in the range of 70 to 80 ft-lb, whereas that for non-Linde flux welds is greater than 90 ft-lb. The weld chemistry for copper, nickel, and phosphorus was similar to that of base metal before the 1973 limits were placed on copper and phosphorus levels; the high copper content in welds was the result of the use of copper-coated weld wires. Because the thickness of the copper coating was not uniform and because more than one heat of weld wire were used to finish a structural weld in the older vessels made before 1973, the copper content in the weld at the vessel inside surface may be different from that at the outside surface. However, the copper content at a given depth in the vessel wall will be about the same. The upper bound for nickel in B&W vessel welds is 0.7 wt%; for CE vessels it is 1.0 wt%. The upper bound for copper in welds is approximately 0.35 wt%.

The inside of the vessel wall was clad with stainless steel to inhibit general corrosive attack. Types 308 and 309 stainless steels were generally weld-deposited using an SAW process whenever possible, and the final stress relief was applied after the cladding process. Some older vessels were clad on the inside surface with Type 304 stainless steel. For example, a portion of the beltline region of the Yankee Rowe vessel is clad with 2.88-mm (0.11-in.) thick sheets of Type 304 stainless steel attached to the base metal by spot welding. The Haddam Neck (Connecticut Yankee) vessel is clad with weld-deposited Type 304 stainless steel with a minimum thickness of 4.1 mm (0.16 in.).

The automatic SAW process was generally used for cladding vessel shell courses, heads, and flanges; single-layer, three- or-six- wire processes and single- or multilayer, one-wire processes were employed. A strip cladding SAW process is used in Europe instead of the multiwire process; CE also uses it in fabricating the more recent reactor pressure vessels. A manual metal arc (MMA) process was used to clad most circumferential welds, and a multiple wire SAW process was used to clad the longitudinal welds (Becker 1982). Some areas of the cladding over the welds were ground to facilitate dye-penetrant testing; very few of these areas would meet European standards for cladding smoothness, which can play an important role during in-service inspection for sizing of underclad flaws.

Single- or multilayer manual metal arc welding processes were use for complex geometric configurations and for most repair welding. The multiwire process provides a smoother cladding surface, as compared to the single-wire process, and facilitates in-service inspection with ultrasonic techniques [Willetts et al. 1986]. Heat input during the cladding process affects the diffusion of base metal into the adjacent cladding layer. Excessive heat input and resulting diffusion of base metal may affect the fracture toughness of irradiated cladding. However, cladding toughness is generally not considered in determining full vessel wall toughness.

All vessel welds were post-weld heat treated at $610\pm14^{\circ}C$ ($1130\pm25^{\circ}F$) followed by a furnace cooling to reduce residual stresses and to temper any martensite in the heat affected zone (HAZ). Residual stresses at the surface can approach yield stress levels before stress relief, but these stresses are reduced to 34 to 60 MPa (5 to 10 ksi) after the stress relief heat

treatment [Zhou et al. 1985]. In the earlier vessels, the total stress relief time was approximately 40 to 50 h. For example, the total stress relief time was 48 h for the Ginna RPV, 40 h for the Maine Yankee RPV, and 40 h for the Palisades RPV [Hoge 1979]. In many newer vessels, the heat treatment time was reduced to about half of the 40 to 50 h maximum time used for treatment of older vessels; the reduced treatment time provides a larger margin of time for additional stress relief after any weld repairs.

All vessels were fabricated to satisfy requirements in the ASME Boiler and Pressure Vessel Code. In terms of general design, most PWR vessels were designed using values near 17.2 MPa (2500 psi) for pressure and 345°C (650°F) for temperature. Before 1963 when Section III of the ASME Code was first released, vessels were designed to meet the requirements of ASME Code, Section VIII (ASME 1968) and, in most cases, were upgraded to meet the intent of Section III through special stress analyses (primarily for fatigue). The allowable stress levels for pressure boundary materials were about 25% lower for Section VIII than those permitted by Section III for similar materials, which generally results in heavier wall thicknesses and larger nozzle-corner radii for Section VIII vessels. A significant change was made in 1972 Addenda to Section III of the ASME Code, in which the test requirements for measuring the reference nil-ductility-transition temperature (RT_{NDT}) were set forth; additionally, non-mandatory Appendix G was added and was made mandatory by Appendix G of 10 CFR 50. Pre-service inspections were performed on reactor pressure vessels at various stages of construction and after installation at the site. Section III of the ASME Code governs these inspections.

3.2.2 Fe-2.25Cr-1Mo Steel

Vanadium-modified 2.25Cr-1Mo steels are developed for the petrochemical refinery industry service at high temperatures and high hydrogen pressures. These steels were developed so that components having wall thickness in excess of 10 in., and diameters and lengths on the order of up to 20 and 200 ft, respectively, can be fabricated [Prager 1998]. These steels offer the fabricability and toughness of bainitic microstructures without the difficulties of welding and heat treating high chromium martensitic materials such as P91.

Realization of the full benefits of this steel required the development of filler metals with properties substantially matching those of the base metal. Prager et al. [1990] have described the development of a filler metal for this steel. Stress rupture tests on weldments to 16000h established that the expected performance of the filler metal, base metal, and HAZ were comparable in strength and within ASME's base metal scatter band. However, for design temperatures in excess of 468°C (875°F), ASME required performance testing of weldments. Such performance testing is not required for service at 468°C or below.

There are three concerns associated with long-term embrittlement of this steel weld in high pressure, high temperature hydrogen reactors: Temper embrittlement, hydrogen attack, and hydrogen embrittlement. Temper embrittlement is caused by reduction of bond strength of grain boundaries relative to the grain due to segregation of impurities (P and Sb) at grain boundaries. If the grains are insufficiently tempered, the effect is the greatest. Test results for base metal, HAZ, and weld metal exposed for 20000 h at 482°C (900°F) have shown that acceptable toughness is retained for the materials, provided impurity levels were maintained within specific limits [Prager 1998].

3.2.3 Fe-9 Cr-1Mo Steel (UNS K90901)

Fe-9Cr-1Mo steels (ASTM P9/T9) have been used successfully in US fossil boilers since 1980. These steels have several enhanced properties over traditional power plant steels, such as 2.25Cr-1Mo (ASTM P22) and 300-series austenitic stainless steels: lower thermal expansion, higher thermal conductivity, and improved resistance to oxidation. P9/T9 steel modified with the addition of niobium (Nb), vanadium (V), and nitrogen (N) exhibits a substantial increase in creep-rupture strength and allowable stress, compared to traditional power plant steels. Figure 3.37 presents a comparison between modified P9/T9 and other steels on the maximum allowable stress over a range of temperature [Kobelco Welding]. The modified steels have higher allowable stress intensities at temperature than annealed P22 steel (ASME 2005, Riou et al. 2006). These properties enable manufacture of the power plant components with thinner walls, thereby reducing thermally induced stresses and minimizing eventual thermal fatigue damage. ASME specifications for the modified P9/T9 steel are SA-213 Grade T91 for tubing, SA-335 Grade P91 for piping, SA-387 Grade 91 for plates, and SA-182 Grade F91 for forgings. All these three steels are hereafter referred to as Grade P91 steel.

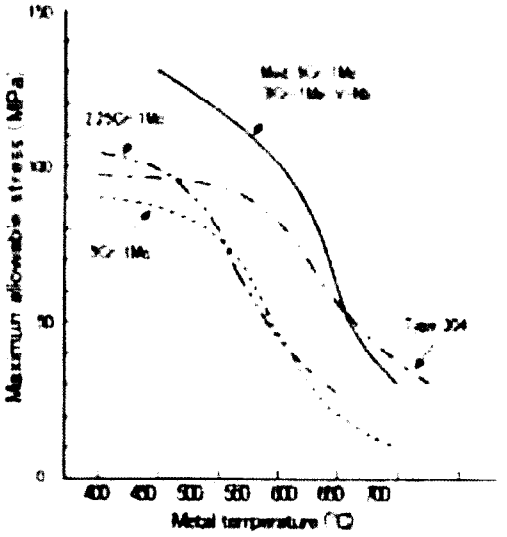

Figure 3.37. A comparison of maximum allowable stress as a function of temperature for P91, P9, P22, and Type 304 steel [Kobelco Welding].

The following two examples illustrate the advantages of using Grade P91 steel over Grade P22 steel. An upgrade of a typical heat-recovery steam generator header from P22 to P91 can reduce wall thickness by 54 percent and component weight by 65 percent [Swanekamp 2004]. The lower thermal expansion coefficient would result in lower thermal stresses. If a pipe run is heated from 21°C to 538°C (1,000°F), the modified Grade P9 will expand about 86% as much as Grade 22 pipe; this will result in about 14% lower pipe stresses [Cohn et al. 2005].

The superior properties of P91 steel depend on a precise addition of Nb, V, and N; optimum heat treatment to create a precise microstructure; and the maintenance of this microstructure throughout the service life. Welding and post-weld heat treatments play critical roles in creating the microstructure. A review of the related literature is presented in this section.

3.2.3.1 Welding Procedure for Thick Sections

Welding P91 generally requires preheating the joint, maintaining interpass temperatures, hydrogen bakes, post heating, and post-weld heat treatment (PWHT). Preheating, typically to

204-260°C (400-500°F), drives off moisture and thereby reduces hydrogen uptake. Hydrogen embrittlement can lead to cold cracking of the finished weld. For the same reason, hydrogen bakes are recommended for P91 if a weld cools to ambient temperature prior to PWHT. Preheating also reduces the thermal gradient between the base material and weld puddle, and it improves weldability by reducing the heat necessary to make the weld while reducing hot-cracking tendency. The typical preheat temperature is 200°C [Cohn et al. 2005]. The typical interpass temperature is in the range of 200-300°C (≈400-600°F). This temperature range should be more spatially controlled for a highly constrained component. Use of electrical resistance or electrical induction heaters is recommended because they provide better temperature control and heat distribution [Cohn et al. 2005].

On cooling from a temperature above the lower critical temperature, no transformation products form until the steel is cooled through the martensitic transformation range. The martensite start, M_s, and finish, M_f, temperatures depend on the chemical composition of Grade P91 steel [Beres et al. 2001]. At the lower end of the composition range for the major alloys (0.08C, 8.0Cr, 0.85Mo, 0.20Si, 0.18V), the M_s and M_f temperatures are about 400°C (752°F) and 209°C (408°F), respectively. At the higher end of the chemical composition range for the alloys (0.12C, 9.5Cr, 1.05Mo, 0.50Si, 0.25V), the M_s and M_f temperatures are about 339°C (642°F) and 149°C (300°F), respectively. Since the M_s and M_f temperatures for weld deposit may be lower than the corresponding base metal temperatures, use of weld deposit M_s and M_f temperatures based on the estimated filler metal chemical composition is recommended [Cohn et al. 2005].

After welding is completed, the weldment should be allowed to cool slowly to at least 93°C (200°F) to insure that all the austenite has transformed to martensite prior to postweld heat treatment (PWHT). If this is not done, there is a risk of martensite formation after PWHT and this may result in hard, brittle welds. For Grade P91 steel weldment, the temperature at which the transformation of austenite to martensite finishes, the M_f temperature, is above 100°C (212°F), varying some with the chemical composition of the filler metal [Sperko Engineering 2005].

Because Grade P91 steel is a high-strength alloy in which austenite normally transforms completely to martensite during air-cooling, the handling of weldments between completion of welding and PWHT is an important practical matter. Weldments that are cooled to room temperature before PWHT will transform more completely to martensite than weldments that are maintained at or above minimum preheat temperature prior to PWHT. Therefore, the weldments that are cooled to room temperature are less likely to contain untempered martensite. Santella et al. [2003] reported that phase transformations taking place in Grade P91 base metal and weld metal are different and concluded that weld metal samples exhibit retained austenite due to incomplete martensite formation from austenite. This retained austenite at room temperature then transforms to fresh martensite during cooling from post-weld heat treatment temperature. This transformation behavior was not observed in the base metal samples. The origin of such transformation in welds is attributed to micro segregation that occurs during weld solidification. As a result, the transformation to martensite will not be uniform throughout the microstructure and will be influenced by local chemical composition.

A postweld hydrogen bakeout may be of critical importance, especially for thick-walled components if there is concern regarding the presence of residual hydrogen. It typically includes soaking of the weldment at 320°C (≈600°F) for a minimum of 20 min for thin components, including at least 75 mm (3 in.) on each side of the weld. The process facilitates hydrogen diffusion from the weldment and it is especially important if the weldment is not

subject to an immediate PWHT. The time should be appropriately increased for thicker components [Cohn et al. 2005]. Kobelco Welding recommends post-heating the weld by 250-350°C for 30-60 min, if PWHT is not conducted before the weld cools to ambient temperature after welding is completed.

Welding thicker materials and high-alloy steels usually requires maintaining minimum preheat and maximum interpass temperatures. If a material cools below the minimum temperature between passes, restraint issues may arise or hydrogen may contaminate the weld. If the material becomes too hot, which can happen during multiple-pass welding, some steels can lose their corrosion resistance. With P91, interpass temperature higher than 300°C usually makes the weld puddle too fluid and difficult to control.

Weld Filler Metal

The performance of Grade 91 welds depends entirely on having the correct chemical analysis of the weld metal. As mentioned in the earlier section of this report, Grade P91 steel is alloyed with considerable amount of vanadium, niobium and nitrogen in addition to chromium and molybdenum to improve the elevated temperature strength. However, filler metals cannot accommodate as much niobium and nitrogen as contained in the steel because such elements result in poor weldability. Simple alloying of conventional 9Cr-1Mo filler metal with vanadium and niobium would create a heterogeneous microstructure consisting of coarse, polygonal ferrite precipitates in the martensitic matrix, thereby decreasing strength and impact toughness.

Sperko Engineering [2005] recommends that a minimum carbon content of 0.09 wt.%, a minimum niobium content of 0.03 wt.%, and minimum nitrogen of 0.02wt.% be specified to ensure adequate creep strength in the weld metal. In addition, the sum of Mn plus Ni should not exceed 1.5 wt.%. Manganese and nickel depress the lower transformation temperature, and if it exceeds 1.5 wt.%, the transformation temperature drops below 788°C (1450°F), narrowing the range in which heat treatment can be done safely. In addition, the M_f temperature goes down, increasing the possibility of retained austenite after PWHT.

Industry has developed filler metals having unique chemical composition that provides good mechanical properties and welding workability in out-of-position welding. For example, Table 3.12 presents typical chemical compositions of filler metal CM-9Nb developed by Kobelco Welding for shielded metal arc welding (SMAW) in comparison with Grade T91 steel. Note that this chemical composition is unique and it does not satisfy the Sperko Engineering requirement of (Mn + Ni) less than 1.5 wt.%. CM-9Nb filler metal offers fine, homogeneous microstructures created by its unique chemical composition as shown in Figure 3.38.

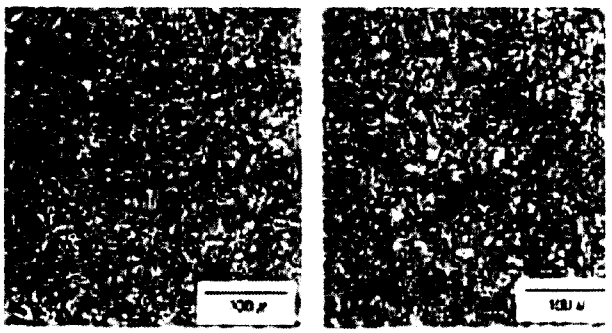

Figure 3.38. Homogeneous microstructure of CM-9Nb deposits consisting of tempered martensite with the absence of polygonal ferrite after PWHT (750°C x 5h), exhibiting a dendritic zone (left) and a pass-to-pass tempered zone (right).

CM-9Nb filler material satisfies the mechanical properties requirement of the AWS standard and it has been used for many ultra-supercritical pressure boilers fabricated by Japanese manufacturers. High temperature strength and creep rupture strength of CM-9Nb filler metal are presented in Figures 3.39 and 3.40, respectively. These figures verify that CM-9Nb satisfies the minimum yield strength, tensile strength and rupture strength of Grade P91 steel. Kobelco Welding has modified the chemical composition of CM-9Nb filler metal and developed CM-96B9, which conforms to both the chemical and mechanical requirements, respectively, of the AWS standards as shown in Table 3.13 and Figure 3.41 [Kobelco Welding].

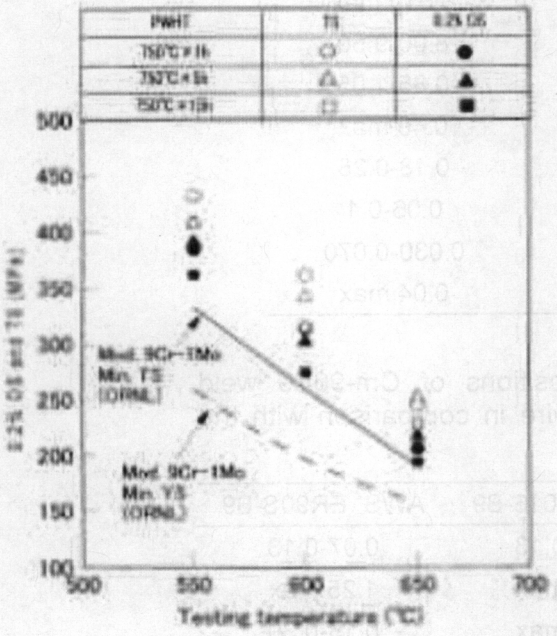

Figure 3.39. High-temperature strength of CM-9Nb weld metal in flat position, satisfying the minimum strength of P91 steel within the given PWHT conditions.

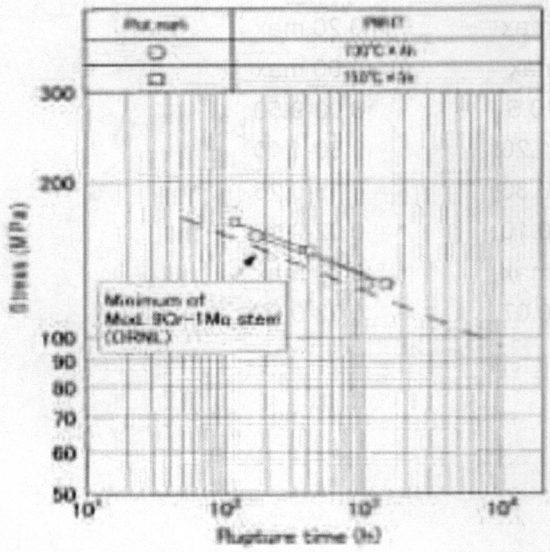

Figure 3.40. Creep rupture strength of CM-9Nb weld metal in flat position, satisfying the minimum rupture strength of P91 steel.

Table 3.12. Typical chemical composition of CM-9Nb weld metal in comparison with A213 T91 tube chemistry range (in wt.%)

Brand	CM-9Nb	ASTM A213T91
C	0.06	0.08-0.12
Mn	1.51	0.30-0.60
Si	0.31	0.20-0.50
P	0.006	0.020 max
S	0.003	0.010 max
Cr	9.11	8.00-9.50
Mo	1.06	0.85-1.05
Ni	0.94	0.40 max
V	0.18	0.18-0.25
Nb	0.03	0.06-0.1
N	0.030	0.030-0.070
Al	-	0.04 max

Table 3.13. Typical chemical compositions of Cm-96B9 weld metal (DC-EP) and TGS-9089 filler wire in comparison with the AWS requirements (wt%)

Element	CM-96B9	AWS[1] E9016-B9	AWS[2] ER90S-B9
C	0.11	0.08-0.13	0.07-0.13
Mn	1.12	1.25 max	1.25 max
Si	0.23	0.30 max	0.15-0.30
P	0.009	0.01 max	0.010 max
S	0.002	0.01 max	0.010 max
Cu	0.01	0.25 max	0.20 max
Ni	0.83	1.0 max	1.00 max
Cr	9.13	8.0-10.5	8.00-9.50
Mo	0.99	0.85-1.20	0.80-1.10
V	0.23	0.15-0.30	0.15-0.25
Nb	0.037	0.02-0.10	0.02-0.10
Al	-	0.04 max	0.04 max
N	0.027	0.02-0.07	0.03-0.07

[1]Weld metal; [2]Filler wire.

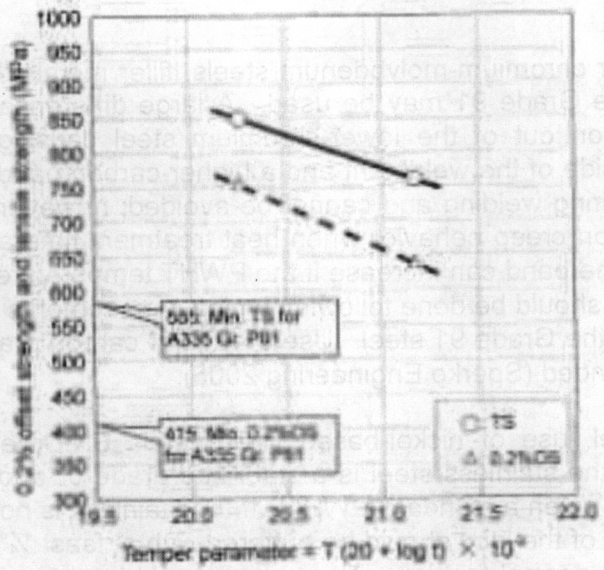

Figure 3.41. Tensile properties of CM-96B9 weld metal as a function of temper parameter where T is PWHT temperature in Kelvin and t is soaking time in hour.

Since Grade P91 is modified with vanadium, nickel, aluminum, niobium, and nitrogen, it develops very high hardness. Tramp residual elements in this steel, such as phosphorous, sulfur, lead, tin, copper, antimony, and others will segregate to the grain boundaries during solidification of the weld pool with propensity for cracking. It is, therefore, very important to use low residual filler metal.

The welding electrodes should be procured to a recognized specification, such as AWS, with a classification of "B9". A low hydrogen electrode with low moisture content is required. Rigorous filler metal control is required for SMAW and SAW. For SMAW, E9015-B9, electrodes are preferred. Use of E9018-B9 electrodes is not recommended for welding Grade 91 steels unless the tramp residuals are controlled to low levels. When using SAW, a basic flux is preferred since other flux types will burn out carbon and permit elevated oxygen and nitrogen levels reducing the strength and toughness of the weld metal. Welding Grade 91 using flux core arc welding (FCAW) requires even more care since many FCAW wires do not provide adequate toughness at 70°F (the lowest hydrostatic test temperature permitted by ASME).

Since Grade P91 steel is a highly hardenable alloy, it is subject to hydrogen cracking. Therefore, use of E9015-B9-H4 electrode is recommended. The “H4” designation indicates that the electrode exhibits less than 4 ml of hydrogen per 100 grams of weld metal. This is truly a very low hydrogen electrode, which is superior for welding highly hardenable steel like Grade 91. Even with diffusible hydrogen control of the electrodes, it is recommended that the electrodes be stored in heated portable rod boxes at the welding location rather than just distributed in the normal fashion. SAW wire/flux combinations and FCAW wire should have “H4” designations also, although FCAW wire may not be available except as “H8.”

The welding technique is also important. Since a wide, flat bead is best, a slight weave technique and high travel speed should be specified. Ropy beads are bad since tall, narrow beads tend to crack. Concave beads should also be avoided, particularly with SAW. Bead thickness should not exceed 1/8 in. for SMAW and FCAW to promote tempering of previous passes [Sperko Engineering 2005].

Dissimilar Metal Welds

For a weld between Grade 91 and lower chromium-molybdenum steels, filler metals that match either the lower chromium grade or the Grade 91 may be used. A large difference in chromium causes a gradient that pulls carbon out of the lower-chromium steel causing a depleted carbon band in the lower-chromium side of the weldment and a higher-carbon band in the grade 91-side of the joint. This occurs during welding and cannot be avoided; however, it has been shown to have no significant effect on creep behavior when heat treatment time and temperature are not excessive. The width of the band can increase if the PWHT temperature is high and/or at longer times. Therefore, PWHT should be done following typical requirements for the lower-chromium steel rather than those of the Grade 91 steel. Use of regular carbon grade filler metal, not low carbon grades, is recommended (Sperko Engineering 2005).

For welding to austenitic stainless steel, use of nickel-based filler metals ENiCrFe-2, ENiCrFe-3, or ERNiCr-3 is recommended. If the stainless steel is a stabilized grade or a low-carbon grade, the completed weldment can be given a standard PWHT. If the stainless is not a stabilized or low-carbon grade, the P/T-91 side of the joint should be buttered with at least ¼" of nickel-alloy weld metal and heat treated in the normal fashion. The buttered and heat treated end can then be welded to the stainless steel using nickel alloy filler metal without preheat or PWHT.

3.2.3.1 Post-Weld Heat Treatment

PWHT requires controlling temperature in four phases to relieve the stress caused by welding. The following example describes the four phases with Grade P91 and follows ASME B31.1 (see Fig. 3.42).

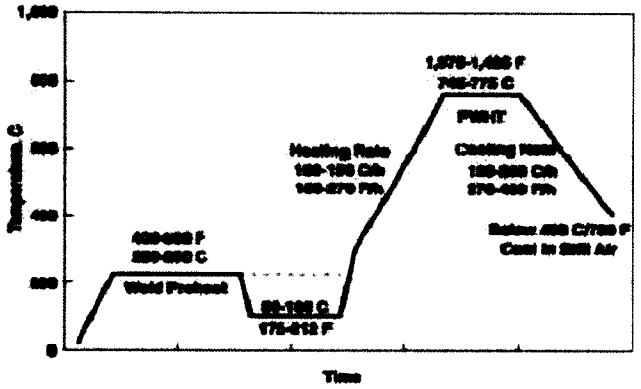

Figure 3.42. Temperature control during postweld heat treatment following the requirements of ASME B31.1 code [Roth 2002].

1. Control temperature. The weldment usually may be brought to this temperature, generally 316°C (600°F), without any time constraint.

2. Control-temperature rise. Once the control temperature is reached, the code requires a controlled temperature rise of no more than 316°C per hour divided by one-half the maximum thickness, but in no case more than 316°C per hour.

3. Soak or hold temperature. This is the stress-relieving temperature. For heavy-wall Grade P91 weldments, that temperature is typically 760±14°C (1,400 ±25°F). For other alloys, it may be between 593-760°C (1,100-1,400°F). Soak time depends on the thickness of the

material. One hour per inch is common for most alloys, but Newell recommends that heavy-wall (greater than 19 mm or 3/4 in.) P91 components should have a minimum soak time of two hours.

4. **Control cool**. After the soak time, the material must be cooled at a controlled rate to prevent stressing the part, which could lead to cracking. Typically, the control-cooling rate is same as the control-temperature rise — cool from 760 to 316°C at a rate of no more than 204°C (400°F) per hour. Below 316°C (600°F), the weldment can be air-cooled to ambient temperature.

Stress relieving restores ductility. Without ductility at ambient temperature, power piping and other chromium-molybdenum components may not withstand hydrostatic testing and other aspects of fabrication, transportation, start-up, and shutdown phases. The hardness of Grade P91 steel weldment changes during postweld heat treatment as shown in Fig. 3.43. Prior to stress relieving, an as-welded P91 weldment usually has Rockwell C hardness in the mid 40s to low 50s and a Charpy V-notch toughness of just 3 foot-pounds. After PWHT, P91 is significantly more ductile. Its Rockwell C hardness drops to the low 20s and its Charpy V-notch toughness can increase to 40 to 70 foot-pounds, depending on the welding process [Roth 2002].

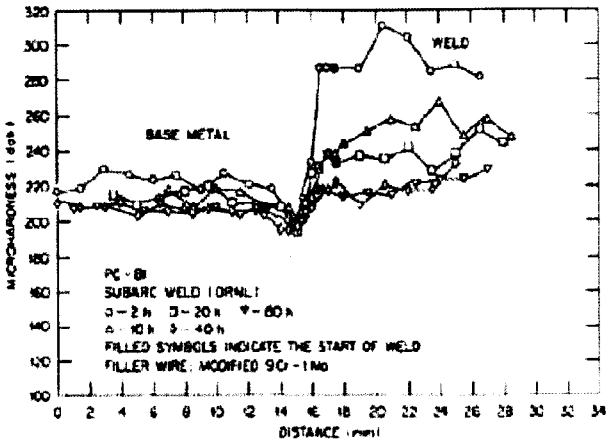

Figure 3.43. Changes in hardness of Grade P91 steel weldment during postweld heat treatment [Klueh 2002].

Proper PWHT of Grade P91 steel is essential in order to temper Grade 91 material and to eliminate the risk of stress corrosion cracking (SCC). It should be emphasized that P91 provides no forgiveness when fabricators and installers fail to stress-relieve the material properly. It will fail under circumstances that P22 would not. Also, like most heavy-wall, large-diameter piping, a P91 pipe's inside diameter (ID) and outside diameter (OD) can exhibit a substantial temperature gradient (50 to 100 degrees) if the procedure and technique are not carefully evaluated and qualified, so installers need to bring ID and OD temperatures as close together as possible. The lower critical transformation temperature can be as low as 788°C (1450°F); if this temperature is exceeded during PWHT, the weld should be allowed to cool to below 93°C (200°F) followed by reheat treating or the condition of the joints should be evaluated by hardness testing. AWS D10.10, *Recommended Practice for Local Heating of Welds in Piping and Tubing*, provides guidance on locating and attachment of thermocouples, the extent of insulation needed, heating coils arrangement, etc. if local heating (preheat, postweld baking, PWHT, etc) is planned.

The PWHT rules in ASME B&PV Code, Section 1 have been recently modified because of the risk of tempering at too high a temperature, and because recent studies have shown that

certain alloying elements – principally nickel and manganese – alter the transformation characteristics of the materials [ASME Code 2005a]. The modified rules are presented in Table 3.14. The modified rules state that the maximum PWHT temperature for P-No. 5B, Group 2 materials (Grade P91 materials) should not be greater than 774°C (1425°F), except as indicated below:

If Ni + Mn < 1.5% but ≥ 1.0%, the maximum PWHT temperature is 788°C (1450°F).

If Ni + Mn < 1.0%, the maximum PWHT temperature will be 800°C (1470°F).

Table 3.14. Mandatory Requirements for Postweld Heat Treatment of Pressure Parts and Attachments‡(ASME 2005a)

Material	Minimum holding temperature, °C (°F)	Minimum holding time at normal temperature for weld thickness		
		≤50 mm	50 to 125 mm	>125 mm
P-No. 5A Group No. 1 and P-No. 5B Group No. 1	675 (1250)	2 min/mm, 15 min minimum	2 min/mm	5 hr plus 15 min for each 25 mm over 125 mm
P-No. 5B Group No. 2	705 (1300)	2 min/mm, 15 min minimum	2 min/mm	5 hr plus 15 min for each 25 mm 125 mm

‡This table is a part of Table PW-39, ASME Boiler and Pressure Vessel Code, Section 1, 2005 Addenda.

The new rules also provide some provision for microstructure recovery if these limits are exceeded during processing.

After PWHT, the weld hardness should be in the range of 200 to 275 Brinnel hardness number (BHN). Hardness up to 300 BHN may be acceptable, but any hardness >300 BHN is an indication of inadequate PWHT. SMAW and SAW weld metal will exhibit higher hardness when compared to gas tungsten arc welding (GTAW) and FCAW. Hardness below 175 BHN indicates overheating of the joint, and such joints should either be replaced or the part should be normalized and tempered [Sperko Engineering 2005].

Grade 91 can be hot bent using furnace heating or induction heating between 870 to 1,090°C (1600 to 2000°F), but the low end of this range is preferred. Pipes that are hot bent should be given a full-furnace normalizing heat treatment at 1,040 to 1,065°C (1900 to 1950°F) for 30 minutes per inch of wall thickness, air cooled to below 93°C (200°F) and tempered in the PWHT range of 746-774°C (1375 to 1425°F) for 1 hour per inch of thickness. Cold bent pipe should be given a stress-relieving heat treatment at the above tempering temperature for 15 minutes per inch of wall thickness.

Local heating using a heating torch is acceptable, but the temperature must be monitored and not ever allowed to exceed 760°C (1400°F) in order to stay below the lower transformation temperature. A good working limit is 705°C (1300°F). Cold deformation should be limited to not more than 10% strain in the metal, and if this limit is exceeded, the part should be renormalized and tempered. Preheating to 150°C (300°F) is recommended when thermal cutting or using carbon or plasma arc gouging [Sperko Engineering 2005].

When performing hydrostatic testing, there is always danger of brittle failure due to the presence of flaws and inadequate toughness of the metal. Weld metal can be somewhat unpredictable in toughness due to variations in welding techniques by different welders and the possibility of weld discontinuities. Accordingly, Grade 91 should be hydrostatically tested at 19°C (90°F) or higher insure that the weld metal is above 15 ft-lbs or 15 mils lateral expansion.

This is usually adequate toughness to ensure failure by leak-before-break rather than brittle failure [Sperko Engineering 2005].

3.2.3.3. Technical Issues in Welding

Type IV Cracking

One of the most significant problems with Grade 91 is post-production exposure to temperatures in the intercritical region. This is above the temperature where martensite begins to transform back into austenite (referred to as the lower critical transformational temperature or AC_1) and below the temperature where phase transformation is complete (called the upper critical transformational temperature, AC_3). Transformation curves for Grade P91 steel during heating are shown in Fig. 3.44. When Grade P91 is exposed to this intercritical region, the martensite is partially reaustenitized and the carbon-nitride precipitates are coarsened but do not fully dissolve back into solution. The resulting material is a part austenite/part martensite metal that lacks the "pinning" effect of the precipitates, and therefore has substantially reduced creep-rupture strength.

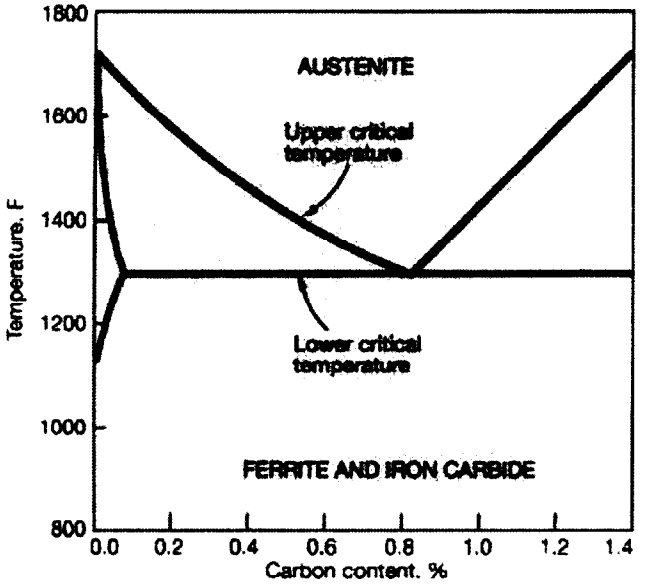

Figure 3.44. Transformation of Grade P91 steel during heating, showing the lower (AC_1) and upper (AC_3) critical transformation temperatures [Henry 2005].

Exposure to the intercritical region and the resulting reduction in strength leads to the Type IV cracking found in many P91 welds. In a Type IV failure, cracking takes place in the fine-grain section on the base-metal side of the heat-affected zone of a weldment as shown in Fig. 3.45. Abrupt changes in wall thickness or other features that create high stresses in the region of the weld set up the conditions necessary for this cracking. Type IV failures are a matter of significant concern because they occur at a relatively early stage in component life — 20000 to 40000 hours — at lower operating temperatures than the maximum design temperature of 600°C (1,110°F) for steam plant components.

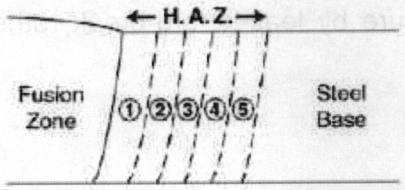

Figure 3.45. Five different microstructural regions formed in the heat-affected zone of Grade P91 steel weldment [Klueh 2002].

Fusion Zone (FZ): $T > T_m$

Heat - Affected - Zone (HAZ) [as-welded]:

Region 1	$T_m > T > T_{\gamma\delta}$	$\gamma + \delta \rightarrow$ Martensite + δ
Region 2	$T_{\gamma\delta} > T > Ac_3$	Coarse grained $\gamma \rightarrow$ Martensite
Region 3	$T_{\gamma\delta} > T > Ac_3$	Fine grained $\gamma \rightarrow$ Martensite
Region 4	$Ac_3 > T > Ac_1$	$\gamma \rightarrow$ Martensite + Overtempered Martensite
Region 5	$Ac_1 > T > T_T$	Overtempered Martensite

Type IV cracks can initiate and grow in the sub-surface for some distance before breaking through to the surface. Figure 3.46 shows the profile and optical microstructures of the cross section of a fractured P91 weldment with Type IV cracking. The weldment was at 600°C and subjected to 80 MPa for 12414 h. On the opposite side of the fractured surface, it can be clearly observed that the cracks in the HAZ have nucleated inside the plate thickness as shown in Figure 3.46(a). The crack initiation is in the fine grained HAZ about 400-500 μm away from the boundary between base metal and HAZ, as shown in Figure 3.46(a)-(c). Figure 3.47 presents the schematic of the Type IV cracking shown in Figure 3.46. It is also noted that the hardness is minimum at this crack initiation site [Watanabe 2006].

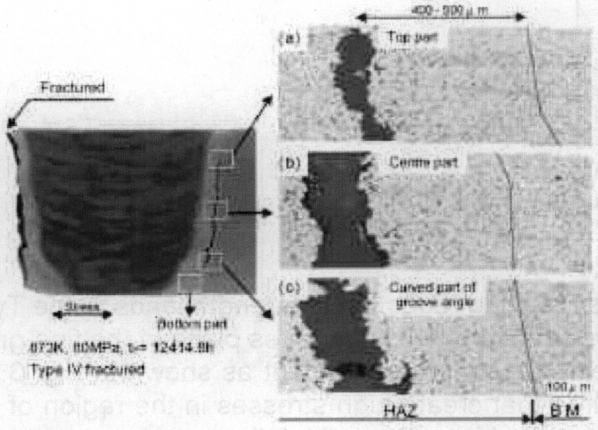

Figure 3.46. Profile and optical microstructure of fractured P91 weldment with Type IV cracking [Watanabe 2006].

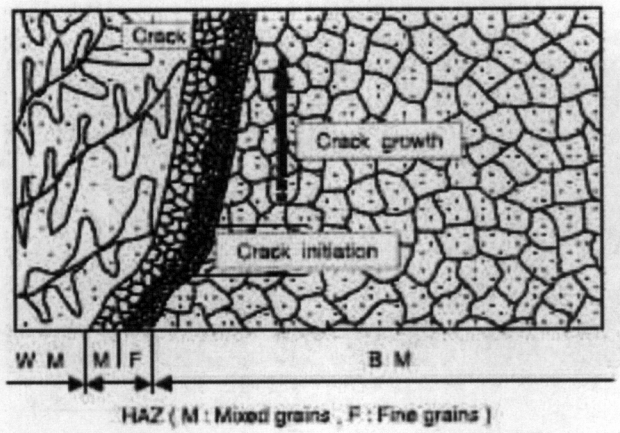

Figure 3.47. Schematic of Type IV crack growth in fractured P91 weldment [Watanabe 2006].

There have been about a dozen Type IV cracking failures in P91/T91 components, mostly in the U.K. where the alloy has been in service longer than in the USA. One U.S. user has reported several P91 weld failures in steam piping of his company's relatively new fleet of F-class combined cycles. A related problem is over-tempering, which occurs when P91 or T91 components experience prolonged exposure to elevated temperatures below the lower critical transformation temperature. This does not affect the martensite, but it does cause coarsening of the precipitates, with a corresponding loss in creep-rupture strength due to the loss of their "pinning" effect. Over-tempering is a lesser risk during fabrication because of the relatively short times of the thermal treatments. But in cases where multiple heat treatment cycles are applied in the fabrication of thick-walled components, weakening could become a significant issue at higher tempering temperatures.

It is the intercritical heating – rather than the over-tempering often cited in the literature – that causes the substantial reduction in strength observed in the Type IV region of welds made using these alloys (see Figs. 3.48 and 3.49). In a Type IV failure, cracking takes place in the fine-grained section of the heat-affected zone of a weldment. These failures are a matter of significant concern because they have occurred at a relatively early stage in component life – 20000 to 40000 hours – and at lower operating temperatures than the maximum design temperature of 599°C (1110°F).

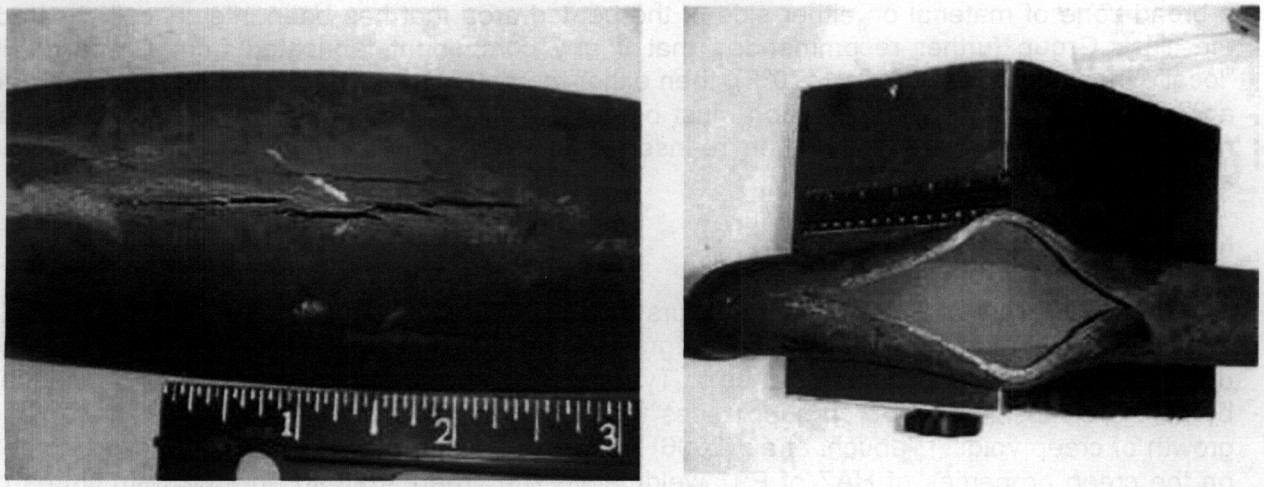

Figure 3.48. Failure of superheater tubes of T91 steel due to improper intercritical heat treatment. Tubes were in service for only four years [Henry 2005].

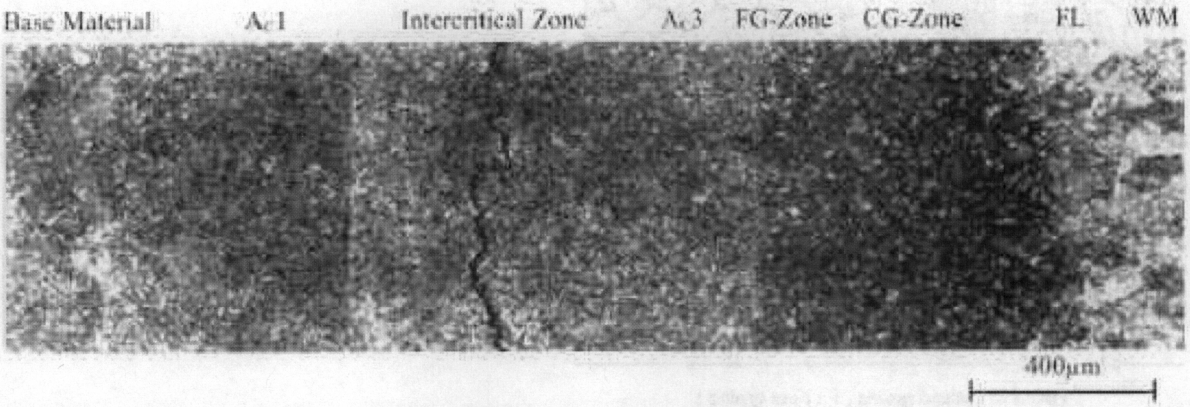

Figure 3.49. Type IV cracking in 9Cr-1Mo-1VNbN (E911) steel after 4295-h exposure at 650°C and 70 MPa [Klueh 2002].

In response to these issues, the ASME Task Group assigned to study Grade P91 material made several recommendations for new rules governing the thermal processing of Grade 91. These include:

- Normalizing in a tightly defined temperature range of 1040°-1080°C (1900°F-1975°F). The minimum temperature limit for normalizing will be established to insure complete re-solution of the most temper-resistant of the precipitates, while the maximum temperature limit will be imposed to minimize detrimental grain coarsening.

- Tempering in a tightly defined temperature range of 730-800°C (1350-1470°F). The minimum temperature limit for tempering will be established to ensure that sufficient precipitation is induced to stabilize the structure, and that a reasonable level of ductility is imparted to the material. The maximum temperature limit will be established to minimize the risk of the reduction in rupture strength that can occur when heating above AC_1.

During the course of its work, the Task Group learned that some US manufacturers had adopted the practice of hot-bending thick-walled pipe at temperatures above AC_3, and then performing a local re-normalization and tempering of the bend area. Since this practice leaves a broad zone of material on either side of the heated area that has been intercritically heated, the Task Group further recommended that if any component fabricated from Grade 91 is "locally" heated above 800°C (1470°F), then either the entire component must be re-normalized and tempered, or the heated section must be removed from the component in its entirety, re-normalized and tempered, and then re-inserted into the component by whatever means is appropriate.

Mitigation of Type IV Cracking

Type IV failure of P91 weldment occurs as a result of formation and growth of creep voids and cracks on the grain boundaries in fine-grained HAZ. In order to improve the creep strength of fine-grained HAZ and the resistance to Type IV cracking, strengthening of grain boundaries by boron is considered. Boron suppresses the coarsening of grain boundary precipitates and growth of creep voids. Tabuchi et al. (2006) have investigated the effect of boron and nitrogen on the creep properties of HAZ of P91 weldment. The creep strength and microstructures of P91 base metal and simulated HAZ were investigated with varying boron content from 0.005% to 0.014% and nitrogen content from 0.003% to 0.028%. The chemical compositions of five

P91 plates with thickness of 25 mm are given in Table 3.15. Effects of boron and nitrogen on creep behavior of these plates were investigated. Nitrogen content was lower than the conventional steel in order to avoid the formation of boron nitride and maximize the grain boundary strengthening effect of boron.

Table 3.15. Chemical composition (in wt.%) of P91 steels [Tabuchi et al. 2006]

Steel	C	Si	Mn	P	S	Cr	Mo	V	Nb	B	N
TA1	0.12	0.29	0.52	0.001	0.001	9.06	1.01	0.20	0.069	0.005	0.003
TA2	0.12	0.31	0.52	0.002	0.001	9.07	1.01	0.21	0.070	0.010	0.003
TA3	0.12	0.29	0.52	0.001	0.001	9.01	1.01	0.21	0.070	0.014	0.003
TA4	0.12	0.30	0.51	0.001	0.001	9.04	0.99	0.21	0.071	0.011	0.010
TA5	0.12	0.29	0.51	0.001	0.01	9.01	0.98	0.21	0.070	0.010	0.028

The measured Ac_3 temperature of the plates was about 900-920°C. The simulated HAZ specimens were produced by induction heating to the peak temperature of 900°C, which corresponds to intercritical HAZ, and gas cooling. PWHT was conducted at 740°C for 4h. Evaluation of HAZ microstructure showed that fine-grained HAZ structure (grain size <10μm) was formed independent of boron and nitrogen contents in the specimens. The creep tests were conducted at 600°C.

Creep test results for base metal at 600°C for 140 MPa are shown in Fig. 3.50. The average creep rupture time of P91 base metal is about 3000h under the same conditions [Kimura 2005]. Creep rupture lives of base metal with boron were comparable to the regular P91 steel in spite of its lower nitrogen content. The TA5 steel with 0.01% B and 0.028% N showed much higher creep strength than the other steels. This high creep strength may be due to the strengthening effect of vanadium nitride precipitates.

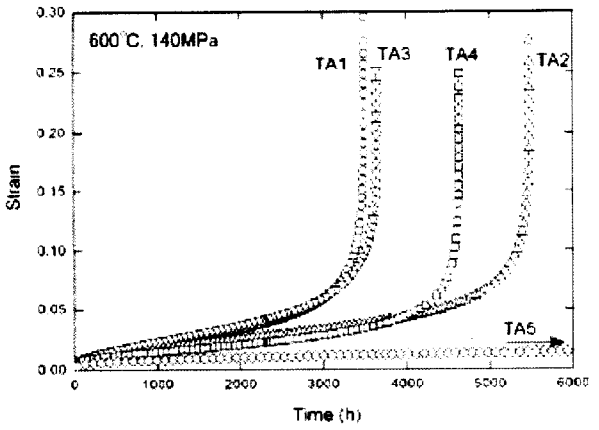

Figure 3.50. Creep test results for base metal of P91 with added boron at 600°C for 140 MPa [Tabuchi et al. 2006].

Creep test results for simulated P91 HAZ specimens at 600°C for 140 MPa are shown in Figure 3.51. The creep rupture lives of simulated HAZ specimen were lower than base metals because of their fine-grained structures. The creep rupture lives of simulated fine-grained HAZ of regular P91 steel (without any boron addition) under the same conditions was less than 100h as shown in Figure 3.51. The simulated HAZ of TA2, TA3 and TA4 steels with higher boron and lower nitrogen shower about 7 to 10 times better creep rupture times than that of simulated HAZ

of P91 steel. This is considered due to the grain boundary strengthening effect of boron [Horiuch 2002].

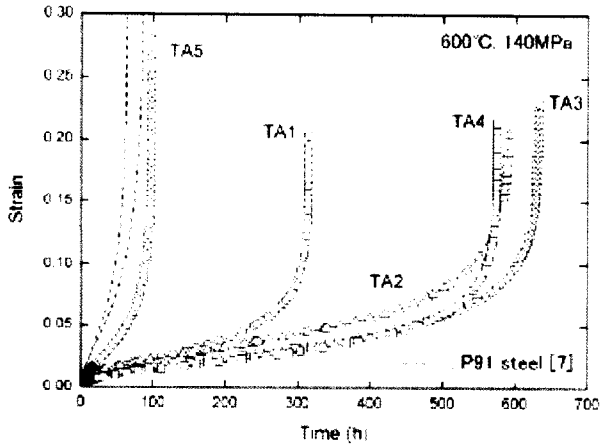

Figure 3.51. Creep test results for the simulated P91 HAZ with added boron at 600°C for 140 MPa [Tabuchi et al. 2006].

On the other hand, the simulated HAZ of TA5 steel with higher nitrogen showed lower creep rupture times, which are comparable with HAZ of regular P91steel, whereas its base metal showed the highest creep strength. For the TA5 steel, TEM micrograph revealed a fairly large amount of coarse BN precipitates. Therefore, it is considered that the grain boundary strengthening effect of boron is not sufficient for the fine-grained HAZ of higher nitrogen steel. From these results, the most appropriate content of boron is about 0.01% and that of nitrogen is <0.01% in order to improve the creep strength for both HAZ and base metal.

Boron addition also reduces susceptibility to Type IV cracking in other high-Cr steels. For example, specimens of 9Cr-3W-3Co-VNb steel plates with boron content varying from 47 to 180 ppm, welded by gas tungsten arc welding, were creep tested at 923K. It was found that the microstructures of the HAZ were quite different from those of conventional high Cr steels such as P91; the fine-grained HAZ did not exist in the steel weldment used in testing. Boron addition also has the effect of suppressing the coarsening of grain boundary carbides in the HAZ during creep. As a result of these phenomena, the welded joints of 9Cr-3W-3Co-VNb steel showed no Type IV fractures and much better creep life than those of conventional steels [Tabuchi et al. 2004].

Stress Corrosion Cracking of Grade P91 Weldments

If Grade P91 steel weldments are left in the untempered or as-welded condition, they can be susceptible to SCC. Although case histories of this failure mechanism in Grade P91 are still rare and the specific conditions under which SCC will occur have not been fully defined, it is known that the mechanism requires some combination of a susceptible microstructure, a high local tensile stress, and presence of a contaminant. In fact, it appears that mere condensation from exposure to a moist atmosphere may concentrate sufficient contaminant under certain circumstances to produce SCC in P91 piping left in the as-welded condition. Contamination with sulfur-bearing compounds (cutting fluids, lubricants, markers, etc.) will cause transgranular cracking, so they should not be used around Grade 91 in the as-welded condition. With Grade 91 steel, weldments should be heat treated as soon as practical after welding.

To eliminate the risk of SCC in P91, the weldment may be kept sufficiently warm to prevent condensation between the completion of welding and the initiation of PWHT. A disadvantage of this option, however, is that it might prevent users from performing the

radiographic testing typically performed on welds prior to PWHT. Mandating a sufficiently dry environment, rather than an elevated temperature, may be an alternative way to eliminate SCC while still allowing pre-PWHT radiographic examination. If warm or dry conditions cannot be assured, it would be prudent to limit the time between completion of welding and initiation of PWHT, to minimize the time that contaminants can enter the weldment. The risk of undetected SCC can be minimized by inspecting the weldment by liquid-penetrant or magnetic-particle testing following completion of PWHT. Because SCC can initiate on both the inner- and outer-diameter, these nondestructive tests need to be performed on all surfaces of the weldment

Cold Working of Grade 91 Steel

Recent studies have indicated that cold strain can adversely affect the creep-rupture strength of creep-strength-enhanced ferritic alloys. Even at low levels of cold strain, there is a discernable reduction in Grade 91's creep-rupture strength. Based on the results of the studies, the ASME Task Group assigned to study Grade P91 steel is considering action that will establish maximum limits for cold strain, above which it will be necessary to re-normalize and temper the full extent of the strained component. The likely maximum limit for cold strain, based on the available data, will be around 15-20% for Grade P91.

3.2.3.4 Mechanical Properties of Welded Sections

The mechanical properties of weld metal and heat-affected zone of P91 weldment are different that those of the base metal. The variations in hardness of P91 weldment were shown earlier in Figure 3.43. Note that the minimum hardness is in the heat-affected zone. The creep rupture time and creep-fatigue crack growth data are summarized in this section.

Figure 3.52 shows stress versus creep rupture time for the P91 weldment materials (base metal, weld metal, and HAZ) at 550, 600, and 650°C. In addition, failure locations in the weldments are also shown. Creep rupture properties of the weld metal and HAZ are lower than those of the base metal at all three temperatures. All the weldments failed in weld metal at 550°C. At 600°C, fracture occurred in the weld metal at the higher stress and shorter time. For rupture times greater than 4000 h, the failure location shifted to the HAZ. At 650°C, though fracture occurred in the weld metal for rupture time less than 1000 h, failure location was in the HAZ for rupture times greater than 7000 h [Watanabe 2006].

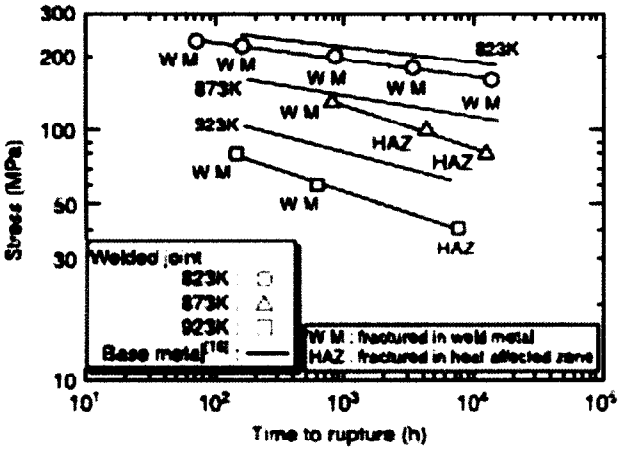

Figure 3.52. Stress versus rupture time for the P91 weldment materials: base metal, weld metal, and heat-affected zone.

Tabuchi and Takahashi [2006] have analyzed 370 creep rupture data points for P91 weldment from seven Japanese companies and institutes. The data were for P91 plate (238 data points), pipe (122 data points) and tube (10 data points) welded mainly by SAW and SMAW. PWHT was conducted at the temperature between 740 and 750°C. The creep tests were performed in the temperature range of 550 to 700°C; most tests were performed at 550°C (82 data points), 600°C (134 data points), and 650°C. The analysis of these data indicated that the creep strength of weldment was lower by a factor of 0.75 than that of base metal at 600°C due to Type IV fracture in HAZ. Weld strength reduction factors for 100000 h were determined as 0.85 at 575°C, 0.75 at 600°C, and 0.70 at 650°C.

Creep-fatigue interaction of high-temperature alloys can reduce life in a nonlinear manner. Figure 3.53 shows that interaction for P22 steel is quite severe as compared to Type 304 and 316 stainless steels, and interaction for P91 is more severe than that for P22 [ASME 2005]. The curves in Figure 3.51 are for base metal but the same rule is likely to apply to the welded components. As discussed earlier, some of the older plants are now using or planning to use P91 as a replacement material and new high efficiency advanced power plants are using 9Cr martensitic steels for thick section components. This is considered useful from the standpoint of fatigue damage because thinner section components made of high strength P91 steel will be less prone to fatigue cracking during the cyclic operation due to smaller temperature gradient through the wall thickness. However, recent creep and high temperature fatigue crack growth tests on welded P91 and P22 components have indicated that the creep-fatigue interaction could be even more severe in P91 components containing welds than in P22, as shown in Fig. 3.54. These tests were conducted at constant temperature but the load was cycled. These tests were funded by the European Commission funded project HIDA [Validation, expansion and standardization of procedures for high temperature defect assessment (HIDA)]. It must be mentioned that the results in Fig. 3.54 are based on tests on a single heat and at one test temperature. However, the results showed that cycling can be more harmful to P91 than to P22 on both large welded pipes (including both circumferential and seam welded) and fracture mechanics-type laboratory specimens [Shibli 2002].

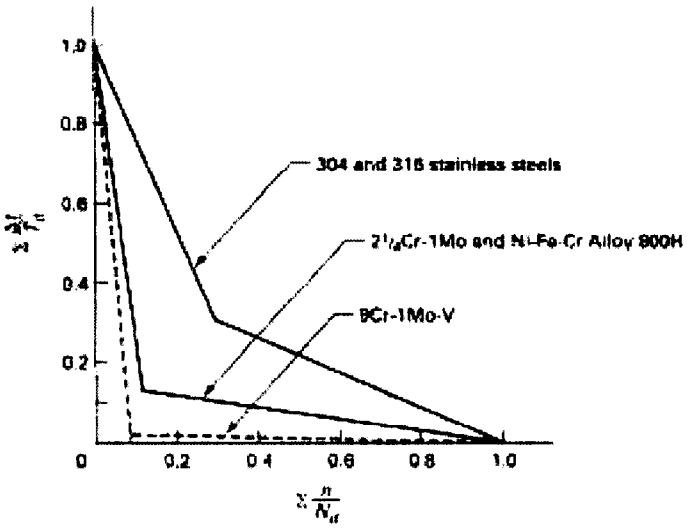

Figure 3.53. Creep-fatigue interaction for some of the high-temperature alloys including P22 and P91 steels [ASME 2005].

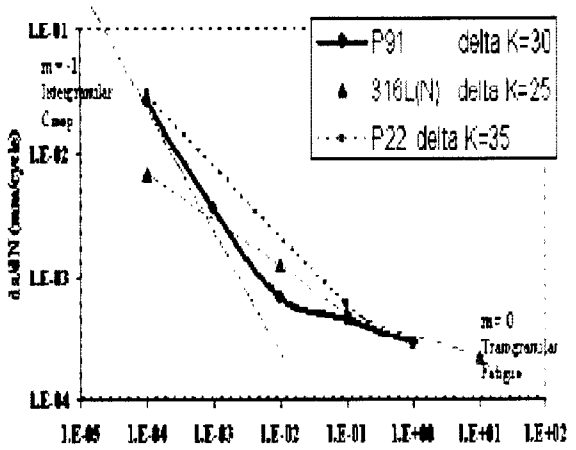

Figure 3.54. Creep-fatigue crack growth curves for some of the high-temperature alloys including P22 and P91 [Shibli 2002].

Takahashi [2006] has presented some additional results of creep-fatigue tests on P91 base metal, weldment, and simulated fine-grained HAZ (FGHAZ) at 550 and 600°C. In weldment, the failure always occurred in the FGHAZ regardless of test temperature and test duration. The shortest test duration at 550°C was 600 h. No Type IV failure with equally short duration has been previously reported in pure creep tests within the same temperature range. This suggests that Type IV failure tends to take place more easily in creep-fatigue conditions in comparison to pure creep conditions.

Creep-fatigue test results for P91 weldment at 550 and 600°C are presented in Fig. 3.55 [Takahashi 2006]. Results for two strain ranges (0.5% and 1.0%) are presented. The number of cycles to failure is plotted against hold time together with the results from the earlier Japanese tests on base metal. Introduction of hold time reduces the number of cycles to failure. The reduction was larger in weldment than in base metal at each temperature and strain range. The reduction was relatively large in the weldment even at 550°C, where the decrease in number of cycles to failure was insignificant in the base metal. The reduction in number of cycles to failure increases with increase in hold time.

The results of reduced number of cycles for P91 weldment during creep-fatigue tests is consistent with other test results presented in literature. Mannan et al. [2001] reports that with introduction of tensile hold, fatigue life of P91 steel decreases rapidly with increasing hold time up to 1 h. Tensile hold of 1 h reduces life to ≈25% of the continuous cycling life (i.e. no hold time). The reduction in life under creep-fatigue condition is attributed primarily to the reduction in strength of P91 steel due to microstructural degradation associated with the coarsening of precipitates and dislocation substructures.

Cabrillat et al. [2006] has analyzed results of uniaxial fatigue-relaxation (strain-controlled during hold time) tests and creep-fatigue (stress-controlled during hold time) tests on P91 steels at 550°C. The hold time was either in tension or in compression and it ranged from 0.5 min to 30 min. The authors then present results for creep-fatigue life evaluations using creep-fatigue rules and material data codified in RCC-MR and ASME Codes and the predictions are compared to experimental results. The paper concludes that the use of RCC-MR procedure provides a good prediction of experimental results of the uniaxial creep-fatigue tests. All the experimental results are correctly located in the RCC-MR creep-fatigue interaction diagram, which is similar to the one for stainless steel shown in Fig. 3.53 (interaction point coordinates 0.3, 0.3). With respect to ASME Code creep-fatigue interaction curve for P91 (see Fig. 3.53), the results show that the interaction diagram is too severe for the uniaxial tests considered here.

In order to complete the validation of RCC-MR Code, it will be necessary to (1) analyze available fatigue-relaxation results, (2) consider hold time of 60 minutes and longer, and (3) perform multiaxial tests and analyze the results.

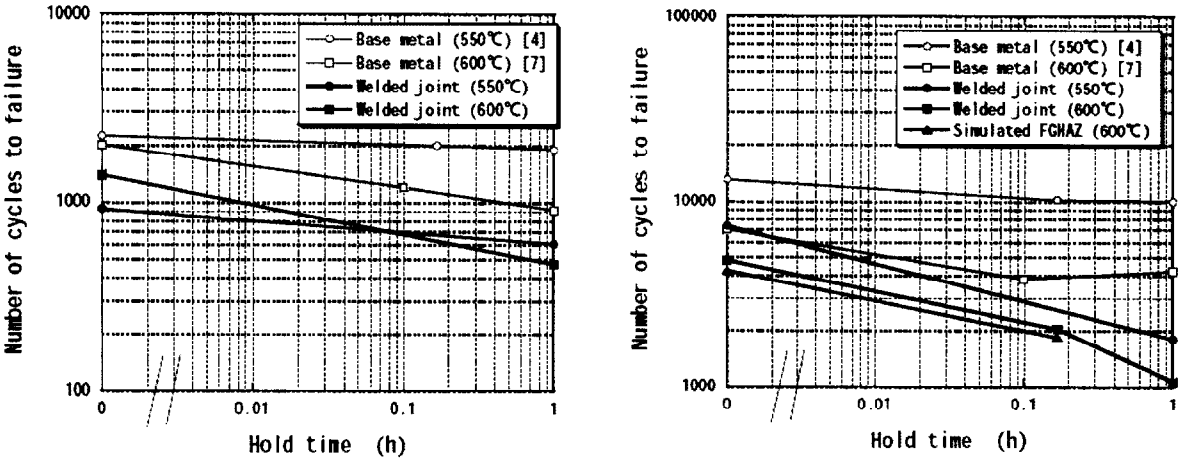

(a) Strain range : 1.0%

(b) Strain range : 0.5%

Figure 3.55. Comparison of creep fatigue lives of P91 base metal and welded joint specimens [Takahashi 2006].

3.2.3.5 Service Experience of Welded Sections

Grade P91 steels require special treatment because they air harden and exhibit very little ductility in the as-welded condition. Preheating at elevated temperature, interpass temperature control, and PWHT are necessary for all weldments, regardless of the component thickness. However, there is a lack of understanding of the significant differences in welding of P91 steel versus the low-alloy steels, traditionally used in the power industry. P91 steel is less tolerant to temperature variations during welding and in post-weld heat treatment. This lack of understanding has resulted in several failures in the field. Problems that significantly impair the creep-rupture strength of P91 steels are over-tempering, under-tempering, and exposure to temperatures in the intercritical region. Other concerns for use of these materials are the reduced creep strength of the Type IV region within the HAZ compared to the base metal, reduced strength of the softer carbon-depleted zone in a dissimilar metal weld, persistent fabrication- or service-induced residual stresses for components that operate below 566°C, a higher sensitivity to transient or steady state over-temperature events, and improper fabrication. Since Grade 91 steel is primarily used in fossil plants as tube and piping materials, all the failures discussed here are the ones experienced in those plants.

Exposure to the Intercritical Region and Type IV Cracking

This example includes a rupture of a superheat header outlet terminal tube. The header was designed to operate at a temperature of 566°C (1,050°F) and a pressure of 16.7 MPa (2460 psi). Both tube and headers were specified to be Grade 91 material. The tube size was 53.98-mm (2.125-in.) outer diameter with a 6.10-mm (0.24-in.) wall thickness. The failure was at 16.5-mm (6.5-in.) radius bend as shown in Fig. 3.56 and the failure mechanism was determined to be creep or creep-fatigue. The metallurgical investigation confirmed the chemical composition as

that of SA-213-T91 material, and the tubing dimensions beyond the failure area were within specification.

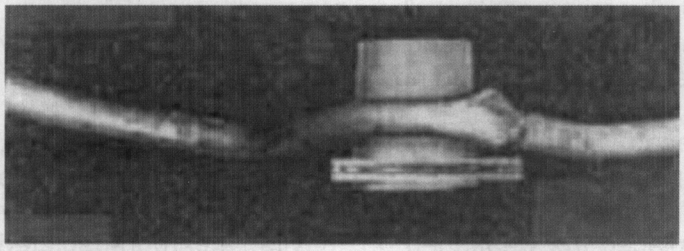

Figure 3.56. Creep or creep/fatigue failure of superheat outlet tube [Cohn et al. 2005].

The metallurgical investigation of the microstructure and hardness measurements did not reveal any obvious evidence of significant overtempering. However, a review of mill test reports revealed that tempering was performed at 816°C (1500°F), which is above the lower critical temperature (AC_1) (See Fig. 3.39). The investigation suspected that partial re-austenization of the microstructure occurred during the mill tempering process.

A series of creep rupture tests performed on the tubing material indicated that the rupture strength of the tubing was slightly better than that of SA-213-T22 (2.25 Cr-1 Mo) tubing. The investigation concluded that the mill heat treatment was deficient for the tubing. All of the T91 material supplied by the mill had to be either heat treated again or replaced.

Improper Fabrication and Undertempering

A girth weld of a small bore of a P91 pipe in a heat-recovery steam generator (HRSG) unit failed during erection on light impact. The weld was extremely brittle, with a measured weld hardness of 445 HV. This indicates that there was no PWHT of the small bore Grade P91 pipe. It was determined that the welding procedure for the pipe did not require cooling below the M_f temperature. In addition, there were fabrication issues with Grade T91 harps in the HRSG unit. The fabricators attempted to perform PWHT on too many harps at the same time, with an insufficient number of thermocouples. As a result, the effective temperature of PWHT was around 650°C (1200°F) and many of the tube weldments in the harps were undertempered and had hardness up to 470 HV.

Improper Joint Design

Another problem that has been experienced in the field is imprudent joining of Grade P91 material to dissimilar alloys – typically to Grade 11, 22, or austenitic stainless steels. One plant owner in the US was forced to rework the welded connection between the main-steam piping and the steam-turbine stop valve on three of its 500-MW, F-class combined-cycle plants [Henry 2005].

The oldest of the three plants, which had fewer than 5000 service hours, found a through-wall crack 135 deg around the circumference of the weld, and 24.5 in. long, while the steam line was in service. The second oldest plant used liquid-penetrant testing to locate a crack that was 20 deg around the joint but had not yet penetrated the wall. In the latest of the three plants, cracks could not be detected with liquid-penetrant testing, but the welds were replaced anyway because joint design was similar to those in the other two plants.

The failed weld connected an 18-in.-diameter Grade P91 pipe with a wall thickness of 1.56 in. to a valve casing made of 1.25Cr-1Mo-0.2V with a wall thickness of 3.00 in. The filler metal

selected was B3 (2.25Cr-1Mo) with no dimensional transition piece. An investigation confirmed that no codes were violated in the welding or PWHT procedures. But the failure determined to be initiation and propagation of the crack through the carbon-depleted zone that is an inevitable feature of weld joining materials of different chromium content. In other words, the joint design, with its lack of a dimensional transition piece between P91 and a dissimilar alloy, was entirely inappropriate and was susceptible to fail prematurely, yet it did not violate existing code rules.

At all three plants, the joint was replaced with a Grade P91 dimensional transition piece, which matched the pipe-wall thickness at one end and the valve nozzle at the other. The piece featured a P91-to-P91 weld at the thin end, and a P91 to 1.25 Cr-1Mo-0.2V weld at the thicker end using B9 filler. This new joint design placed the weakened but inevitable carbon-depleted zone in the thicker section of the joint where the stresses were lower and more favorably distributed.

During the root-cause analysis of this piping failure, investigators learned that many, if not all, Grade P91 piping systems are installed without "cold spring." This common practice is based on the faulty assumption that Grade 91, like traditional alloys, will relieve high-temperature steady-state stresses by creep relaxation during the early stages of operation. In many cases, however, the high-temperature creep strength of the Grade 91 material is such that at normal operating temperatures the material will not "relax" sufficiently fast to relieve these stresses. This can lead to a condition of "elastic follow-up" in which the joint is subjected to a secondary stress that behaves like a primary stress. Thus, a better industry practice would be to install Grade P91 piping with cold spring, so that the piping system is not stressed at elevated temperatures, where accelerated creep damage will occur.

3.3 RPV Fabricability

The NGNP RPV is anticipated to have dimensions ≈8 m diameter and ≈24 m height, similar to the GT-MHR design indicated in Table 3.16. The wall thickness of the NGNP RPV is expected to be between 100–300 mm depending on the material used and the operating conditions. The candidate materials should be manufactured to the required dimensions using a method that provides the maximum life of the pressure vessel with minimum inspection requirements. There are two possible ways of manufacturing the pressure vessel as described below.

- Forged seamless rings of required vessel diameter and thickness, and welding of these rings to achieve the required height. The advantage of this method is the presence of only circumferential welds in the finished pressure vessel.

- Plates (either rolled or forged) of required thickness that are initially machined to a circular shape and, subsequently welded longitudinally to the required vessel/ring diameter. In addition, many such rings have to be welded circumferentially to achieve the final height of the pressure vessel. Understandably, this method will introduce additional welds in the longitudinal direction that may provide more hot spots for weld failure thereby requiring more stringent inspection requirements.

As the radiation levels in the NGNP vessel are expected to be very low (<0.001 dpa), radiation embrittlement along the welds may not be a concern in the NGNP. Nevertheless, it is preferable to manufacture the vessel by a seamless ring forging method simply because the number of welds (and resulting hot spots) are lower in this method.

Table 3.16. Forging capability of UNSK90901 (9Cr-1Mo-V-Nb) for NGNP RPV (dia. ≈8 m, ≈24 m height and thickness 100-300 mm)

Manufacturer (Contact)	Current Ring Forging Capability	Future/Upgrade Plans	Viability to forge K90901
Japan Steel Works, Japan (Mr. Tom Noda)	8 m Outer Diameter (OD) but not for K90901 (experience only on SA-508)	May be inclined to try 2.25Cr-Mo steel but not K90901 steel	RINGS - NO PLATES - NO
Bruck Forgings, Germany (Ms. Rita Roland)	5.2 m OD (max)	8m rings in 2-3 years (not necessarily for K90901)	RINGS - NO PLATES - NO
Saarschmeide, Germany (Dr. Dieter Bokelmann)	< 5 m	Probable investment in large forging press by 2009 (not necessarily for K90901)	RINGS - NO PLATES - YES*. ≈6 m length, ≈ 2.5 m width for a total of about 55 plates
Scot Forge, IL (Mr. Bill Michaud)	6 m OD (max)	None	RINGS - NO PLATES - NO
Doosan Heavy Industries, South Korea KAERI)	Overall experience in using modified 9Cr-1Mo for fossil applications but not for nuclear applications. Korean Atomic Energy Research Institute (KAERI) is in talks with DHI to fabricate the thick section vessel using modified 9Cr-1Mo steel. Also, KAERI is interested in investing/funding DHI for this project.		

* No experience in manufacturing plates of Grades 91 or 22V.

3.3.1 Low Alloy Steel

SA508 forgings and SA533 plates are currently being used in LWR pressure vessels. Capabilities do exist for manufacturing 508 forgings of the required NGNP vessel dimensions. Japan Steel Works have fabricated ring forgings of SA508 steel of 8 m diameter. Manufacture of plates is also not anticipated to be a problem with SA508/SA533 material. Fig. 3.57 shows a picture of large diameter forging manufactured by Japan Steel Works.

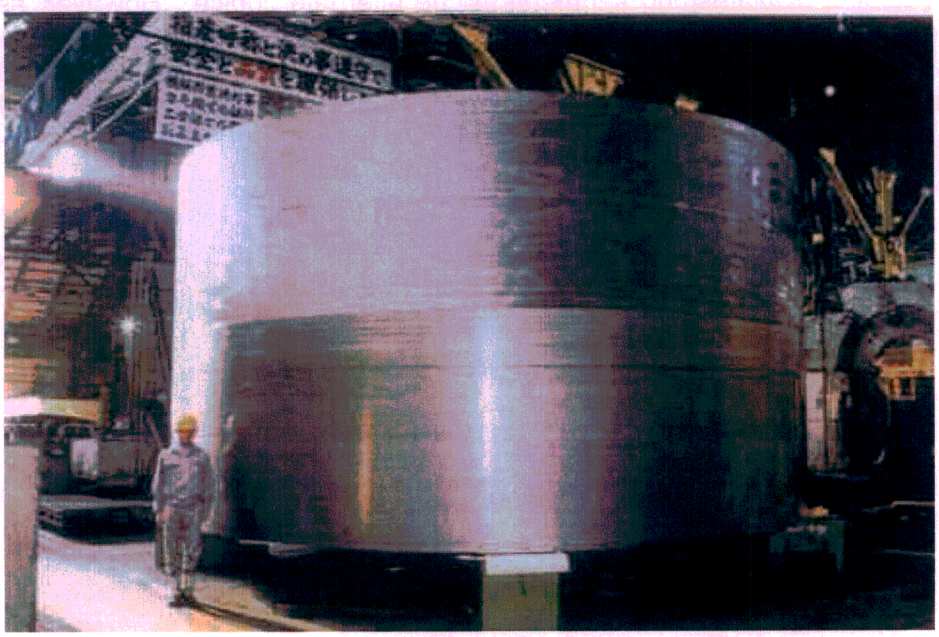

Figure 3.57. Large diameter ring forgings manufactured by Japan Steel Works [Nanstad, 2004].

3.3.2 Fe-2.25 Cr-1 Mo- V Steel

Fe-2.25Cr-1Mo-V steel (UNS K31835) is extensively used in the fossil industries and hydrogenation reactor pressure vessels. There is no available information on existing pressure vessels having dimensions similar to that required in the NGNP RPV. However, due to the large scale use of this material in fossil, petrochemical industries, etc. there is relatively more experience in forging/rolling thick-sections of this material than say, modified 9Cr-1Mo. There have been studies to evaluate the thick-section properties of this material as discussed earlier. A recent paper by Doosan Heavy Industries (DHI), South Korea [Kim et al. 2006] discusses the aging response of a forged 2.3-m inner dia. and 400-mm thick 2.25Cr-1Mo-V material. Although this study was aimed at petrochemical applications, the ability of DHI to fabricate thick-section forging of this material suggests that it should not be a difficult task to fabricate the NGNP RPV from this material. Japan Steel Works, if persuaded, may be willing to invest in large diameter thick-section forgings of this steel.

3.3.3 Fe-9 Cr-1Mo Steel

Modified 9Cr-1Mo steel (UNS K90901) has overall superior mechanical properties among the three candidate materials that makes them primary candidates for use in the NGNP RPV. As there is not much information on thick-section properties/fabrication experience of this material, a concentrated effort was focused on finding vendors from all over the world to assess their capability for forging modified 9Cr-1Mo steel. Table 3.16 also gives the forging capability of several vendors who had significant experience and capability to forge large diameter steel rings. As seen from the table, none of the vendors have the capability, at present, to forge thick-section large diameter rings of modified 9Cr-1Mo steel. From our conversation with Japan Steel works, it was clear that they are not willing to upgrade their existing facility to facilitate forging of F91 unless an incentive is offered to them (in terms of assured market/customers to order RPV of F91, or in some other form). Without any incentive, they seem not willing to invest in forging F91 grade. Other vendors who were contacted did not have enough experience and have little or no capability in forging large diameter steel rings.

As ring forging of RPV using modified 9Cr-1Mo steel does not appear to be a feasible option at present, axial welding of plates/ring segments is the alternate choice. However, as indicated in the table above, none of the vendors have experience in manufacturing thick-section plates too. Saarschmeide, Germany is confident that they can fabricate plates of this steel, but as indicated in the table, it would require ≈55 plates to achieve the final RPV. As one can imagine, there would be a lot of welds in the completed RPV.

4. ASME-Code Compliance Calculations

The ASME Boiler and Pressure Vessel Code, Section III allows the use of Subsection NB for designing Class I ferritic steel nuclear components operating at temperatures ≤371°C (700°F). Limited excursions into higher temperatures are permitted provided it can be shown that the resulting creep strains are negligible. If creep strains are not negligible, Subsection NH must be applied. The permissible materials under Subsection NH are much more limited than under Subsection NB. However, the reactor pressure vessels of both the prismatic and pebble bed designs are proposed to be made of the ferritic alloy 9Cr-1Mo-V, which is permitted under both Subsections NB and NH.

We have analyzed both RPV designs for normal operation as well as a postulated depressurized conduction coolant accident. The coolant temperature and pressure data were obtained from Idaho National Laboratory [Davis 2006, Gougar and Davis 2006].

The RPV for the prismatic core design has an outside diameter of 7.658 m with a wall thickness of 0.216 m, while the outside diameter and wall thickness for the pebble bed core design are 7.204 m and 0.180 m, respectively. Both designs operate under a nominal He coolant pressure of 7 MPa during normal operation. During a depressurized conduction coolant accident, the coolant pressure rapidly reduces to atmospheric, but the temperature of the RPV goes through a transient heat up which can exceed 371°C significantly. The temperature and heat flux data for the normal operation as well as the accident condition were obtained from Davis [2006]. Both thermal conduction and stress analyses were conducted using the finite element code ABAQUS.

4.1 Primary Membrane Stress

The primary membrane stress intensity during normal operation is required by Subsection NB to be limited by S_m, evaluated at the thickness-averaged temperature. The maximum primary membrane stress intensity and the maximum thickness-averaged temperature (calculated by RELAP5) for the prismatic core design RPV are 117 MPa and 427°C, respectively, and the same for the pebble bed core design RPV are 133 MPa and 360°C, respectively. The maximum RPV wall temperature for the pebble bed RPV, as calculated by an alternative pebble bed specific code, is greater than 371°C. The negligible creep curve, defined in Appendix T-1324 of Subsection NH, for 9Cr-1Mo-V as reported by Riou et al. [2006] is plotted in Fig. 4.1. The maximum allowable time at 427°C below which creep effects can be ignored is much less than the 60 yrs design lifetime whether one uses the more conservative RCC-MR creep data or the less conservative ASME creep data. Therefore, creep effects cannot be ignored for the prismatic core design and we have to use Subsection NH, which requires the primary membrane stress intensity to be limited by S_{mt}, evaluated at the thickness-averaged temperature and design lifetime. The maximum value of the design lifetime for which Subsection NH provides data for 9Cr-1Mo-V steel is $3x10^5$ h. A plot of the allowable primary membrane stress intensities (S_m and S_{mt}) vs. temperature for the primary candidate alloy 9Cr-1Mo-V steel is shown in Fig. 4.2, which also shows (symbols) the primary membrane stress intensities for prismatic and pebble bed core designs where the temperature for the pebble bed design was calculated by RELAP5. As mentioned earlier, an alternative code specific to pebble bed design predicted higher temperature (>371°C) than RELAP5. It is clear that both designs satisfy the general primary membrane stress criterion for this material, even if the RPV temperature for the pebble bed design is 50°C higher than shown in Fig. 4.2.

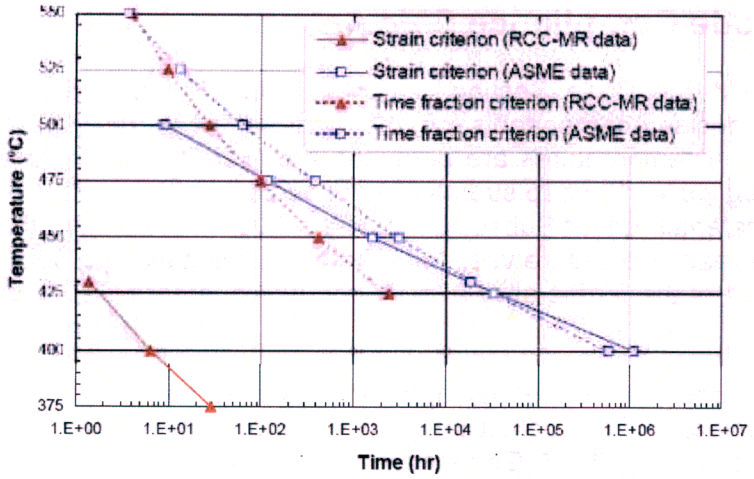

Figure 4.1. Negligible creep curve for 9Cr-1Mo-V steel [Riou et al. 2006]

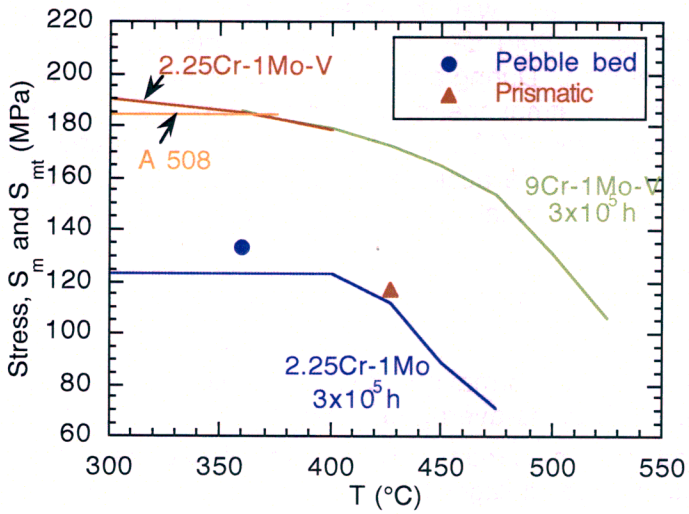

Figure. 4.2. Variation of primary membrane stress intensity and allowable primary membrane stress intensities as functions of temperature and time.

Figure 4.2 also shows the allowable primary membrane stress intensity plots for 2.25Cr-1Mo (permitted in Subsections NB and NH), A 508 (permitted in Subsection NB but not in NH), and 2.25Cr-1Mo-V (not permitted in Section III, but permitted in section VIII up to 400°C) steels. It is evident that the Subsection NH-approved 2.25Cr-1Mo steel does not have sufficient strength for either design. A 508, which is used extensively as a light-water reactor pressure vessel material, also has sufficient strength for the pebble bed design provided the temperature is ≤371°C. Code Case N-499 allows the use of this material up to 427°C for Service level B and 538°C for service levels C and D (accidents) for limited excursions not exceeding 1000 h. But this time limit is much shorter than the design lifetime (60 y) envisioned for the RPVs. Figure 4.2 shows that 2.25Cr-1Mo-V also has sufficient strength up to 400°C and there is limited creep rupture data in the literature that indicate that it may have adequate high temperature strength for both designs. However, this material is currently not permitted in Section III.

4.1.1 Weldment

Although the precise fabrication method for the RPV is yet to be determined, either axial or circumferential welding will be used. According to Subsection NH Table E 1-14.10 E-1, the

stress rupture factor for 9Cr-1Mo-V welded with code-approved weld and procedure is 1.0 up to 425°C. Therefore, there is no reduction in the stress rupture strength for the welded structure compared to the base material.

4.2 Primary Plus Secondary Stress

4.2.1 Prismatic Core Design RPV

Distributions of the steady-state temperature at the OD and ID surfaces of the prismatic core design RPV during normal operation are plotted in Figs. 4.3 and 4.4, respectively. The maximum ID temperature is 448°C and the corresponding OD temperature is 394°C. Stress distribution during normal operation due to pressure and temperature was determined using elastic finite element analysis. The distributions of the von Mises effective stress at the OD and ID surfaces are plotted in Figs. 4.5 and 4.6, respectively. The maximum stresses at the OD and ID are 161 and 108 MPa, respectively. Since the peak temperature is >371°C, Subsection NH needs to be applied.

There are several tests in Subsection NH T-1320 for satisfying the strain limits for structural integrity using elastic analysis. The simplest Test A-1 in T-1322 requires the following inequality to be satisfied:

$$X + Y \leq S_a / S_y \qquad (1)$$

where $X = P_L/S_y$, and $Y = Q_R/S_y$, P_L is primary membrane stress intensity, Q_R is the maximum thermal stress intensity range, S_y as the average of the two S_y values corresponding to the maximum and minimum wall-averaged temperatures during the cycle and S_a is the lesser of

(1) 1.25 S_t using the highest wall-averaged temperature during the cycle, and a time of 10000 h, which in the case of the prismatic core design RPV is 276 MPa (420°C), and

(2) The average of the two S_y values corresponding to the maximum and minimum wall-averaged temperatures during the cycle, which for the prismatic core design RPV is 377 MPa.

For the Prismatic core RPV, P_L=117 MPa, Q_R = 44 MPa, and S_y = 377 MPa. Substituting these values into Inequality 1, X + Y = 0.43 and S_a/ S_y =0.73, showing Inequality 1 is satisfied.

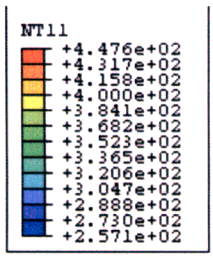

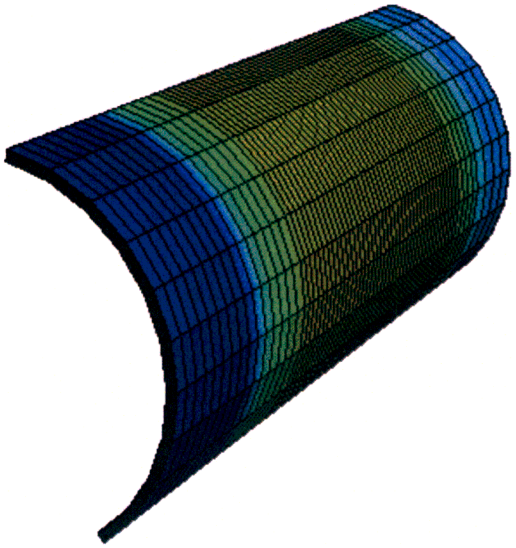

Figure 4.3. Distribution of temperature at the OD surface of prismatic core design RPV during normal operation.

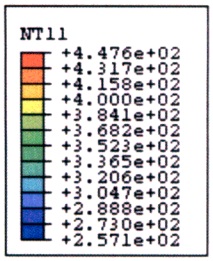

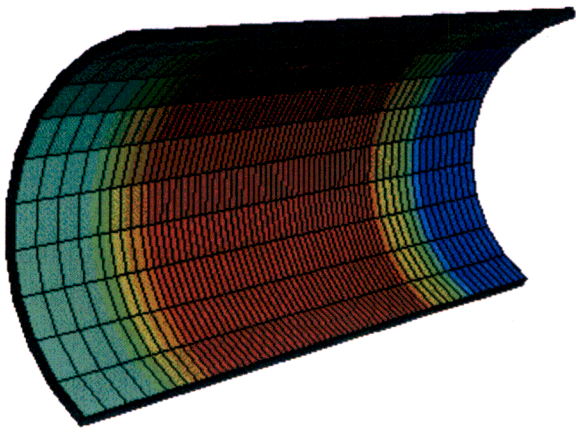

Figure 4.4. Distribution of temperature at the ID surface of prismatic core design RPV during normal operation.

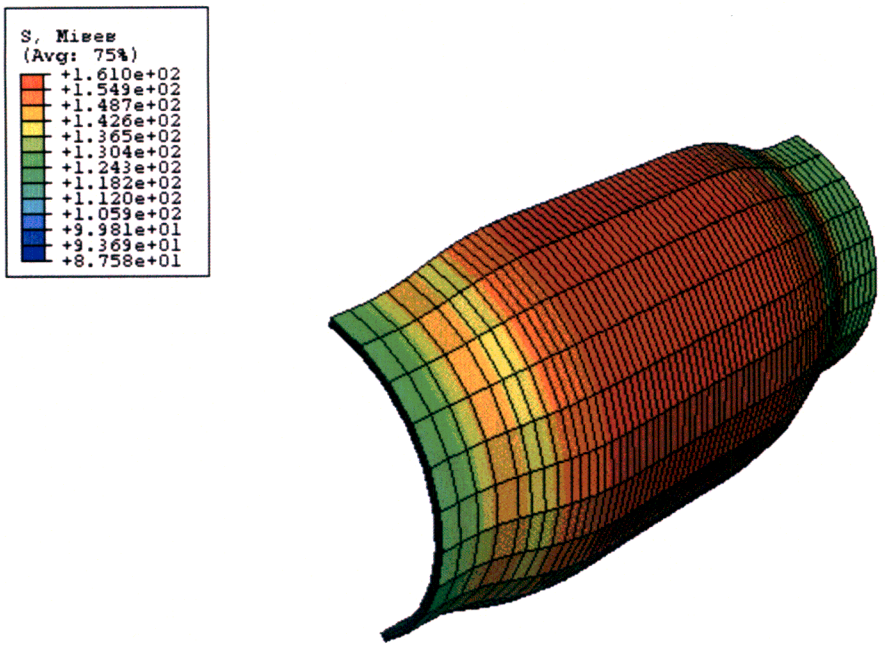

Figure 4.5. Distribution of von Mises effective stress at the OD surface of prismatic core design RPV during normal operation.

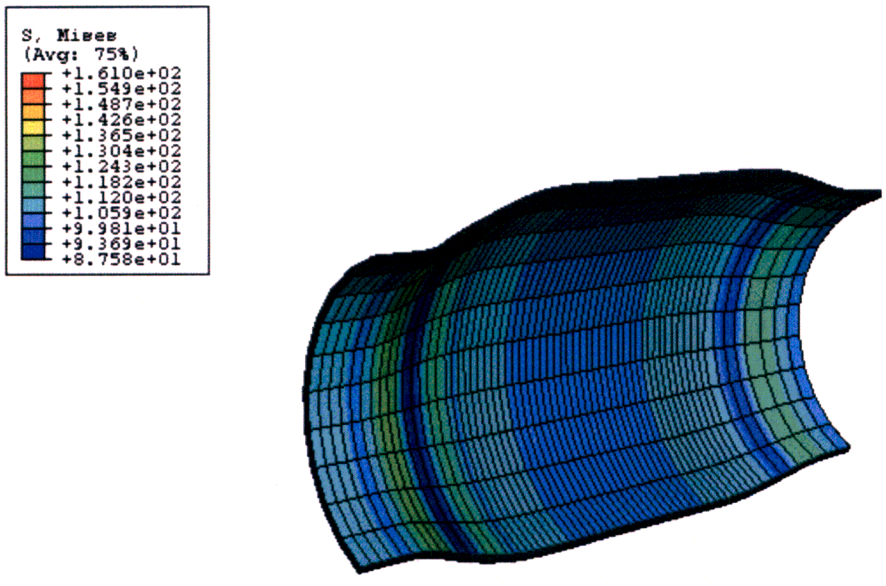

Figure 4.6. Distribution of von Mises effective stress at the ID surface of prismatic core design RPV during normal operation.

4.2.2 Pebble Bed Core Design RPV

Distributions of the steady-state temperature at the OD and ID surfaces of the pebble bed core design RPV during normal operation are plotted in Figs. 4.7 and 4.8, respectively. In contrast to the prismatic core design, the maximum ID temperature occurs near the bottom end of the RPV and is equal to 375°C and the corresponding OD temperature is 337°C. Stress distribution during normal operation due to pressure and temperature was determined using elastic finite element analysis. The distributions of the von Mises effective stress at the OD and

ID surfaces are plotted in Figs. 4.9 and 4.10, respectively. The maximum stresses at the OD and ID are 163 and 128 MPa, respectively.

Since the peak temperature is close to 371°C, we can use Subsection NB rules for this case. The thermal stress ratchet rule in NB 3222.5 requires the following inequality (Bree diagram) to be satisfied:

For $0<X<0.5$, $Y \leq 1/X$, and (2a)

For $0.5<X<1$, $Y \leq 4(1-X)$ (2b)

where X and Y have the same definitions as in Eq. 1.

For the pebble bed case, X = 133/377 = 0.35 and Y = 30/377 = 0.08. Therefore, we need to satisfy inequality 2a, i.e., Y ≤ 2.86, which is easily satisfied.

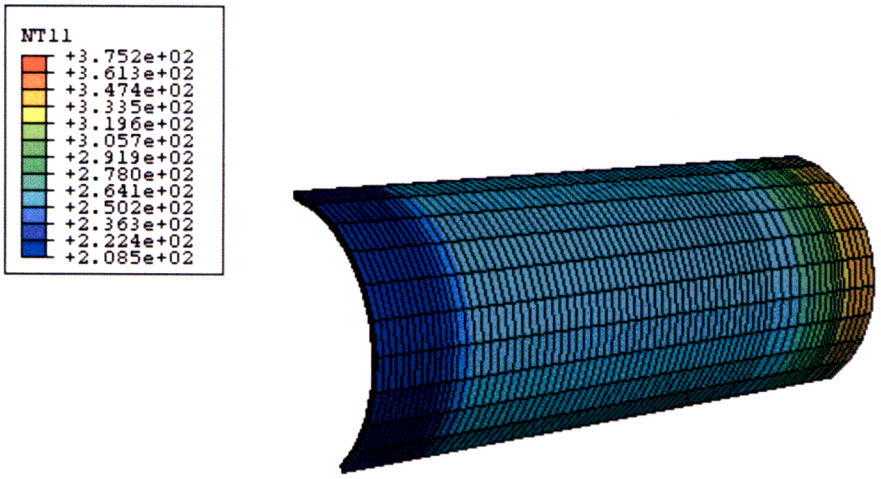

Figure 4.7. Distribution of temperature at the OD surface of pebble bed core design RPV during normal operation.

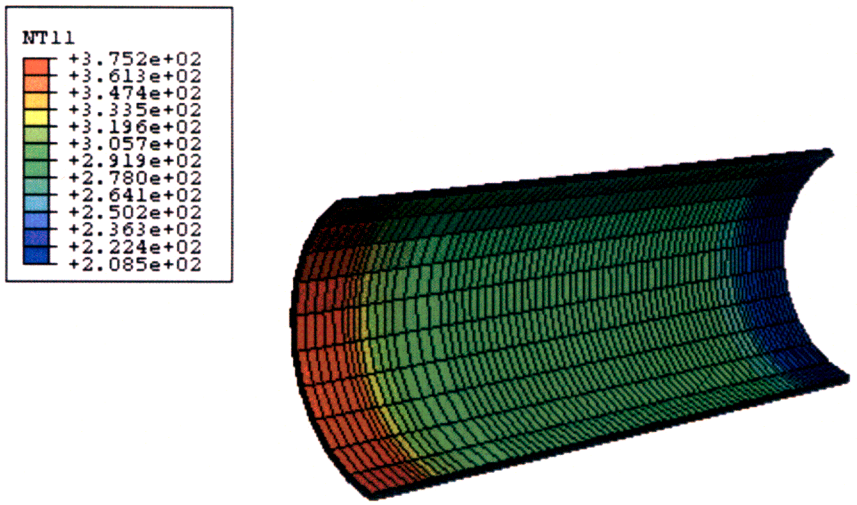

Figure 4.8. Distribution of temperature at the ID surface of pebble bed core design RPV during normal operation.

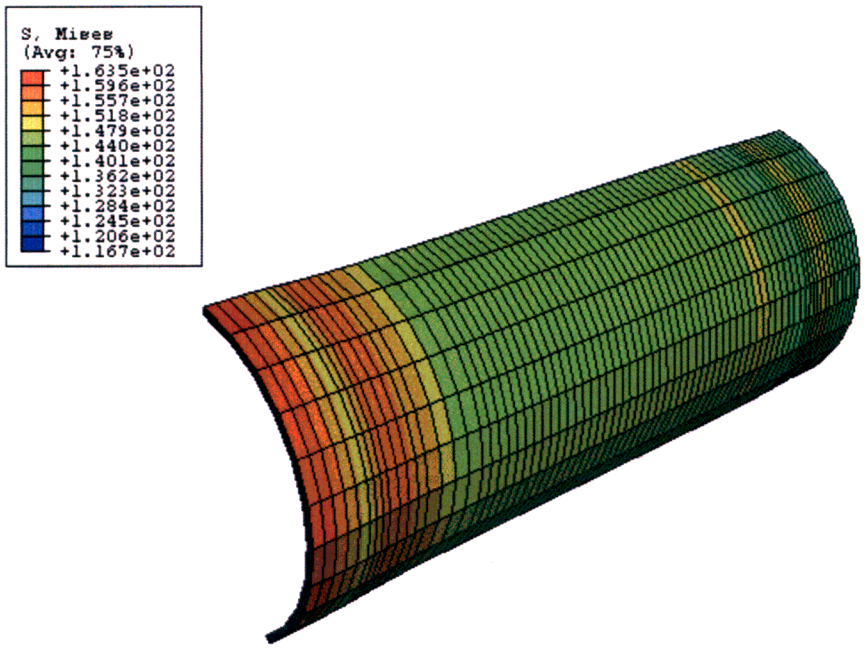

Figure 4.9. Distribution of von Mises effective stress at the OD surface of pebble bed core design RPV during normal operation.

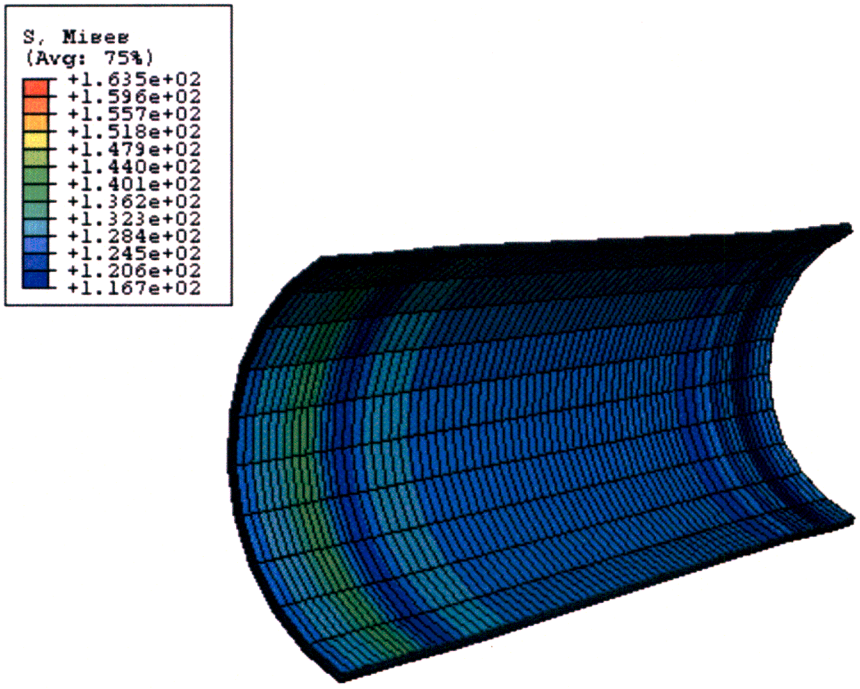

Figure 4.10. Distribution of von Mises effective stress at the ID surface of pebble bed core design RPV during normal operation.

4.3 Depressurized Conduction Coolant Accident

Since the RPV of both designs are rapidly depressurized during this accident there are no primary stress limits to satisfy. However, both designs undergo a time-dependent transient during which the temperature of the RPV exceeds 371°C into the creep range of the material

and thermal stresses are generated. Therefore, stress analyses were conducted allowing for both elastic and creep deformation to occur.

4.3.1 Prismatic Core Design

A transient heat conduction analysis was conducted with surface heat fluxes prescribed at the ID and OD surfaces up to a time of 3.5×10^5 s. These heat fluxes were obtained from a RELAP5 run conducted by C. Davis at INL.[1] In the RELAP5 analysis, heat flow was assumed to be in the radial direction and all axial heat conduction in the RPV was ignored. A comparison of the temperature distributions at the ID and OD surfaces at 2.25×10^5 s calculated using ABAQUS and RELAP5 is shown in Figs. 4.11a-b, respectively. As a result of ignoring axial heat conduction in the RELAP5 run, although the results are close, the peak temperature computed by ABAQUS is lower than that by RELAP5. A similar comparison for the temperature variation at a given location with time, plotted in Fig. 4.12, shows results that are close at short times ($<2 \times 10^5$ s) but the temperatures calculated at longer times by ABAQUS are less than those by RELAP5.

The temperatures calculated by ABAQUS were input into a stress analysis that accounted for elastic as well as creep deformation. Variations of the axial and hoop stresses along the axial direction at the ID and OD surfaces at 2.2×10^5 s are shown in Figs. 4.13 a-b, respectively. Similar variations of the von Mises effective stress and effective creep strain are shown in Figs. 4.14 a-b, respectively. Note that the maximum accumulated creep strain is negligible. Fig. 4.15 shows the time variations of the temperature and von Mises effective stress at the critical location. The temperature reaches a peak and then decreases slightly with time at the end of the transient. For reference, the minimum value of the yield strength of 9Cr-1Mo-V steel at 525°C is 377 MPa and the minimum time to stress rupture at a constant stress of 120 MPa and at a constant temperature equal to the peak temperature of 525°C is $>3 \times 10^5$ h.

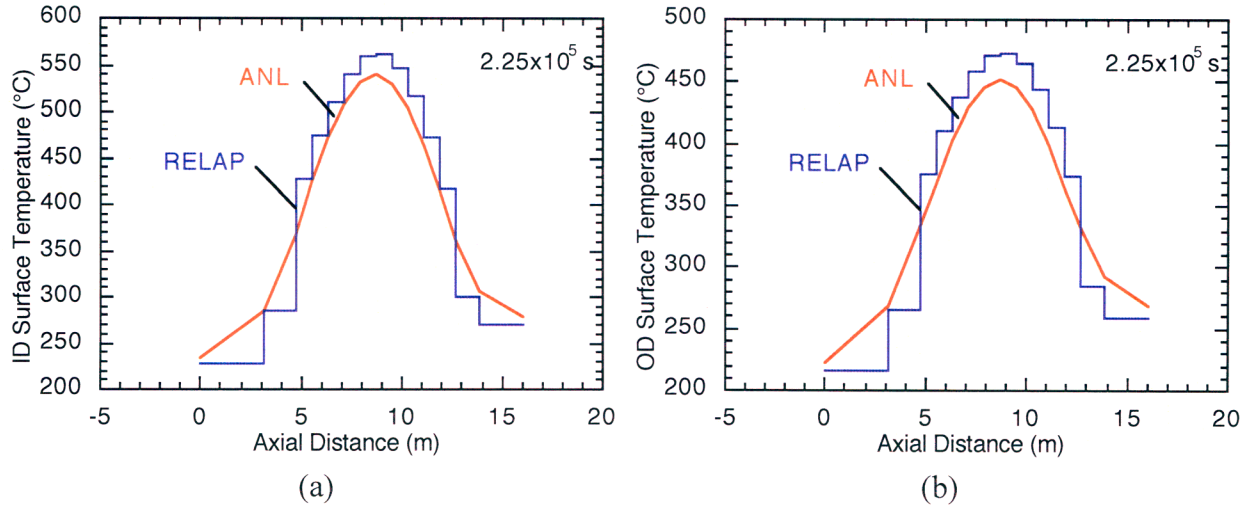

Figure 4.11. Distribution of temperature at the (a) ID and (b) OD surface of the prismatic core RPV at 2.25×10^5 s during a depressurized conduction coolant condition.

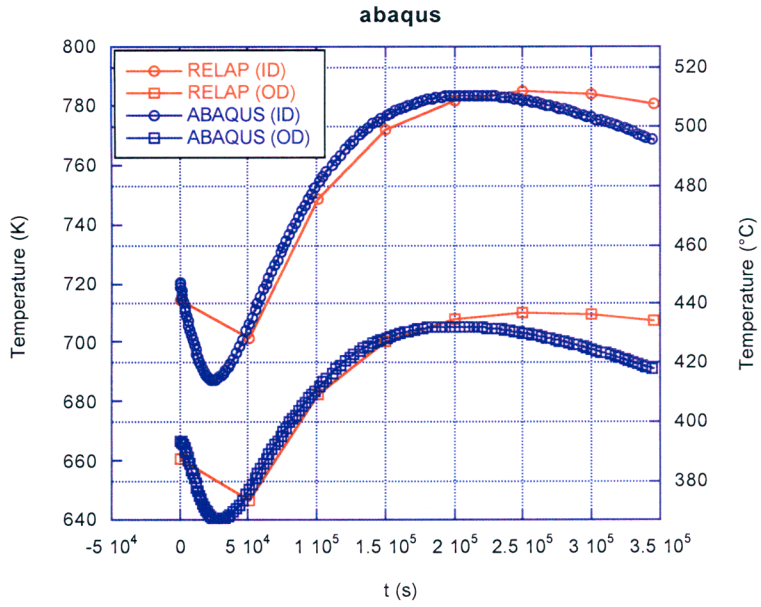

Figure 4.12.. Comparison of ID and OD temperature variations as computed by RELAP5 and ABAQUS.

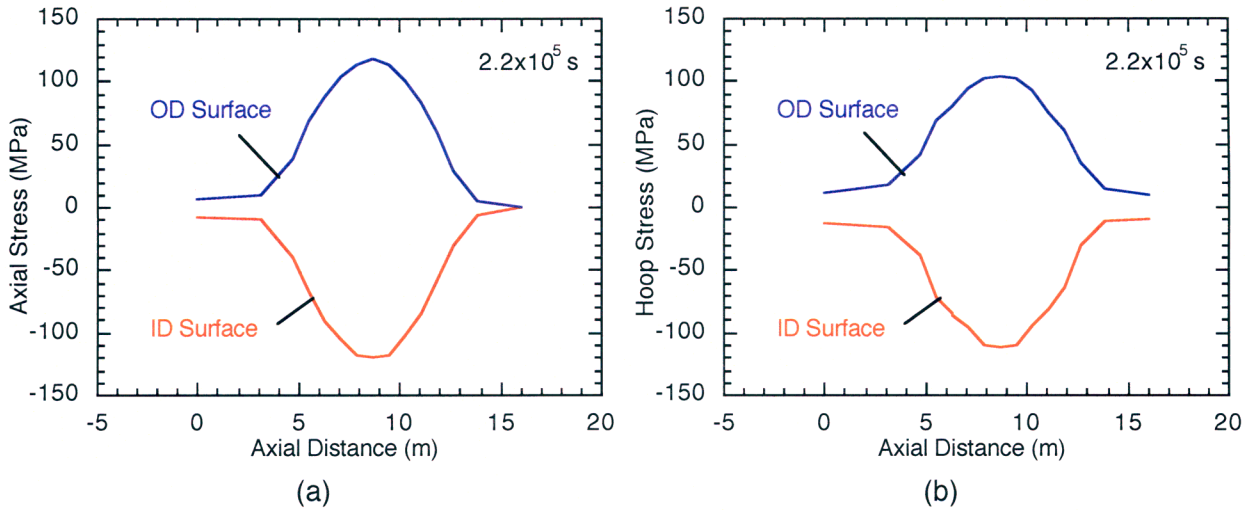

Figure 4.13. Distribution of (a) axial stress and (b) hoop stress at the ID and OD surfaces of the prismatic core RPV along the axial direction at 2.2×10^5 s.

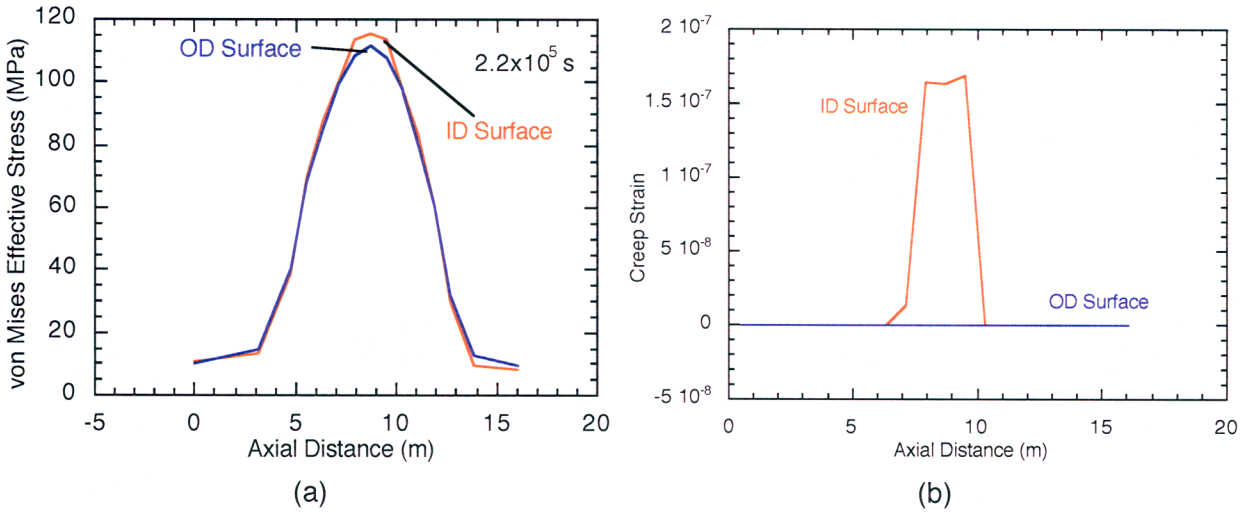

Figure 4.14. Distribution of (a) von Mises effective stress and (b) effective creep strain at the ID and OD surfaces of the prismatic core RPV along the axial direction at 2.2×10^5 s.

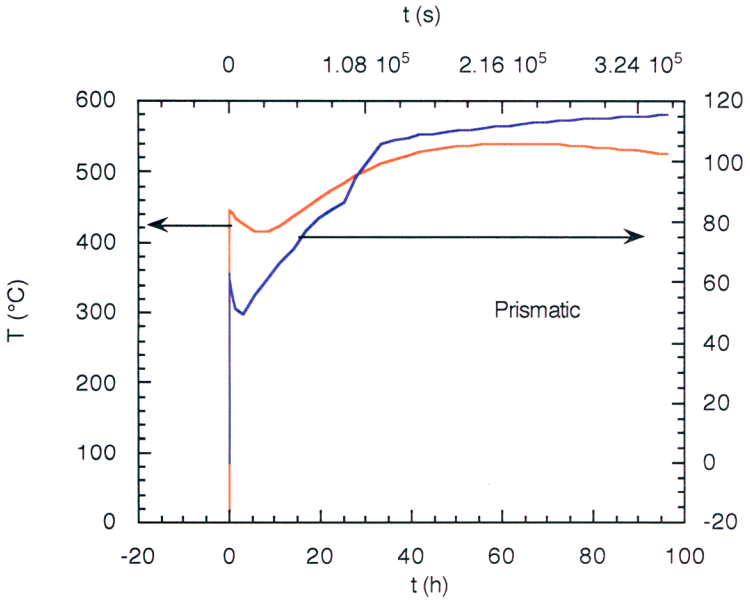

Figure 4.15. Variations of temperature and von Mises effective stress with time at the peak temperature location of the prismatic core RPV.

4.3.2 Pebble Bed Core Design

As in the case of the prismatic core design, a transient heat conduction analysis was conducted with surface heat fluxes prescribed at the ID and OD surfaces up to a time of 3.5×10^5 s. These heat fluxes were obtained from a RELAP5 run conducted by C. Davis at INL [Davis 2006]. In the RELAP5 analysis, heat flow was assumed to be in the radial direction and all axial heat conduction in the RPV was ignored. A comparison of the temperature distributions at the ID and OD surfaces at 2×10^5 s conducted using ABAQUS and RELAP5 is shown in Figs. 4.16a-b, respectively. As a result of ignoring axial heat conduction in the RELAP5 run, although the results are close, the peak temperature computed by ABAQUS is lower than that by RELAP5.

Note that although the peak temperature during normal operation occurs at the bottom end of the RPV, during the accident transient its location moves closer to the mid point.

The temperatures calculated by ABAQUS were input into a stress analysis that accounted for elastic as well as creep deformation. Variations of the axial and hoop stresses along the axial direction at the ID and OD surfaces at 2.5×10^5 s are shown in Figs. 4.17 a-b, respectively. The stress levels and temperatures are lower in the pebble bed case compared to the prismatic core case. Thus, the accumulated creep strains during the transient are also negligible. Fig. 4.18 shows the time variations of the temperature and von Mises effective stress at the critical location. The temperature reaches a peak and then decreases slightly with time at the end of the transient. For reference, the minimum value of the yield strength of 9Cr-1Mo-V steel at 480°C is 377 MPa and the minimum time to stress rupture at a constant stress of 100 MPa and at a constant temperature equal to the peak temperature of 480°C is $>>3 \times 10^5$ h. It can be shown that even if the temperature history is arbitrarily increased by 50°C, the maximum creep deformation still remains negligible.

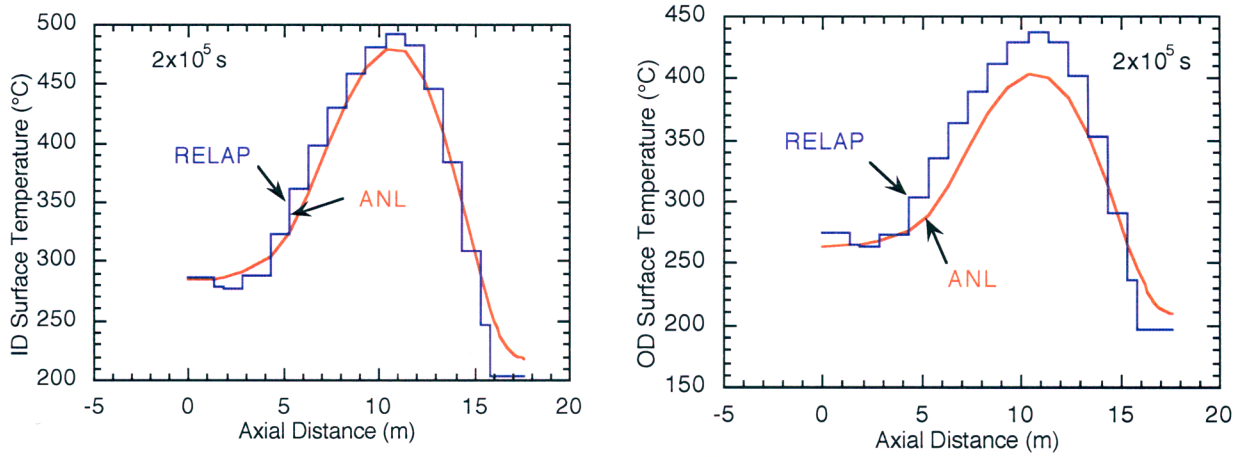

Figure 4.16. Distribution of temperature at the (a) ID and (b) OD surface of the pebble bed core RPV at 2×10^5 s during a depressurized conduction coolant condition.

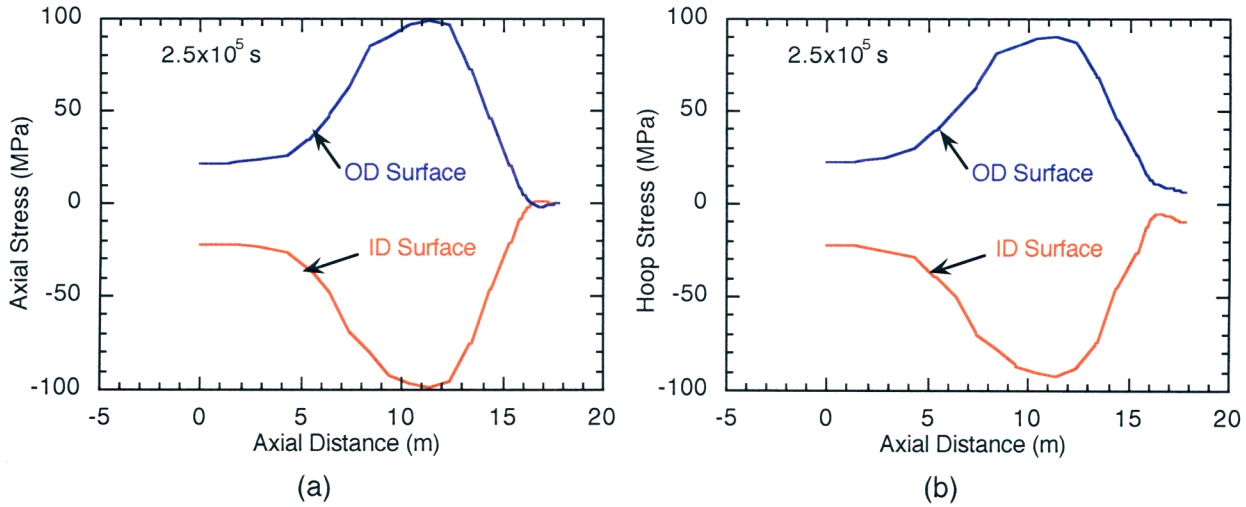

Figure 4.17. Distribution of (a) axial stress and (b) hoop stress at the ID and OD surfaces of the pebble bed core RPV along the axial direction at 2.5×10^5 s.

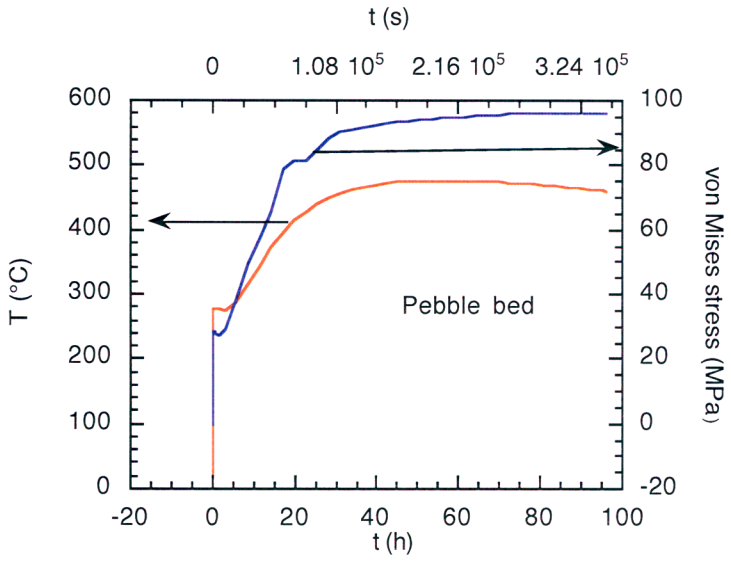

Figure 4.18. Variations of temperature and von Mises effective stress with time at the peak temperature location of the pebble bed core RPV.

4.4 Discussions and Conclusions

Thermal and stress analyses were conducted for the prismatic core and pebble bed core RPVs during normal operation as well as a depressurized conduction coolant accident. For normal operation, Subsection NH rules were applied for the prismatic core RPV and Subsection NB rules were applied for the pebble bed RPV. The peak primary membrane stresses for the prismatic core design RPV are within the ASME Code Subsection NH allowable ($3x10^5$ h) and the peak primary membrane stresses for the pebble bed core design RPV are within the ASME Code Subsection NB allowable for the reference alloy 9Cr-1Mo-V steel.

A-508 forgings, which are used extensively in light water reactors, can be a potential candidate material for the pebble bed design RPV because the peak temperatures as calculated by RELAP5 is ≤371°C. However, a pebble bed-specific code calculates temperatures higher than 371°C, which makes the use of this material uncertain unless the RPV is actively cooled. A-508 forging is also unacceptable for the prismatic core design RPV because the calculated temperatures during normal operation exceed 371°C significantly unless it is actively cooled.

2.25Cr-1Mo-V steel could also be a potential candidate alloy because it appears to have sufficient strength at low temperatures and limited data show that it might have sufficient high temperature strength up to 500°C. However, its use is currently not permitted under Section III.

Thermal stress analysis showed that both designs satisfy the thermal stress ratchet requirements of the ASME Code, Section III, Subsection NB (for the pebble bed RPV) and Subsection NH (for the prismatic core RPV) during normal operation.

Thermal conduction analyses were performed for a depressurized conduction coolant accident scenario for both designs. A comparison of the temperature profiles and histories calculated by ABAQUS and RELAP5 showed that the peak temperatures may have been overestimated by RELAP5 because axial heat conduction in the RPV is ignored in the current RELAP5 model. The peak temperatures attained in the prismatic and pebble bed core RPVs during the transient are 525°C and 480°C, respectively.

Stress analyses showed that although the peak temperatures are in the creep range for 9Cr-1Mo-V steel, the stresses are too low to cause significant creep deformation. Also, the peak stresses are well within the expected minimum yield strength of the material at peak temperature.

Finally, the results of all the thermal hydraulic analyses used as input in this report are based on an emissivity of 0.8 at all surfaces. A sensitivity analysis is needed to determine whether the conclusions of this report are valid, if the emissivity was significantly different.

5. RPV Inspection Requirements

5.1 Inspection of Low-Alloy Steel Pressure Vessels

This section summarizes the experience related to inspection of light-water reactor pressure vessels. Ultrasonic examination methods are generally used to characterize flaws in the LWR reactor pressure vessel welds and heat-affected zones. Section XI of the ASME Code provides the requirements for these examinations. Evaluation of the results of these examinations performed to the minimum ASME Code Requirements as of 1994 indicates a significant level of uncertainty in detection, size, and orientation of defects in RPV weldments, particularly of underclad flaws. This uncertainty has led to fairly conservative regulatory requirements involving indication evaluations, pressure-temperature (P-T) limit determination based on a large hypothetical flaw size (one-fourth thickness), and probabilistic evaluation of pressurized thermal shock (PTS) events based on hypothetical flaw sizes and distributions. Additional guidance and recommendations for in-service examination of vessels are provided in USNRC RG 1.150, Rev. 1 [USNRC 1983]. These recommendations are intended to increase the reliability of examinations and significantly exceed the ASME Section XI requirements. A number of efforts have been undertaken to improve inspection reliability and repeatability; these efforts include NRC [Muscara 1985] and EPRI programs and international efforts such as the Program for the Inspection of Steel Components (PISC) Round Robin Tests [Crutzen 1987, Nichols and Crutzen 1988]. These efforts have led to the development of in-service inspection techniques and procedures that have improved ability to detect and size small underclad cracks and weld defects.

In-service Inspection Requirements

In-service inspection is a mandatory requirement based on the ASME Code, Section XI (ASME 1986b). The general philosophy of Section XI in-service inspection and the status of improvements in the code requirements for the RPV are presented by Cook [1987]. There are basically four inspection intervals during which certain welds must be examined; most plants use four 10-year intervals over a 40-year period. All shell, head, shell-to-flange, head-to-flange and nozzle-to-vessel welds, and repair welds (repair depth greater than 10% of wall thickness) in the beltline region must be subjected to a 100% volumetric examination. The nozzle inside radius sections must all be subjected to a volumetric examination during each of the four inspection intervals. Twenty-five percent of the partial-penetration nozzle welds (control rod drive mechanism and instrumentation) are required to have a visual examination of external surfaces during each inspection interval (leading to total coverage of all nozzles). All of the nozzle-to-safe end butt welds are dissimilar metals (i.e., ferritic steel nozzle to stainless steel or Inconel) are subjected to volumetric and surface examinations at each interval. All studs and threaded stud holes in the closure head are to have surface and volumetric examinations at each inspection interval. Any integrally welded attachment is required to have surface or volumetric inspection of welds at each inspection interval. Visual examination of accessible interior attachment welds is also required at each inspection.

Thus, the inspection plan for the RPV requires close monitoring of potential fatigue-crack formation and growth in all the relevant welds. The additional monitoring and recording of transients are usually conducted in accordance with the plant technical specifications.

Advanced Ultrasonic Examination Methods

Smooth, sharp-edged flaws (such as fatigue cracks) oriented in a plane normal to the vessel surface and located in the beltline region near the cladding/base-metal interface are the most critical type of flaws because the material in that region of the pressure vessel exhibits the highest degree of neutron embrittlement and corresponding high RT_{NDT}, and high tensile stresses (thermal) occur near the vessel inner surface during a PTS accident or a cooldown violating the P-T limits. Such flaws are difficult to detect and size with an ultrasonic technique based on signal-amplitude alone, which is the technique generally used in the United States for vessel inspection [Willetts et al. 1989]. PISC II results show that reliable detection of these flaws is achievable with advanced inspection techniques, but sizing is far from adequate even when advanced techniques are used [Njo et al. 1991].

In the amplitude-based technique, the sensitivity setting of the ultrasonic equipment is referenced to a distance-amplitude correction curve, which can be obtained from an ASME reference block with one 3-mm (0.125-in.) side-drilled hole [Halmshaw 1987]. ASME Code Section XI specifies an amplitude cut-off level of 20T of the distance-amplitude correction curve and only defect indications that exceed that level are recorded. ASME Section XI Code also specifies use of an additional scan angle of 70-degrees longitudinal wave to inspect clad-base metal interface regions [ASME 1989, Bush 1988].

The amplitude-based technique uses the decibel-drop method to determine flaw sizes much larger than the width of the sound field [Willetts et al. 1989, Halmshaw 1987]. In the decibel-drop method, the transducer is positioned to obtain a maximum height for an echo from the defect, and then it is traversed until the height of the echo drops to a specified threshold (50% of the maximum height for the 6-decibel-drop method). This position of the transducer is assumed to be over the edge of the flaw. Similarly, the transducer is moved in other directions from the maximum height position, and finally the flaw size is determined. A flaw size much smaller than the width of the sound field can be determined by the 20-decibel drop method (beam edge method) or by comparing the amplitude of the reflection from the flaw with a range.

Automated systems potentially have better detection capability (more sensitivity) than manual techniques and they are used in laboratory testing and are occasionally applied to field inspections of RPVs. One such automated system is the Ultrasonic Data Recording and Processing System (UDRPS), which features automatic flaw detection software and may be used with many different ultrasonic inspection techniques, for example, amplitude-based techniques, and tip-diffraction techniques [Willetts et al. 1986]. The UDRPS uses signal averaging techniques to provide a better signal-to-noise ratio, thereby improve the detection capability of the system. Use of UDRPS with the tip-diffraction technique, discussed in the next paragraph, has demonstrated better capability to detect underclad and embedded flaws than that demonstrated by several conventional manual techniques. Laboratory evaluations show that UDRPS can effectively detect a near surface flaw as small as 2.5 mm (0.1-in.). In application, UDRPS has been used to characterize a 35.6 mm (1.4-in.) long and <25.4 mm (1-in.) deep indication in the Calvert Cliffs-2 reactor vessel during its 10-year in-service inspection [Nucleonics Week 1989b]. The UDRPS results show that the apparent crack was a slag deposit rather than an unacceptable crack-like defect.

Tip-diffraction techniques developed in the United Kingdom can accurately size underclad and embedded flaws. With one of the tip-diffraction techniques (the time-of-flight diffraction technique), the difference in the travel times of ultrasonic waves diffracted from each of the flaw tips is measured to estimate the flaw size [Silk et al. 1987]. Flaw orientation and roughness,

which interfere with flaw size measurements using amplitude-based techniques, have very little effect on flaw sizing with tip-diffraction techniques. Tip-diffraction techniques have a potential advantage over amplitude-based techniques in differentiating closely spaced flaws from a continuous crack. Laboratory test results, including PISC II test results, show that the tip-diffraction techniques are the most accurate for sizing underclad and embedded flaws [Willetts et al. 1989, Browne 1989]. These techniques, commonly used in Europe, are increasingly applied in the United States. These techniques have also been used to size fatigue cracks [Liddington et al. 1976].

Flaws located in the nozzle-to-shell welds are also of considerable interest in assessing RPV integrity. The nozzle-to-shell welds can be ultrasonically inspected from the nozzle bore; however, sizing of the flaws is difficult when conventional (unfocused) transducers are used [Willetts et al. 1989]. The main reason for this difficulty is the large distance between the nozzle bore and nozzle weld. At these large distances, the ultrasonic beam of conventional transducers provides poor resolution of flaws in the welds. A large-diameter, focused ultrasonic transducer produces a small diameter beam at the flaw location and can be used for accurate mapping of flaw edges. Laboratory results show that the large-diameter focused transducers are substantially more accurate than unfocused transducers in sizing flaws in the nozzle-to-shell welds [Clayton 1989].

Focused transducers are used commonly in France and Belgium, but infrequently in the United States. Examples of the applications of focused transducers are inspection of reactor pressure vessel welds and heat-affected zones in Westinghouse 350-MWe and Framatome 900-MWe reactors in Belgium and in a 660-MWe reactor at Krsko in Croatia [NEI 1989]. Also, a large-diameter focused transducer was used to inspect nozzle-to-vessel welds of the Ginna plant reactor vessel during its second in-service inspection interval [Stone et al. 1989]. The inspection with the focused transducer characterized the earlier detected ultrasonic indications as closely spaced indications. Earlier, a focused transducer was used to characterize the flaws in the vessel head cladding at the Yankee Rowe plant [ACRS 1990].

The Program for the Inspection of Steel Components (PISC) has planned further evaluations of various advanced ultrasonic inspection methods. The PISC III project will address the practical problems encountered during in-service inspection of the pressure vessel, which were not addressed in the PISC II project. The problems include, for example, accessibility and inspectability, hostile environments, and qualification of inspection personnel.

Recently, the ASME Section XI Code has developed more stringent requirements for demonstrating performance of ultrasonic inspection procedures, equipment, and personnel used to detect and size flaws at the susceptible sites in the pressure vessels. These requirements are introduced to ensure that inspectors apply the appropriate ultrasonic inspection techniques in the field to correctly characterize the flaws. These requirements are presented in the two mandatory appendices of ASME Section XI: Appendix VII, Qualification of Nondestructive Examination Personnel for Ultrasonic Examination; and Appendix VIII, Performance Demonstration for Ultrasonic Examination Systems. Implementation of Appendices VII and VIII will take several years. The susceptible sites include the clad-base metal interface, nozzle inside radius section, reactor vessel structural welds, nozzle-to-vessel welds, and bolts and studs. The enhanced inspection program will provide more reliable in-service inspection data on U.S. reactor pressure vessels, which then may be used for the development of a plant-specific vessel flaw distribution or a generic flaw distribution, more representative of operating PWR vessels than currently used distributions such as the Marshall distribution [UKAEA 1982].

Advanced in-service inspection methods with highly reliable flaw detection and accurate flaw sizing capabilities can also provide the precision needed to reduce the highly conservative safety factors used in fracture mechanics calculations. Thus, there is potential support to relax the hypothetical one-fourth thickness reference flaw size used as the basis for plant operating limits (pressure-temperature limits). The regulations could allow a reduced reference flaw size, if the smaller flaw size can be justified by plant-specific NDE practice and proven verification results.

An ASME Code, Section XI, task group is evaluating the effects of improved in-service inspection methods for RPVs on overall vessel reliability[p]. The implementation of Appendix VIII for demonstration/qualification of future vessel inspections will be considered as it relates to margins of safety for vessel integrity. The task Group is currently reviewing the basis for the Section XI flaw acceptance standards and the relationship with the Appendix G ¼-thickness reference flaw used to establish plant operating pressure-temperature limits. This work evolved out of the White Paper on RPV integrity requirements [ASME 1993]. Guidance on sizing accuracy for mid-wall flaws will be also developed for code action. The Task Group will prepare recommendations for modifying the ¼-thickness reference flaw requirement through credit for results from the use of improved NDE techniques.

Acoustic Emission Monitoring

Acoustic emission methods may be used to monitor potential crack growth in the RPV welds and base metal if the outside surface of the vessel is accessible. Some PWR vessels are supported by neutron shield tanks, which will prevent access to the vessel outside surface. Acoustic emission monitoring could also be used to detect any leakage during a hydrotest. It is used in Europe during hydrotests and was responsible in detecting the leakage through the control rod drive penetration crack in a French PWR plant [1991].

Earlier, an acoustic emission method for crack growth detection was tested for continuous surveillance of selected areas of the Watts Bar 1 primary pressure boundary during hot functional testing. A preloaded, precracked fracture specimen was also placed in the primary system to test the capability of the acoustic emission method to detect a signal during reactor operation. The specimen was designed such that the system operating temperature would impose thermal loads and cause crack growth. The test results showed that coolant flow noise can be filtered out, and that the acoustic emission signals from a fracture specimen can be detected under operating conditions [Hutton et al. 1984]. Acoustic emission was also used to monitor possible crack growth during the 1987 hydrotest of the High Flux Isotope Reactor located at the Oak Ridge National Laboratory; no evidence of crack growth was detected [Hutton 1989].

Several significant steps have been taken to validate continuous, on-line acoustic emission monitoring in the field. Recent work on the application of the acoustic emission method at Watts Bar 1 has shown that it can be effectively used for in-service monitoring of crack growth in thick wall, geometrically complicated components such as RPV nozzles [Hutton et al. 1988]. Field application of continuous acoustic emission monitoring is also currently being evaluated by Pacific Northwest Laboratory at the Limerick Unit 1 reactor to monitor a flaw indication in an inlet nozzle safe end weld [Doctor et al. 1991a]. In addition, ASME Code Case N-471 has been developed and approved, which provides for continuous on-line acoustic

[p]ASME Code, Section XI, Task Group on Application of NDE for Plant Operating Criteria, J. Spanner, Jr., Chairman, which reports to the Working Group on Plant Operating Criteria, T. J. Griesbech, Chairman.

emission monitoring for growth of known flaws. The Code Case applies to components in which flaws exceeding the acceptance criteria (ASME Section XI, IWB-3410.1) have been identified, and for which the analytical evaluation of the flaws found the components acceptable for continued service according to ASME Section XI, IWB-3132.4.

5.2 Testing and Inspection of Grade P91 Steel Testing of Grade P91 Steel

Hardness Testing

To determine whether the processing of creep-strength-enhanced ferritic steels has been performed correctly, users need tools that can quickly and inexpensively provide information on the overall condition of the material. Because hardness provides a direct indication of material's room-temperature tensile strength, which can be used to roughly estimate its elevated-temperature properties, portable hardness testing has been used as one such tool. However, this has created significant problems because of a lack of understanding of the variables that can affect the accuracy of hardness readings. For example, there are several types of portable hardness testers available that operate on entirely different principles, each of which exhibits certain peculiarities that are capable of influencing the accuracy of the measurements relative to testing with a laboratory instrument. In addition, the condition of the work piece itself can create considerable difficulty in accurately assessing the hardness.

When performing hardness tests, it is important to prepare the surface properly, particularly for heat-affected zone (HAZ) readings. Since the base metal may have a layer of decarburization on the surface, about 1/32 inch of metal should be removed by grinding, and that should be followed by polishing to a 120 grit finish. This preparation will also make readings more consistent and should also be followed when measuring the hardness of the weld metal.

One possible action that could be taken is to identify a recommended hardness range for each grade that would be considered acceptable for all applications, with the stipulation that hardness readings outside of that range would require evaluation to determine (1) accuracy of the measurement and (2) fitness for service. It also should be emphasized that, for Grade P91 material that has been heated into the intercritical temperature range, the hardness may not be adequate to indicate damage, since the re-formed martensite can mask the effects of the undesirable heat treatment.

Ultrasonic Measurements

Grade P91 steel is recommended for use in the normalized and tempered condition. It is susceptible to the formation of undesirable microstructures during fabrication and/or heat treatment processes. It is important to nondestructively characterize the microstructure of this steel for quality control during fabrication and heat treatment to ensure the desirable microstructure and mechanical properties. The ultrasonic technique is a promising technique for such characterization. Ultrasonic velocity and attenuation measurements have been used for characterization of the microstructures obtained by various heat treatments.

Kumar et al. (2002) measured ultrasonic velocity and attenuation for estimating hardness and characterizing microstructure in Grade P91 steel subject to various heat treatments. Their results are summarized here. Samples of a 10 X 10 mm cross-sectional area and 60-mm length were prepared from the normalized (1333 K/6h/air cooled) and tempered (1043 K/4 h/air cooled) from forged rounds of 70 mm in diameter. The samples were soaked for 5 minutes at

different temperatures, starting from α-phase region (1073 K) to γ + δ-region (1623 K), followed by oil quenching. These treatments were given to obtain different microstructures and grain sizes in the different regions in the heat-affected zones of the weldments. Table 5.1 gives the details of the heat treatments employed.

Table 5.1. Details of heat treatment given to P91 steel and the corresponding microstructure, average grain size, hardness, and ultrasonic parameters (Kumar et al. 2002)

Specimen	Heat Treatment Temperature (K)	Microstructure	Grain Size (μm)	Hardness (VHN)	Longitudinal Wave Velocity at 15 MHz (m/s)	Shear Wave Velocity at 5 MHz (m/s)	Attenuation Coefficient at 15 MHz (dB/mm)	Spectral Peak Ratio
1	1073	α + C	48	205	5998	3310	0.227	0.8208
2	1098	α + C	49	205	5996	3310	0.219	0.7826
3	1123	α + m + C	45	277	5990	3306	0.209	0.7166
4	1148	α + m + C	30	370	5972	3290	0.072	0.5213
5	1173	α + m + C	19	397	5962	3283	0.0735	0.4556
6	1223	m + C	19	430	5952	3274	0.037	0.4906
7	1273	m + C	18	433	5951	3272	0.037	0.4599
8	1323	m + C	29	435	5951	3271	0.047	0.4728
9	1373	m + C	40	445	5949	3272	0.072	0.5617
10	1423	m	92	420	5948	3270	0.252	1.0268
11	1473	m	131	410	5952	3270	0.417	1.3911
12	1523	m + δ	116	393	5952	3267	0.387	1.8406
13	1573	m + δ	85	380	5948	3271	0.352	1.7129
14	1623	m + δ	55	345	5949	3272	0.337	1.6452

α—ferrite, m—martensite, C—carbide, and δ—δ-ferrite.

Figure 5.1 shows the variation in hardness with increase in the soaking (heat-treatment) temperature. Below the lower critical temperature (Ac_1, 1100 K), the hardness is the lowest and almost constant. As the soaking temperature increased above Ac_1 temperature, the hardness is found to increase with increasing temperature. This is due to the increase in the amount of martensite formed with an increasing soaking temperature in the α + γ-phase region. Above about 1373 K, the grain size increases rapidly, leading to a lower hardness with a further increase in soaking temperature. Beyond 1473 K, the formation of soft δ ferrite further decreased the hardness, even though it refined the grain size.

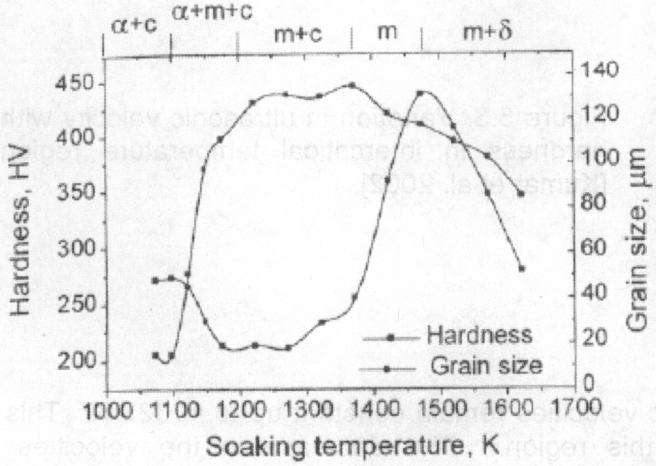

Figure 5.1. Variation in hardness and grain size with soaking temperature [Kumar et al. 2002].

Ultrasonic Velocity

Figures 5.2(a) and (b) show, respectively, the variation in the ultrasonic longitudinal- and shear-wave velocities with the soaking temperature. In the samples with soaking temperatures below Ac_1 temperature, the ultrasonic velocities are the highest and almost constant. As the soaking temperature is increased beyond Ac_1, the velocities decreased sharply with an increase in soaking temperature until the Ac_3 temperature (1180 K) is reached. The sharp decrease in the ultrasonic velocities in the intercritical region is due to increase in the amount of martensite with the increase in the soaking temperature. This change in microstructure is also reflected in the variation in hardness (see Fig. 5.1). The lower velocity in martensite is attributed to the lower modulus of elasticity of martensitic structure compared to that of ferritic structure. There is a continuous variation in the ultrasonic velocity and hardness in the intercritical temperature region (Ac_1 and Ac_3), as shown in Fig. 5.3. Comparison of velocity changes in Figs. 5.2(a) and (b) indicates that ultrasonic shear wave velocity is more sensitive to hardness change compared to longitudinal wave velocity (Kumar et al. 2002).

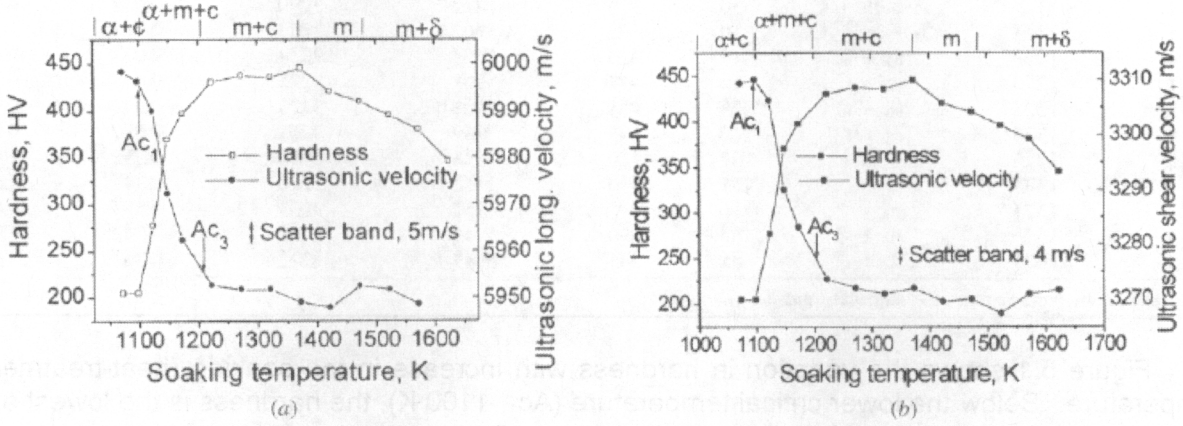

Figure 5,2. (a) Variations in ultrasonic longitudinal wave velocities and hardness with soaking temperature. (b) Variation in ultrasonic shear wave velocity and hardness with soaking temperature [Kumar et al. 2002].

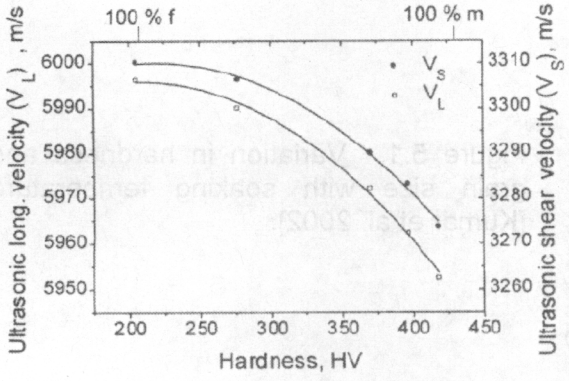

Figure 5.3. Variation in ultrasonic velocity with hardness in intercritical temperature region [Kumar et al. 2002].

Above Ac_3 temperature, the ultrasonic velocities remain constant up to ≈1323 K. This is due to more uniform microstructure in this region. The decrease in the velocities at temperatures beyond 1323 K is due to increase in the grain size. Beyond the Ac_4 temperature, the ultrasonic velocity is found to be constant. This may be due the fact that a very small amount of δ ferrite is formed up to the highest soaking temperature applied in these tests.

Ultrasonic velocity can also be used to determine the weld profile. Figure 1(a) shows the variation in ultrasonic velocity with scanning distance across the P91 weld line in as-welded and PWHT conditions. In as-welded condition, ultrasonic velocity is maximum in the base metal and minimum in the weld metal. As the amount of weld metal increases in the propagation direction of ultrasonic beam, ultrasonic velocity is decreases and hence the amount of weld metal and base metal can be determined in the propagation direction of the ultrasonic beam, which can be used to determine the weld profile. The lower velocity in the weld metal is due to the presence of martensitic structure with lower ultrasonic velocity. The ultrasonic velocity plot shown in Figure 5.4(a) appears to be an almost replica of the weld profile shown in the photograph of the macroetched weldment [see Figure 5.4(b)]. After PWHT at 760°C for 1h, ultrasonic velocity was found to be slightly lower than that in base metal but higher than that in the weld metal under as-welded condition. Thus the adequacy of PWHT can be assessed using ultrasonic velocity and weld profile can also be determined even in the PWHT condition. These results are consistent with those obtained from a study carried out in the specimen with thermally simulated microstructures corresponding to different regions of the weldment and presented earlier in this section [Kumar et al. 2002].

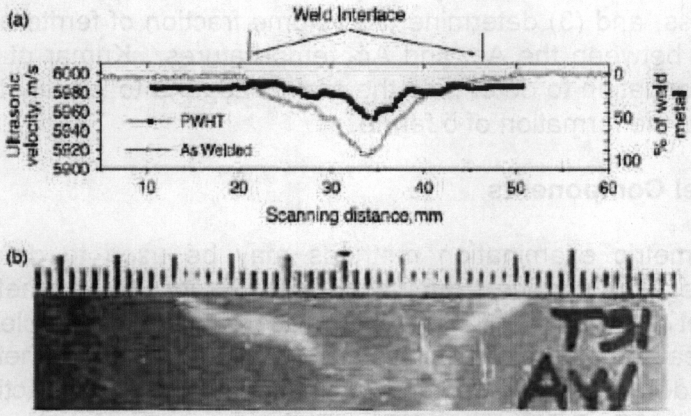

Figure 5.4. (a) Variation in ultrasonic longitudinal wave velocity with scanning distance across the weld line in as-welded and PWHT conditions and (b) Micrograph of the etched weldment.

Ultrasonic Attenuation

Figure 5.5 shows the variation in the ultrasonic attenuation with the soaking temperature. In the samples heat treated at the soaking temperatures less than Ac_1 temperature, the attenuation is found to be almost constant. As the soaking temperature increased above Ac_1 temperature, the attenuation found to be decreased due to the increased amount of martensite, which has a lower attenuation. The ultrasonic attenuation was found to be at a minimum in the sample quenched from just above the Ac_3 temperature (1210 K) where the prior-austenite grain size was also at a minimum. It starts increasing again in the samples heat treated above 1323 K, due to the increase in grain size. The attenuation increases sharply after 1373 K due to rapid increase in the grain size, which is associated with the carbide (V_4C_3 and NbC) dissolution. Above about 1473 K, the ultrasonic attenuation decreases because of the decrease in the grain size consequent to the formation of δ ferrite. Kumar et al. [2002] also presents the quantitative analysis of ultrasonic attenuation.

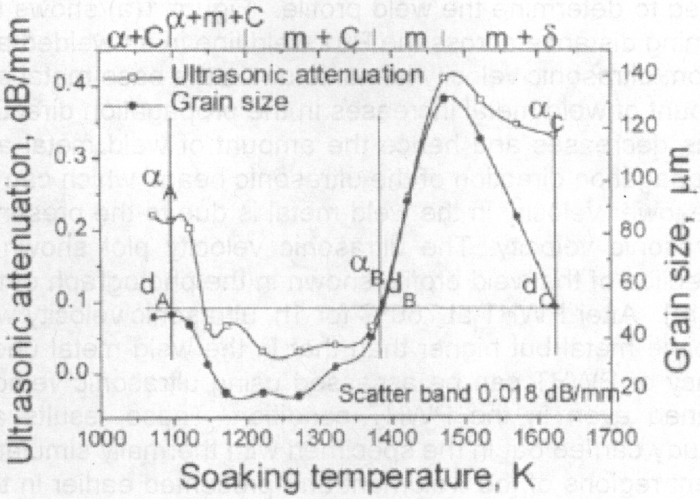

Figure 5.5. Variation in ultrasonic attenuation and grain size with soaking temperature [Kumar et al. 2002].

Kumar et al. (2002) have used ultrasonic velocity to (1) identify the Ac_1 and Ac_3 temperatures, (2) determine the hardness, and (3) determine the volume fraction of ferrite and martensite in the quenched specimens between the Ac_1 and Ac_3 temperatures. Kumar et al. [2002] have also used the ultrasonic attenuation to determine the grain size, and to identify the onset of dissolution of V_4C_3 and NbC and the formation of δ ferrite.

5.2.1 Inspection of Grade P91 Steel Components

The traditional surface and volumetric examination methods may be used to detect cracking in the P91 welds during service. The surface examination methods include magnetic-particle testing (MT) and liquid-penetrant testing (PT). These examinations may not be able to detect initiation of Type IV cracking because these cracks initiate subsurface. The volumetric examination methods include amplitude-based ultrasonic examinations and tip-diffraction techniques. Also acoustic emission monitoring may be used to detect the presence of cracks.

European Pressure Equipment Research Council (EPERC) has identified several innovative NDE techniques for reactor pressure vessels of ultra-supercritical nuclear power plants operating at up to 350 bar pressure and 750°C temperature. The candidate materials include P91, P92, E911, and Alloy 617. The innovative NDE techniques being considered are X-ray diffractometry, portable X-ray diffractometer, and acoustic emission [Tonti 2005].

Non-destructive inspection methods are being developed to maintain the reliability and to carry out preventive maintenance for aged P91 components such as tubing and steam headers. These techniques could be used for inspection and evaluation of thick-walled, P-91 reactor pressure vessels during fabrication and operation (Mitsubishi Heavy Industries).

NDE Method for Creep Damage. Mitsubishi heavy industries (MHI) has developed a non-destructive creep damage detection and evaluation technology based on vast database of metallurgical analysis by electric resistance method. This technique is being used for life assessment of high-temperature pressure retaining components.

NDE Method for Fatigue Damage. Life consumption of low cycle fatigue at attachment welding edges is assessed by analysis of micro-crack with MT Replica Method.

NDE Method for Fatigue, Corrosion Fatigue, and Tube Thinning Damage. MHI has developed a NDI apparatus so called M-MAUS (Mitsubishi Multi-sensor Automatic UT System) for fatigue and corrosion fatigue damage detection at furnace wall. Also, UT equipment for tube wall thickness measurement and fatigue damage inspection from tube inside has been developed.

Magnetic Brakhausen Noise Analysis: Magnetic Barkhausen noise (MBN) analysis has been used for the assessment of residual stresses in P91 weldment before and after PWHT. The results of the MHN analysis have been correlated with those obtained by the micro-hardness measurements. Since MBN is related to the nucleation and movement of magnetic domain walls which get influenced by presence of residual stresses and microstructural features, MBN measurements can be used to assess residual stresses and for characterization of microstructural features.

MBN measurements for FBR steam generator tube-to-tube weld are presented in Fig. 5.6. (Tubes were made from modified 9Cr-1Mo material.) The measurements were made at the weld center, and 5, 15, and 25 mm from the weld center on both sides of the weldment. The measurement locations were selected in such a way as to cover base metal, HAZ, and weld region. Microhardness measurements were made at these locations using a Vicker's hardness tester with a load of 5 kg. After the measurements in as-welded condition, the tubes were post-weld heat treated at 700°C for 1 h followed by air cooling. Again the measurements were repeated at the same locations after removing the oxide layer. The results showed that, in the as-welded condition, there is maximum MBN peak height in the base metal region and there is gradual decrease in peak height with decreasing distance from weld centerline. The weld shows the minimum MBN peak height. The large variation in MBN peak height indicates a large difference in the hardness in the weld, HAZ, and base metal regions. This is supported by the corresponding variation in the measured hardness values. After PWHT, the MBN peak height become about the same at all locations. This is also supported by the narrow variations in the hardness values after PWHT. This is attributed to the removal of residual stresses and reduction in dislocation density in the weld and HAZ during PWHT. It is possible to develop an acceptance criterion based on MBN peak height values to ensure the effectiveness of PWHT.

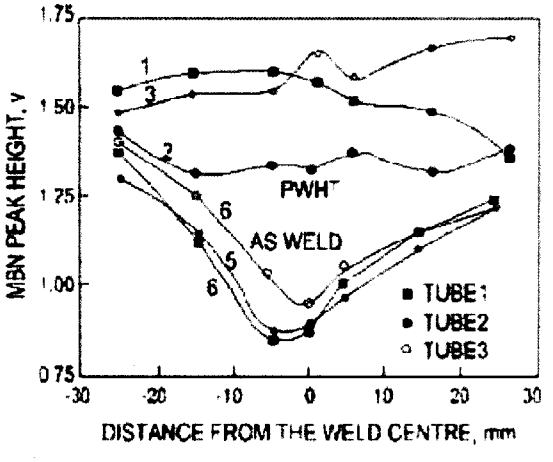

Figure 5.6. Variation in MBN peak height with distance from the weld centerline in as-welded and PWHT conditions.

6. Summary

The NGNP, which is an advanced HTGR concept with emphasis on both electricity and hydrogen production, involves helium as the coolant and a closed-cycle gas turbine for power generation with a core outlet/gas turbine inlet temperature of 900-1000*C. In the indirect cycle system, an intermediate heat exchanger is used to transfer the heat from primary helium from the core to the secondary fluid, which can be helium, nitrogen/helium mixture, or a molten salt. The system concept for the VHTR can be a reactor based on the prismatic block of the GT-MHR developed by a consortium led by General Atomics in the U.S. or based on the PBMR design developed by ESKOM of South Africa and British Nuclear Fuels of U.K.

This report has reviewed the available information on candidate materials for the construction of RPV and has made a preliminary assessment of several relevant factors to make a judicious selection of the material for the RPV. In addition, calculations were made to address the ASME Code compliance for the candidate RPV materials under steady state and during depressurized conduction ccooldown conditions. The assessment included three primary candidate alloys namely, low alloy steel SA508 (UNS K12042), Fe-2.25Cr-1Mo-0.25V steel (UNS K31835), and modified 9Cr-1Mo steel (UNS K90901) for the RPV.

Several conclusions were drawn from this evaluation:

Baseline Mechanical Properties: There is sufficient database available for the mechanical properties of SA-508 steel. There is limited data available on the thermal aging effects on the mechanical properties and additional information needs development on the long-term aging effects. The steel is approved for use up to 371°C (700°F) under the ASME Code. At present no data is available on the effects of impure helium on the long-term corrosion and mechanical properties of the material.

There is adequate tensile data on the Fe-2.25Cr-1Mo-0.25V in the temperature range of interest in NGNP RPV. There is only limited creep data available for the steel and additional data are needed, especially at elevated temperatures that encompass conduction cooldown conditions. However, substantial data on the creep fatigue properties, thermal aging affects on the mechanical properties, performance characteristics in impure helium, properties of thick section material are needed prior to its selection for NGNP RPV. Furthermore, the steel is approved under ASME Code Section VIII (for non nuclear applications) and is not approved under Section III for use in nuclear systems.

Substantial database on the baseline mechanical properties is currently available for the Modified 9Cr-1Mo steel. Sufficient data are also available on the long-term thermal aging effects on the mechanical properties for this steel. One of the strong points for the selection of this steel is that it is approved in Section III of the ASME Code for nuclear applications. However, the creep-fatigue limits for the steel in the Code is highly conservative and it may preclude its selection for the NGNP RPV application. Furthermore, additional data are needed for the steel in the areas of compatibility in impure helium and mechanical properties of thick sections.

Welding Issues: Pressure vessels of Low alloy steels have been fabricated and used in U.S. light-water reactors and there is substantial experience in welding of both plates rings to form the vessels. Vessels with wall thicknesses varying between 203 to 254 mm (8 to 10 in.) and diameter-to-thickness ratios of ≈20 have been fabricated for the PWRs. In contrast, BWR

vessels with much larger diameter and a wall thickness of 152-mm (6-in.) have been fabricated. Pressure vessel materials have performed well in service, and no fatigue-driven cracks have been found in any PWR vessels. The only materials-related variable that appears to affect fatigue is the sulfur content (and distribution as sulfides) in the steel. Low alloy steels with average to high sulfur levels generally exhibit higher crack growth rates in the laboratory than low sulfur steels (<0.010 wt%).

Vanadium-modified 2.25Cr-1Mo steels are developed for the petrochemical refinery industry service at high temperatures and high hydrogen pressures. These steels were developed so that components having wall thickness in excess of 10 in., and diameters and lengths on the order of up to 20 and 200 ft, respectively, could be fabricated. These steels offer the fabricability and toughness of bainitic microstructures without the difficulties of welding and heat treatment of high chromium martensitic materials such as P91. Stress rupture tests on weldments to 16000 h established that the expected performance of the filler metal, base metal, and HAZ were comparable in strength and within ASME's base metal scatter band. However, for design temperatures in excess of 468°C (875°F), ASME required performance testing of weldments, and additional long-term test data are needed to qualify the welded components for application in NGNP RPV. Temper embrittlement, caused by reduction of bond strength of grain boundaries relative to the grain due to segregation of impurities (P and Sb) at grain boundaries, is of concern. If the grains are insufficiently tempered, the effect is the greatest. Test results for base metal, HAZ, and weld metal exposed for 20000 h at 482°C (900°F) have shown that acceptable toughness is retained for the materials, provided impurity levels were maintained within specific limits.

Modified 9Cr-1Mo steel is a leading candidate for NGNP RPV and it is being evaluated in several programs conducted worldwide. The superior mechanical properties of 9Cr-1Mo weldment strongly depend on creation of a precise microstructure and maintaining it throughout the service life of the welded component. Welding procedure and post-weld heat treatment play critical roles in creating the microstructure. The most significant problem in welding of 9Cr-1Mo steel is its propensity to Type IV cracking in the heat-affected zone. Boron addition seems to reduce cracking susceptibility but additional data are needed to quantify the effect over the long term. Creep-fatigue interaction could be more severe in 9Cr-1Mo weldment compared to weldment of 2.25Cr-1Mo steel. The creep-fatigue data show that the number of cycles to failure decreases with increase in tension hold time for the weldment. Significant additional data are needed to quantify this effect and establish, if any, the maximum reduction in life.

Procurement Issues: The current schedule for the NGNP plant requires that the conceptual and preliminary designs and the application for the construction permit from NRC be completed by the middle of calendar year 2010. The selection of material for the NGNP RPV is one of the critical item to meet the schedule. The NGNP RPV will have dimensions of 8-9 m in dia. and probably 200-300 mm in thickness. Such a vessel is much larger than the current LWR vessels and requires field welding of either ring forgings or plates of the selected material. In the selection of the candidate material for the RPV, the key technical/design issues are the reactor outlet temperature, active vs. passive cooling of the vessel, ASME code compliance under normal and transient conditions, high temperature design methodology currently available, welding and post-weld heat treatment in the field, fabrication expertise to achieve uniform through-thickness properties in thick sections, and vendor experience and availability in fabrication with different candidate materials.

At present, there exists a substantial experience in fabrication of RPV from SA-508 with several vendors around the world and procurement of a vessel of this material may depend primarily on the availability of a vendor to meet the schedule and not on the technical issues with the material.

Fe-2.25Cr-1Mo-V steel is extensively used in the fossil industries and hydrogenation reactor pressure vessels. There is no available information on existing pressure vessels having dimensions similar to that required in the NGNP RPV. Because of the extensive use of this material in fossil, petrochemical industries, etc. it can be concluded that there is some experience in forging/rolling thick-sections of this material. However, application of this material for NGNP RPV requires substantial additional data on the long term (>10000 h) mechanical properties and ASME Code approval for nuclear service.

Modified 9Cr-1Mo steel has overall superior mechanical properties among the three candidate materials that makes it a primary candidate for use in the NGNP RPV. However, information is lacking on thick-section properties/fabrication experience of this material. An assessment of the potential vendors from all over the world showed that capability and experience to fabricate a modified 9Cr-1Mo vessel of the size required for NGNP are severely lacking. At present, none of the vendors have the capability to forge thick-section large diameter rings of the modified 9Cr-1Mo steel. It was clear that none of the vendors was willing to upgrade their existing facility to facilitate forging of this steel unless an incentive is offered to them (in terms of assured market/customers to order RPV of the modified steel, or in some other form). As ring forging of RPV, using modified 9Cr-1Mo steel, does not appear to be a feasible option at present, axial welding of plates/ring segments is the alternate choice. However, none of the vendors has experience in manufacturing thick-section plates. Based on our assessment, the selection of this material for RPV may not meet the NGNP schedule because of the procurement limitation.

ASME Code Compliance of RPV: The NGNP RPV needs to be designed using the ASME Section III Code rules. If the RPV wall temperature can be maintained at a sufficiently low temperature, Subsection NB of the Code can be used. Otherwise, Subsection NH has to be followed.

SA508/SA533 steels are ASME Code approved for Class 1 nuclear components and Subsection NB rules are applicable up to 371°C for normal operation. Limited high temperature excursions under off-normal and depressurized conduction cooldown conditions are permitted under Code Case N 499. SA-508 forging can be a potential candidate for the pebble bed RPV design since the peak temperature as calculated by RELAP5 is ≤371°C. However, temperatures ≥371°C were calculated when a pebble-bed-specific code was used, which necessitates active cooling of the RPV made of this steel to comply with the ASME Code for transient operation. SA-508 steel is unacceptable for the prismatic core RPV design because the calculated temperatures during normal operation exceed 371°C and active cooling is mandatory, if this steel is selected for the prismatic RPV design.

At present, Fe-2.25Cr-1Mo-V steel is not approved under ASME Code Section III for nuclear service and therefore, no calculation was performed to assess its suitability for both designs of NGNP RPV.

Calculations performed for the modified 9Cr-1Mo steel showed that the peak membrane stress for the pebble bed design RPV is within the ASME Code Subsection NB allowable for the steel. The peak membrane stress for the prismatic design RPV is within the ASME Code

Subsection NH allowable (300000 h) for the steel. Stress analysis of the depressurized conduction cooldown condition for both pebble bed and prismatic designs showed the peak temperatures to be in the creep range for the steel, but the stresses are too low to cause any significant creep deformation ($<10^{-6}$).

7. References

ACRS 1990. Proceedings of the ACRS Subcommittee on Materials and Metallurgy, September 5, Ann Riley & Associates, Ltd., Washington D.C. 2006.

Alexander, D. J., Maziasz, P. J., and Brinkman, C. R., 1993. "Microstructures and Mechanical Properties of Aging Material," Liaw, P. K., Viswanathan, R., Murty, K. L., Simonen, E. P., and Frear, D., (Eds.), TMS, p. 343.

Anderson, P., Bellgardt, T., and Jones, F. L., 2003. "Creep Deformation in a Modified 9Cr-1Mo Steel," Materials Science and Technology, 19, pp. 207-213.

ASM Handbook, 1990. 2, p. 617.

ASME 1968. ASME Boiler and Pressure Vessel Code, Section VIII, "Unfired Pressure Vessels Built by Welding," American Society of Mechanical Engineers, New York.

ASME 1986b. ASME Boiler and Pressure Vessel Code, Section XI, "rules for Inservice Inspection of Nuclear Power Plant Components," American Society of Mechanical Engineers, New York.

ASME 1989. ASME Boiler and Pressure Vessel Code, Section XI, "rules for In-service Inspection of Nuclear Power Plant Components, "IWA-2232 and Mandatory Appendix I, Ultrasonic Examination," American society of Mechanical Engineers, New York.

ASME 1993. White Paper on Reactor Vessel Integrity Requirements for Level A and B Conditions, prepared by ASME Section XI Task Group on Reactor Vessel Integrity Requirements, EPRI TR-100251, Electric Power Research Institute, Palo Alto.

ASME 2005. ASME Boiler and Pressure Vessel Code, Section III, Division 1– Subsection NH, Class 1 Components in Elevated Temperature Service, 2005 Addenda, July 1, 2005.

ASME 2005a. ASME Boiler and Pressure Vessel Code, Section I, Part PW– Requirements for Boilers Fabricated by Welding, 2005 Addenda, July 1, 2005

ASME Code Case 2098-1, 1991.

ASME Code Case N-499-2, 2001.

ASME Code, Section II Part D, 2004.

Barlow, D. J., Middleton, C. J., and Metcalfe, E., 1990. Proceedings of International Conference on Steam Plants of the 1990s, Inst. Mech. Eng., London, pp. 265-274.

Becker, F. L. 1982. "Near surface Crack Detection in Nuclear Pressure Vessels," Quantitative NDE in the Nuclear Industry: Proceedings of the Fifth International conference on Nondestructive Evaluation in the Nuclear Industry, San Diego, California, May 10-13, 1982, American Society for Metals, Metals Park, Ohio, pp. 52-55.

Beres, L., Balogh, A., and Irmer, W., 2001. "Welding of Martensitic Creep-Resistant Steels," Welding Journal, 80, pp. 191-s to 195-s.

Brinkman, C. R., Alexander, D. J., and Maziasz, P. J., 1990. "Modified 9Cr-1Mo Steel for Advanced Steam Generator Applications," presented at the Joint ASME/IEEE Power Generation Conference, Boston, MA, October 21-25, 1990, 90-JPCINE-8.

Bush, S. H. 1988. "Impact of PISC II on ASME XI 'Rules for In-Service Inspection of Nuclear Power Plant Components'," Ultrasonic Inspection of Heavy Section Steel Components: The

PISC II Final Results, R. W. Nichols and S. Crutzen (eds.), Elsevier applied Science, London, p. 617.

Cabrillat, M., et al., 2006. "Creep Fatigue Behavior and Damage Assessment for Mod 9Cr 1Mo Steel," Proceedings of PVP2006-ICPVT-11, 2006 ASME Pressure Vessels and Piping Division Conference, July 23-27, 2006, Vancouver, BC, Canada.

Canonico, 1994

Choudhary, B. K., Saroja, S., Rao, K. B. S., and Mannan, S. L., 1999. "Creep-Rupture Behavior of Forged, Thick-Section 9Cr-1Mo Ferritic Steel," Metallurgical and Materials Transactions, 30A, pp. 2825-2834.

Clayton, W. T. 1989. "New Ultrasonic Flaw-Sizing Procedures," Nuclear Plant Journal, November-December, pp. 72-77.

Cohn, M. J., Henry, J. F., and Nass, D., 2005. "Fabrication, Construction, and Operation Problems for Grade 91 Fossil Power Components," Journal of Pressure Vessel Technology, ASME, May 2005, pp. 197-203.

Cook, J. F. 1987. "Adequacy of ASME Code In-Service Inspection Methodology," Residual Life Assessment of Major Light Water Reactor Components – Overview Volume 1, V. N. Shah and P. E. MacDonald (eds.), NUREG/CR-4731, Vol. 1, pp. 123-129.

Crutzen, S. 1987. "Summary of the PISC II Project: PISC II Report No. 1," presented at the Seminar on Non-Destructive Examination in Relation to Structural Integrity, Ispra, Italy, August 28-29, 1985, in International Journal of Pressure Vessels and Piping 28, Ispra, Italy: Commission of the European Communities, 1-5, 1987, pp. 311-346.

Davis, C, 2006, Idaho National Laboratory, Personal communication.

DeVan, M. J., Lowe, Jr., A. L., and Hall, J. B., 1996. "Fracture Toughness Test Results of Thermal Aged Reactor Vessel Materials," Effects of Radiation on Materials: 17th International Symposium, ASTM STP 1270, pp. 660-669.

DeVan, M. J., Lowe, Jr., A. L., and Wade, C. S., 1993. "Evaluation of Thermal-Aged Plates, Forgings, and Submerged-Arc Weld Metals," Effects of Radiation on Materials: 16th International Symposium, ASTM STP 1175, pp. 268-282.

Doctor, S. R., et al. 1991a. "Advanced NDE Technologies and Characterization of RPV Flaw Distribution," Proceedings of the Eighteenth Water Reactor Safety Information Meeting, Rockville, Maryland, October 22-24, 1990, NUREG/CP-0114, Vol. 3, pp. 137-156.

Ebi, G. and McEvily, A. J., 1984. "Effect of Processing on the High Temperature Low Cycle Fatigue Properties of Modified 9Cr-1Mo Ferritic Steel," Fatigue of Engineering Materials and Structures, 7, p. 299.

Ellis, F. V., and Byrnum, J. E., 1990. "Creep and Tensile Properties of SA-508 Class 3 Forging Material," Damage Assessment, Reliability, and Life Prediction of Power Plant Components, PVP.

Ennis, P. J., and Czyrska-Filemonowicz, A., 2002. "Recent Advances in Creep Resistant Steels for Power Plant Applications," OMMI Internet Journal, 1, pp. 1-28.

Fukakura, J., Asana, M., Kikuchi, M., and Ishikawa, M., 1993. "Effect of Thermal Aging on Fracture Toughness of RPV Steel," Nuclear Engineering Design, 144, pp. 423-429.

Generation IV International Forum, 2002, A Technology Roadmap for Generation IV Nuclear Energy Systems, FIF-002-00.

Gougar, H. D. and Davis, C. B., 2006, Reactor Pressure Vessel Temperature Analysis for Prismatic and Pebble-Bed VHTR Designs, Idaho National Laboratory Report, INL/EXT-06-11057.

Gunawardane, H. P., Hall, J. B., and Rosinski, S. T., 2006. "Mechanical Property Changes in Reactor Vessel Materials Thermally Aged for 209,000 h at 282°C," Journal of ASTM International, 3, Paper ID JAI12430.

Halmshaw, R. 1987. Non-Destructive Testing, Edward Arnold Ltd., London and Baltimore.

Harris, B. L., Shah, V. N., and Korth, G. E., 1986. "Creep Rupture Failure of Three Components of the Reactor Primary Coolant System during the TMLB Accident," EGG-EA-7431.

Hayner, G. O., Bratton, R. L., Wright, R. N., Windes, W. E., Totemeier, T. C., Moore, K. A., Corwin, W. R., Burchell, T. D., Klett, J. W., Nanstad, R. K., Snead, L. L., Katoh, Y., Rittenhouse, P. L., Swindeman, R. W., Wilson, D. F., McGreevy, T. E., Ren, W., 2005. "Next Generation Nuclear Plant Materials Research and Development Program Plan", INL/EXT-05-00758.

Henry, J. F., 2005. "Growing Experience with P91/T91 Forcing Essential Code Changes," Combined Cycle Journal, 1Q/2005.

Hoffman, C., 1982. "The Effects of Mechanical Cycling on the Substructure of Modified 9Cr-1Mo Ferritic Steel," in "Ferritic Steels for High Temperature Applications", Khare, A. K., (Ed.) American Society for Metals, Materials Park, OH, 221.

Hoge, K. G. 1979. Evaluation of the Integrity of SEP Reactor Vessels, NUREG-0569.

Horiuchi, T., et al. 2002. "Improved Utilization of Added B in 9 Cr Heat-Resistant Steels Containing W," ISIJ International, Vol. 42, pp. S67-S71.

Hucinska, J., 2003. "Advanced Vanadium Modified Steels for High Pressure Hydrogen Reactors," Advances in Materials Science, 4, pp. 21-27.

Hutton, P. H. 1989. "An Overview of Development and Application of Acoustic Emission Methods in the United States," Nuclear Engineering and Design, 113, pp. 59-69.

Hutton, P. H., et al. 1984. Acoustic Emission Monitoring of Hot Functional Testing, NUREG/CR-3693, PNL-5022.

Hutton, P. H., et al. 1988. Acoustic Emission System Calibration of Watts Bar Unit 1 Nuclear Reactor, Nureg/CR-5144, PNL-6549.

Imgram, A. G., Ibarra, S., Prager, M., 1990. "A Vanadium Modified 2 1/4Cr-1Mo Steel with Superior Performance in Creep and Hydrogen Service," New Alloys for Pressure Vessels and Piping, PVP 201, MPC-3, pp. 1-28.

Ishiguro, T., Murakami, Y., Ohnishi, K., and Watanabe, J., 1982. "A 2 1/4Cr-1Mo Pressure Vessel Steel with Improved Creep Rupture Strength," ASTM STP 755, pp. 129-147.

Jones, W. B., 1983. "Effects of Mechanical Cycling on the Substructure of Modified 9Cr-1Mo Ferritic Steel," Proceedings of ASM International Conference on Production, Fabrication, Properties, and Application of Ferritic Steels for High-Temperature Applications, Warren, PA, 6-8, October 1981, American Society for Metals, Metals Park, OH, pp. 221-235.

Kim, H. S., Song, B. J., Ryu, W. S., and Hoong, J. H., 2004. "Creep Rupture Properties of Nitrogen added 10Cr Ferritic/Martensitic Steels," Journal of Nuclear Materials, 329-333, pp. 299-303.

Kim, J. T., Kim, B. H., Kong, B. O., and Kim, D. J., 2006. "Effects of V and Carbides on the Temper Embrittlement of the 2.25Cr-1Mo Steel," PVP2006-ICPVT-11-93218, Proceedings of PVP2006-ICPVT-11, 2006 ASME Pressure Vessels and Piping Division Conference, July 23-27, 2006, Vancouver, BC, Canada

Kimura, K., 2005. "Assessment of Long-Term Creep Strength and Review of Allowable Stress of High Cr Ferritic Creep Resistant Steels," PVP2005-71039, Proceedings of ASME Pressure Vessels and Piping Division Conference, Denver, CO, July 2005, pp. 237-244.

Kimura, M., Kobayashi, K., and Yamaguchi, K., 2003. "Creep and Fatigue Properties of Newly Developed Heat-Resisting Steels for Ultra Super Critical (USC) Power Plants," Materials Science Research International, 9, pp. 50-54.

Kloc, L., Sklenicka, V., Dlouhy, A., and Kucharova, K., 1998. "Power-Law Viscous Creep in Advanced 9% Cr Steel," in "Microstructural Development and Stability in High Chromium Ferritic Power Plant Steels," Strang, A., and Gooch, D. J., (Eds.) Number 2, The Institute of Materials, pp. 445-455.

Klueh R. L., and Harries, D. R., 2001. "High Chromium Ferritic and Martensitic Steels for Nuclear Applications," ASTM.

Klueh, R. L., 2002, "Joining and Processing Issues for Ferritic/Martensitic Steels," US Fusion Materials Science Program Strategic Planning Meeting, University of California at Santa Barbara, August 26-30, 2002, PowerPoint slides.

Klueh, R. L., 2005. "Elevated Temperature Ferritic and Martensitic Steels and their Application to Future Nuclear Reactors" International Materials Reviews, 50, pp. 287-310.

Klueh, R. L., and Swindeman, R. W., 1986. "The Microstructure and Mechanical Properties of a Modified 2.25Cr-1Mo Steel," Metallurgical Transactions, 17A, pp. 1027-1034.

Kobelco Welding. "Advanced 9Cr Filler Metals in Welding Power Boilers and Oil Refinery Machinery," Technical Report, Kobelco Welding Today.

Kumar, A., et al., 2002. "Comprehensive Microstructural Characterization in Modified 9Cr-1Mo Ferritic Steel by Ultrasonic Measurements," Metallurgical and Materials Transactions A, Volume 33A, June 2002, pp. 1617-1626.

Kwon, J. D., Woo, S. W., and Choi, Y. H., 2004. "The Study of Thermal Aging of Dissimilar Weld Zone in a Primary Reactor Cooling System," Key Engineering Materials, 261-263, pp. 1689-1694.

Lee, J. S., Armaki, H. G., Maruyama, K., Muraki, T., and Asahi, H., 2006. "Causes of breakdown of creep strength in 9Cr-1.8W-0.5Mo-Vnb Steel," Materials Science and Engineering A, 428, pp. 270-275.

Liddington, B. H., et al. 1976. "Ultrasonic Measurement of the Depth of Fatigue Cracks," British Journal of Nondestructive Testing, 18, 6, p. 165.

Longsdon, W. A., 1982. "The Influence of Long-Time Stress Relief Treatments on the Dynamic Fracture Toughness Properties of ASME SA508 Cl 2a and ASME SA533 Gr B Cl 2 Pressure Vessel Steels," Journal of Materials for Energy Systems, 3, pp. 39-50.

MacDonald, P. E., Bayless, P. D., Gougar, H. D., Moore, R. L., Ougouag, A. M., Sant, R. L., Sterbentz, J. W., and Terry, W. K., 2004, The Next Generation Nuclear Plant – Insignts Gained from the INEEL Plant Design Studies, Proc. ICAPP-04, Pittsburgh, PA, June 13-17, 2004, p. 349.

Mannan S. L., and Valsan, M., 2004. "High Temperature Low Cycle Fatigue of Steels and their Welds," Key Engineering Materials, 274-276, pp. 57-64.

Mannan, S. L., and Valsan, M., 2006. "High Temperature Low Cycle Fatigue, Creep-Fatigue and Thermomechanical Fatigue of Steels and their Welds," International Journal of Mechanical Sciences, 48, pp. 160-175.

Mannan, S. L., et al., 2001. "Selection of Materials for Prototype Fast Breeder Reactor," http://www.igcar.ernet.in/igc2004/PFBR.pdf.

Mannan, S. L., Rao, K. B. S., Valsan, M., and Nagesha, A., 2005. "Strain Controlled Low Cycle Fatigue and Creep-Fatigue Interaction Behavior of Modified 9Cr-1Mo Ferritic Steel," Transactions of the Indian Institute of Metals, 58, pp. 159-168.

Mitsubishi Heavy Industries. "Remaining Life Estimation Technologies."

Muscara, J. 1985, Research Program Plan: Non-Destructive Examination, NUREG-1155, Vol. 4.

Nagesha, A., Valsan, M., Srinivasan, V. S., Rao, K. B. S., and Mannan, S. L., 2005. "High Temperature Low-Cycle Fatigue and Creep-Fatigue Behavior of a Modified 9Cr-1Mo Ferritic Steel," Proceedings of Fourth International Conference on Advances in Materials Technology for Fossil Power Plants, October 25-28, 2004, pp. 1227-1228.

Nanstad, R. K., 2004. "Reactor Pressure Vessel Steels and Irradiation Issues," Presented at the VHTR Materials R&D Collaboration Meeting, INEEL, Idaho Falls, May 2004

NEI 1989. "Faster Work on Pressure Vessels," Nuclear Engineering International, October 1989, pp. 26, 27.

Nichols, R. W. and Crutzen, eds. 1988. Ultrasonic Inspection of Heavy Section Steel Components: The PISC II Final Report, Elsevier Applied Science, London.

Njo, D. H., et al. 1991. "Integration of Fracture Mechanics and NDE: An Essential Requirement for Effective Structural Integrity Assessment," in Pressure Vessel Integrity 1991, S. Bhandari et al. (eds.), PVP-Vol. 213, MPC-Vol. 32, American Society of Mechanical Engineers, New York, pp. 31-38.

Nucleonics Week 1989b. "Outlook On Nondestructive Examination," Nucleonics Week, June 30.

Orr, J., and L. Woolard, L., 1997. "The Development of 9%CrMo Steels from Steel 91 to E911," in "Microstructural Development and Stability in High Chromium Ferritic Power Plant Steels," Strang, A., and Gooch, D. J., (Eds.), Number 1, The Institute of Materials, pp. 53-72.

Prager, M, Yamaura, T, and Takeda, T, 1990. "Development of a Filler Metal for Welding Vanadium Modified 2 1/4 Chrome-1 Moly Steel," New Alloys for Pressure Vessels and Piping, Pressure Vessels and Piping Conference, TN, June 17-21, 1990. pp. 65-77.

Prager, M., 1998. "Long-Term Studies of Strength and Toughness of an Advanced Steel," Fitness-for-Service Evaluations in Petroleum and fossil Power Plants, PVP-Vol. 380, ASME, pp. 291-299.

Raj, B. et al. 2006. "Frontiers in NDE Research Nearing Maturity for Exploitation to Ensure Structural Integrity of Pressure Retaining Components," International Journal of Pressure Vessels and Piping, 83, pp. 322-335.

Reddy, G. B., and Ayres, D. J., 1982. "High Temperature Elastic-Plastic and Creep Properties for SA-533 Grade B Class 1 and SA508 Materials," EPRI NP-2763.

Riou, B., et al. 2006, "Negligible Creep Conditions for MOD 9Cr1Mo Steel," Proc. PVP2006, ICPVT-11, July 2006, Vancouver, Canada.

Roth, M., 2002. "Welding Chromium-Molybdenum Steel Pipe for Power Plants," The Fabricator, July 11, 2002. (3 pages)

Ryu, W. S., ,2006. Private Communication.

Ryu, W. S., 2005. "Korean R&D Program on RPV Materials," GIF VHTR Materials & Components, PMB Meeting, Sep 5-7, 2005.

Santella, M. L. et al. 2003. "Austenite to Martensite Phase Transformation in 9 Cr 1 Mo Steel Weld Metal," presented at the American Welding Society Conference

Seran, J. L., Cabrillat, M. T., and Forest, L., 2004. "CEA R&D Program on Reactor Pressure Vessel: Metallurgical and Mechanical Studies launched on Mod 9Cr-1Mo Steel," VHTR/NGNP Meeting, Idaho Falls, May 4-6, 2004.

Shibli, I. A., 2002, "Performance of P91 Thick Section Welds Under Steady and Cyclic Loading Conditions: Power Plant and Research Experience," OMMI, Vol. 1, Issue 3, pp. 1-17.

Sikka, V. K, Ward, C. T., and Thomas, K. C, 1981. Proceedings of Conference on Ferritic Steels for High Temperature Applications, Warren, PA, October 6-18, 1981, ASM, p. 65.

Sikka, V. K., 1985. "Pressure Vessels and Piping: Materials for Nuclear Steam Generators", ASME.

Sikka, V. K., Cowgill, M. G., and Roberts, B. W., 1983. "Ferritic Alloys for use in Nuclear Energy Technologies," Davis, J. W., and Michel, D. J., (Eds.) TMS, Warrendale, PA.

Silk, M. g., et al. 1987. Reliability of Nondestructive Inspection: Assessing the Assessment of Structures Under Stress, Adam Hilger, Bristol, pp. 69-70.

Sklenicka, V., Kucharova, K., Dlouhy, A., and Krejci, J., 1994. Proceedings of Conference on Materials for Advanced Power Engineering, D. Coutsouradis et al. (Eds.) Kluwer Academic, Dodrecht, 1994, p. 435.

Sperko Engineering, 2005. "Welding Grade 91 Alloy Steel," October 2005.

Stahlkopf, K. E., et al. 1987. "A Review of Materials and Fabrication Methods Used in Light Water Reactor Pressure Vessels," Performance and Evaluation of Light Water Reactor Pressurre Vessels, PVP-Vol. 119, American Society of Mechanical Engineers, New York, p. 1.

Staubli, 1996

Stone, R. M., et al. 1989. Operation of the EPRI Nondestructive Evaluation Center: 1988 Annual Report, EPRI NP-6565, Electric Power Research Institute, Palo Alto, pp. 8-1 to 8-10.

Swanekamp, R., 2004, "Maintenance Workshop Tackles the Challenges of P91/T91 and HRSG Layup," Power Engineering,

Swindeman, M. J., and Swindeman, R. W., 2005. "Creep response of advanced martensitic steels to stress and temperature changes after long times," Proceedings of Fourth International Conference on Advances in Materials Technology for Fossil Power Plants, October 25-28, 2004, 1168-1182.

Swindeman, R. W., Maziasz, P. J., and Brinkman, C. R., 2000. "Aging Effects on the Creep-Rupture of 9Cr-1Mo-V Steel," Proceedings of International Joint Power Generation Conference, Miami, FL, July 23-26, 2000, IJPGC2000-15050.

Swindeman, R. W., Sikka, V. K., and Maziasz, P. J., 1998. "Evaluation of T91 after 130,000 Hours in Service," in "Fatigue, Environmental Factors, and New Materials," PVP-374, ASME, New York, pp. 305-312.

Tabuchi, M., and Takahashi, Y., 2006. "Evaluation of Creep Strength Reduction Factors for Welded Joints of Modified 9Cr-1Mo Steel (P91)," Proceedings of PVP2006-ICPVT-11, 2006 ASME Pressure Vessels and Piping Division Conference, July 23-27, 2006, Vancouver, BC, Canada.

Tabuchi, M., et al. 2006. "Study on Type-IV Damage Prevention in High-Temperature Welded Structures of Next-Generation Reactor Plants, Part II: Effect of Boron on Creep Properties and Microstructures of HAZ for High Cr Steels," Proceedings of PVP2006-ICPVT-11, 2006 ASME Pressure Vessels and Piping Division Conference, July 23-27, 2006, Vancouver, BC, Canada.

Tabuchi, M., et al., 2004, "Improvement of Type IV Creep Cracking Resistance of 9Cr Heat Resisting Steels by Boron Addition," OMMI, Vol. 3, Issue 3, p. 1-11.

Tachibana, Y., 2005. "High Temperature Structural Design Guideline of the HTTR Metallic Components," Presented at the Generation IV International Forum, Oak Ridge, TN.

Takahashi, Y., 2006. "Study on Type-IV Damage Prevention in High-Temperature Welded Structures of Next-Generation Reactor Plants, Part 1 Fatigue and Creep-Fatigue Behavior of Welded Joints of Modified 9Cr-1Mo Steel," Proceedings of PVP2006-ICPVT-11, 2006 ASME Pressure Vessels and Piping Division Conference, July 23-27, 2006, Vancouver, BC, Canada.

Tonti, A. "Strategic Research Agenda – TG 4," European Pressure Equipment Research Council (EPERC), Annual General Meeting, Brussels, 8 Nov. 2005.

Totemeier, T. C., Tian, H., and Simpson, J. A., 2006. "Effect of Normalization Temperature on the Creep Strength of Modified 9Cr-1Mo Steel," Metallurgical and Materials Transactions, 37, pp. 1519-1525.

Tsuchida, Y., Inoue, T., and Suzuki, T., 2004. "Creep Rupture Strength of V-modified 2 ¼ Cr-1Mo Steel," IJPVP, 81, pp. 191-197.

UKAEA (United Kingdom Atomic Energy Authority) 1982. Assessment of the Integrity of PWR Pressure Vessels, W. Marshall (study group chair) CBE, FRS, CEGB/S/64, March, London.

USNRC 1983. "Ultrasonic Testing of Reactor Vessel Welds During Preservice and Inservice Examinations," Regulatory Guide 1.150, Rev. 1, U.S. Nuclear Regulatory Commission.

Wachter, 1985

Wall, M., 1987, "A Review of Thermal Aging Effects in High Chromium Ferritic Steels," UKAEA Report AERE-R 12317.

Watanabe, T., 2006. "Creep damage evaluation of 9Cr–1Mo–V–Nb steel welded joints showing Type IV fracture," International Journal of Pressure Vessels and Piping, Volume 83, Issue 1, January 2006, Pages 63-71

Willetts, A. J., et al. 1986. Evaluation of the Ultrasonic Data Recording and Processing System (UDRPS), EPRI NP-4397, Electric Power Research Institute, Palo Alto.

Willetts, A. J., et al. 1989. Accuracy of Ultrasonic Flaw Sizing Techniques for Reactor Pressure Vessels, EPRI NP-6273, Electric Power Research Institute, Palo Alto.

Wu, R., Sandstrom, R., and Seitisleam, F., 2005. "Low Temperature Creep Crack Growth in Low Alloy Reactor Pressure Vessel Steel," Journal of Nuclear Materials, 336, pp. 279-290.

Zhou, R. J., et al. 1985. "A Study of Residual Stress in Pressure Vessel Steels," Bulletin 302, Welding Research Council, New York, p. 23.